

MDPI

Review

# A Review on Cutting-Edge Three-Dimensional Graphene-Based Composite Materials: Redefining Wastewater Remediation for a Cleaner and Sustainable World

Tahreem Shahzad <sup>1</sup>, Sajawal Nawaz <sup>2</sup>, Hasan Jamal <sup>3</sup>, Taiba Shahzad <sup>4</sup>, Farid Akhtar <sup>5,\*</sup> and Urooj Kamran <sup>5,6,\*</sup>

- Department of Chemistry, University of Narowal, Narowal 51600, Pakistan; shahzad.tahreem987@gmail.com
- <sup>2</sup> Department of Physics, University of Padua, 35122 Padua, Italy; sajawalnawaz3@gmail.com
- Division of Energy Technology, Daegu Gyeongbuk Institute of Science & Technology, 333, Techno Jungang-Daero, Hyeonpung-Myeon, Dalseong-Gun, Daegu 42988, Republic of Korea; hasanjamal13@yahoo.com
- Department of Bio-Technology, University of Narowal, Narowal 51600, Pakistan; taiba.shahzadahmad1024@gmail.com
- Division of Materials Science, Luleå University of Technology, 97187 Luleå, Sweden
- Institute of Advanced Machinery Design Technology, Korea University, 145 Anam-ro, Seongbuk-gu, Seoul 02841, Republic of Korea
- \* Correspondence: farid.akhtar@ltu.se (F.A.); malikurooj9@gmail.com (U.K.)

Abstract: Three-dimensional (3D) graphene-based composite materials (3D GBCMs) have emerged as promising candidates for addressing critical challenges in water pollution remediation. This review selectively highlights the recent advancements in the application of 3D GBCMs to remove a wide range of contaminants, including heavy metals, dyes, salts, and pharmaceutical residues, from water. They owe their efficacy to their large surface area, interconnected porous structure, and functionalization potential. Three-dimensional GBCMs are promising materials for water filtration, offering capabilities such as heavy metal ion adsorption, the photocatalytic degradation of organic pollutants, and advanced desalination techniques like capacitive deionization (CDI) and solar desalination, thus providing sustainable solutions for obtaining freshwater from saline sources. Additionally, the factors influencing the pollutant removal capacities of 3D GBCMs, such as their material morphology, particle size, and porosity, are briefly discussed. Notably, the effect of the particle size on pollutant removal has not been extensively studied, and this review addresses that gap by exploring it in detail. Future research directions are also proposed, emphasizing the optimization and broader application of 3D GBCMs in environmental remediation. This review aims to provide valuable insights into the design and practical implementation of 3D GBCMs, offering guidance for their continued development in sustainable water treatment.

**Keywords:** 3D graphene-based materials; wastewater treatment; solar desalination; capacitive deionization; organic contaminants



Academic Editors: Swadesh Kumar Singh and Julfikar Haider

Received: 1 November 2024 Revised: 5 December 2024 Accepted: 11 December 2024 Published: 3 January 2025

Citation: Shahzad, T.; Nawaz, S.; Jamal, H.; Shahzad, T.; Akhtar, F.; Kamran, U. A Review on Cutting-Edge Three-Dimensional Graphene-Based Composite Materials: Redefining Wastewater Remediation for a Cleaner and Sustainable World. *J.* Compos. Sci. 2025, 9, 18. https:// doi.org/10.3390/jcs9010018

Copyright: © 2025 by the authors. Licensee MDPI, Basel, Switzerland. This article is an open access article distributed under the terms and conditions of the Creative Commons Attribution (CC BY) license (https://creativecommons.org/licenses/by/4.0/).

#### 1. Introduction

Life would not have evolved without water and will eventually die without it, assuring that the availability of water for living organisms is the biggest challenge of the time, as a man can neither survive drought nor floods [1]. Water is a universal solvent; its solvation properties are so good that it is hard to obtain pure water [2]. In recent years, an upsurge in the contamination of aquatic ecosystems has drastically affected living beings. The release of these defilements in water bodies is triggered by both natural and anthropogenic

means. For instance, only 0.01% of available freshwater is stressed due to unsustainable consumption. Treating these biohazards is a prerequisite for access to safe drinking water and aquatic habitat availability [3]. Among the major organic and inorganic eco-hazards, inorganic salts (sulfates, phosphates, and nitrates), organic (acids, bases, and drugs), dyes, heavy metals, pathogens (bacteria and viruses), and radioactive substances introduced into the aquatic and terrestrial environment have been reported in various matrices, indicating their inefficient elimination by conventional water treatment methods [4,5]. Due to their ease of access, waterways such as rivers, lakes, and oceans are the most common sites for waste disposal. Industrial discharge, agricultural runoff, municipal waste, landfill leaching, marine dumping, and atmospheric deposition are common sources of water pollution [6]. Water treatment techniques are being developed using nanotechnology based on sensor technology [7], nanofiltration [8], disinfection [9], biosorption [10], photodegradation [11], and adsorption [12]. Because of their large surface area, small size, and ease of functionalization, nanostructures, and their micro and macro analogs, provide unparalleled opportunities to create more effective catalysts and redox-active media for wastewater purification [13,14]. Many different types of low-dimensional nanomaterials have been developed and researched for their efficacy as water-purification materials [15,16]. These include 0D metal oxide nanoparticles (e.g., Fe<sub>3</sub>O<sub>4</sub> and TiO<sub>2</sub> nanoparticles), 1D nanowires and nanotubes (e.g., silver nanowires and carbon nanotubes), and 2D nanosheets (e.g., graphene and 2D layered transition-metal chalcogen) [17]. Nanomaterials efficiently eliminate several pollutants from wastewater, such as heavy metals [18,19], drugs [20], organic and inorganic solvents [21,22], dyes [23,24], biological toxins [25], pathogens [26,27], and pesticides. Moreover, their small size and huge surface area provide a minimal intraparticle diffusion distance that can be compressed without affecting their surface area [28]. Researchers attempt to create innovative nanomaterials with novel features to broaden their application [29]. One of the primary goals of nanotechnology is to improve wastewater management [30].

There are numerous undesirable consequences associated with nanomaterials like irreversible agglomeration in aqueous media causing significant loss of activity, the extensive membranous extraction required in recovering depleted nanomaterial from treated media, and the ecotoxicity correlated with the remnants of nanomaterials in processed water [31]. As a result, only a few commercially available nano-based water treatment systems have been developed [32,33]. To address these concerns, nanotechnology has evolved to involve different types of membranes [34], beads [35], and filters based on nano-porous ceramics [36], carbon nanotubes [37], surface-immobilized nanomaterials [38] and 3Dprinted nanostructures [39]. Creating 3D macrostructures by assembling low-dimensional nanomaterials represents the most admired approach to addressing the challenges of their practical applicability [40]. A variety of 3D macro architectures, such as graphene-based membranes [41], fibers [42], sponges [43], transition metal nanoparticle hydrogels [44], carbon nanotube (CNT) aerogels [45], and many others, have been successfully introduced at lab scales. These printed 3D materials carry the properties of their nano-sized precursors and are potentially suitable for wastewater treatment [46]. One of the main innovations in this domain is the recent development of 3D graphene-based adsorbents (3D GBAs), which strengthen water purification materials' structural and functional properties [47]. Three-dimensional GBAs are often designed and synthesized through frameworks such as hydrogels, aerogels, sponges, and foams. These assemblies possess high surface areas and porosities and the potential to impart intrinsic functionality to graphene sheets in the form of atoms, molecules, polymers, and nanoparticles to achieve enhanced physical properties and selectivity toward specific contaminants. The 3D GBAs with hierarchical porosity, which leads to a high adsorption capacity and effective pollutant removal effi-

ciency, perform important catalytic activities [48]. The development of 3D graphene-based composite materials (3D GBCMs) offers an important direction for future commercial water purification applications [49]. These materials are effective and environmentally friendly, aiding in meeting the demand worldwide for clean water for drinking and other daily use.

The potential of these materials is immense, but this review highlights the remaining challenges, requiring ongoing work to develop scalable, economical, and environmentally sustainable production approaches. This review provides a thorough and detailed analysis of 3D graphene structures, emphasizing their evolution and varied applications. Unlike previous studies that have briefly addressed the significance of these materials, this review offers a comprehensive historical overview of the development of 3D graphene materials. It explores their potential uses across different fields. It categorizes different 3D graphene-based materials (3D GBMs) based on their structural characteristics, including macroscopic and microscopic forms, and examines various types, such as spheres, cages, and crumpled graphene, highlighting their specific advantages in different applications. This review carefully examines the structural properties of 3D graphene materials, such as their porosity, particle size, and morphology, and investigates how these properties affect their efficiency in pollutant removal, an area that has not been extensively covered before. It emphasizes the critical role of hierarchical porosity and their surface area in boosting their adsorption capacity. Beyond just listing material properties, this review delves into the practical applications of 3D graphene, particularly in the realm of wastewater treatment. It comprehensively analyzes the mechanisms by which GBCMs purify water, including adsorption, catalysis, deionization, and solar desalination. This review outlines how these materials can effectively remove heavy metals, dyes, salts, and pharmaceutical residues from water, positioning them as promising solutions for environmental remediation. By taking a systematic and detailed approach, this review aims to be an invaluable resource for researchers in materials science, environmental engineering, and related disciplines. It integrates historical context, structural analysis, and practical applications to deepen understanding of the complex significance of 3D graphene materials, with a special focus on their utility in addressing global environmental issues, particularly in wastewater treatment. While highlighting the significant potential of 3D graphene materials, this review also acknowledges challenges such as their scalability, cost, and environmental impact, suggesting that future research should focus on overcoming these obstacles to enhance the commercial viability of these materials.

## 2. History of 3D GBCMs

Although 2D graphene layers have been extensively studied, when 2D graphene layers are used in real life, they do not always work as well as expected because they lose some of their unique qualities. In order to conquer this obstacle, researchers have started the development of 3D structures that preserve the advantageous properties of two-dimensional graphene materials while avoiding the complications related to stacking [50]. A range of approaches, including chemical reduction, 3D printing, hydrothermal reduction, and laser casting, have been utilized to fabricate 3D graphene structures. These structures consist of graphene foam and macroscopic hydrogel. Despite the initial challenges, the emergence of 3D graphene materials, specifically the introduction of graphene oxide (GO) films, signified an important change from conventional carbon nanotubes. The films exhibited outstanding durability and the effective utilization of GO, thereby creating opportunities for an extensive array of applications [51]. The natural adaptability of the layered arrangement of GO enabled the fabrication of porous rGO films via chemical or thermal reduction. Simultaneously, alternative research groups have investigated the fabrication of hollow nanostructures composed of graphene-encasing metal oxide nanoparticles and microscopic

J. Compos. Sci. 2025, 9, 18 4 of 53

3D graphene materials [52]. Early developments in 3D graphene were primarily concerned with carbon aerogels, particularly those comprised of carbon nanoparticles and nanotubes. Breakthroughs in freeze-drying graphite oxide dispersion by Wang and Ellsworth initiated the era of 3D graphene aerogels, providing a foundation for further exploration [53]. In 2010, Shi and colleagues advanced the field by creating 3D graphene hydrogels through chemical self-assembly [54]. Overcoming challenges related to hydrothermal methods, Worsley et al. emphasized the importance of high-temperature heating in achieving conductivity, leading to the creation of ultralow-density graphene aerogels [55]. The advancement of the history of 3D graphene continued through the implementation of various methodologies, including 3D printing and laser scribing. In 2011, Cheng et al. utilized chemical vapor deposition (CVD) on structured models to fabricate 3D graphene from the bottom up [56]. Hu et al. introduced the MTU reaction in 2013, which is an innovative chemical reaction pathway that facilitates the exponential synthesis of honeycomb-like graphene in three dimensions. Their breakthrough, involving exothermic chemical reactions, ushered in a new era of 3D graphene materials with intricate structures. Hu's alkali-metal chemistry further expanded the possibilities regarding the use of these materials, allowing the synthesis of inorganic carbon compounds and the development of self-modulated microscale structures in 3D graphene [57]. Table 1 highlights key developments from the introduction of GO films in 1998 and 2014 to recent application advancements.

**Table 1.** Historical evolution of 3D GBCMs' development.

Key Developments of 3D Graphene	Year	Significance	References
Emergence of 3D Graphene Materials	1998 and 2014	Graphene oxide films were introduced, which are different from regular carbon nanotubes. The long longevity and usefulness of GO make it possible for a wide range of applications.	[51,58]
Development of Carbon Aerogels	2009	Freeze-drying graphite oxide dispersion as a breakthrough, paving the way for 3D graphene aerogels.	[53]
Structural Versatility	2010	The field creating 3D graphene hydrogels through chemical self-assembly provides a high degree of structural versatility. This technique enables the controlled arrangement of graphene sheets in three dimensions, offering new possibilities for tailoring the architecture of graphene-based materials.	[54]
Advancements in 3D Printing and Laser Scribing	2011	The fabrication of 3D graphene involves employing CVD in a bottom-up approach.	[56]
Innovative MTU Reaction	2013	Chemical reaction pathway facilitating the exponential synthesis of honeycomb-like graphene. Exploration of alkali-metal chemistry for inorganic carbon compounds and self-modulated microscale structures.	[57]
Metal-Sulfur Batteries (MSBs) Application	2023	Special benefits of 3D graphene shapes for MSBs, addressing sulfur loading and aggregation issues. Improved shape, electrical conductivity, and electrochemical stability for overcoming MSB problems.	[59]

J. Compos. Sci. 2025, 9, 18 5 of 53

Table 1. Cont.

Key Developments of 3D Graphene	Year	Significance	References
Wearable Piezoresistive Sensors Application	2021	Promising use of 3D graphene-based wearable piezoresistive sensors for flexibility, ease of fabrication, low power usage, and simple signal acquisition. Noteworthy for graphene's strong $\pi$ - $\pi$ stacking and self-assembly structures.	[60]
Environmental Remediation Application	2023	Highlighted use of 3D graphene as an adsorbent for environmental remediation. Emphasis on heteroatom-doped graphene adsorbents for water pollutant removal, showcasing improved adsorption effectiveness.	[61]

The applications of 3D graphene span from material design to device usage, particularly in metal (Li/Na/Al/Mg) sulfur batteries. The review by Meetesh et al. delves into the history of 3D graphene, its preparation methods, and its crucial role in battery applications, especially in metal-sulfur batteries (MSBs); the shapes of 3D graphene have unique advantages that help overcome problems in MSBs, allowing for an improved shape, electrical conductivity, and electrochemical stability, as well as low density, rapid charge kinetics, and an adjustable porous structure [59]. The applications of 3D graphene in the development of wearable piezoresistive sensors are highlighted by Minghui et al. in their review. Three-dimensional graphene-based wearable piezoresistive sensors demonstrate great promise as flexible sensors because they are easy to make, have a simple read-out device, use a low amount of power, and are straightforward to signal acquisition with. Nanoparticles, metal nanowires, carbon nanotubes, graphene, and porous silicon are some nanomaterials used to make 3D structures that work very well in wearable piezoresistive pressure devices. One material that stands out is graphene, which is very flexible and lightweight, and has great mechanical strength. Graphene is perfect for manufacturing 3D wearable piezoresistive sensors because its strong  $\pi$ - $\pi$  stacking and the strong van der Waals interaction between its planar basal planes allow for controllable self-assembly structures [60]. A recent work by Wan et al., focusing on its application as an adsorbent, highlighted the use of 3D graphene for environmental remediation. The study gives valuable information about using heteroatom-doped graphene adsorbents to eliminate water pollutants. It shows how 3D heteroatom doping and hydrothermal production can improve the effectiveness of adsorption by graphene. Graphene's unique physicochemical and mechanical qualities and 3D structure, allowing its wide range of uses, have attracted attention. In particular, graphene's large surface area, variable surface functions, many adsorption mechanisms, and improved practical handling make it an attractive adsorbent for cleaning up the environment [61].

# 3. Classification of 3D GBCMs on Structure

There are numerous facets to the classification of 3D graphene materials, including differentiations according to their engineering dimensions, the types of connections in the structures, and the precursors utilized in synthesis. Figure 1 demonstrates a classification scheme for 3D graphene materials based on recently reported works.

At the engineering level, these substances are classified into two types: macroscopic 3D graphene materials (100  $\mu$ m or greater), which consist of monoliths, films, filaments, and millispheres, and microscopic 3D graphene materials (less than 100  $\mu$ m), which manifest as powders but have 3D structures on the micrometer or nanometer scale [62]. When

J. Compos. Sci. 2025, 9, 18 6 of 53

examining the connections within 3D graphene structures, it becomes evident that their joint architectures consist of interknitted graphene sheets held together by van der Waal's forces. In contrast, their integrated networks demonstrate uninterrupted carbon atom connections via chemical bonds, which contribute to their enhanced mechanical robustness, conductivity, and integrity [56].

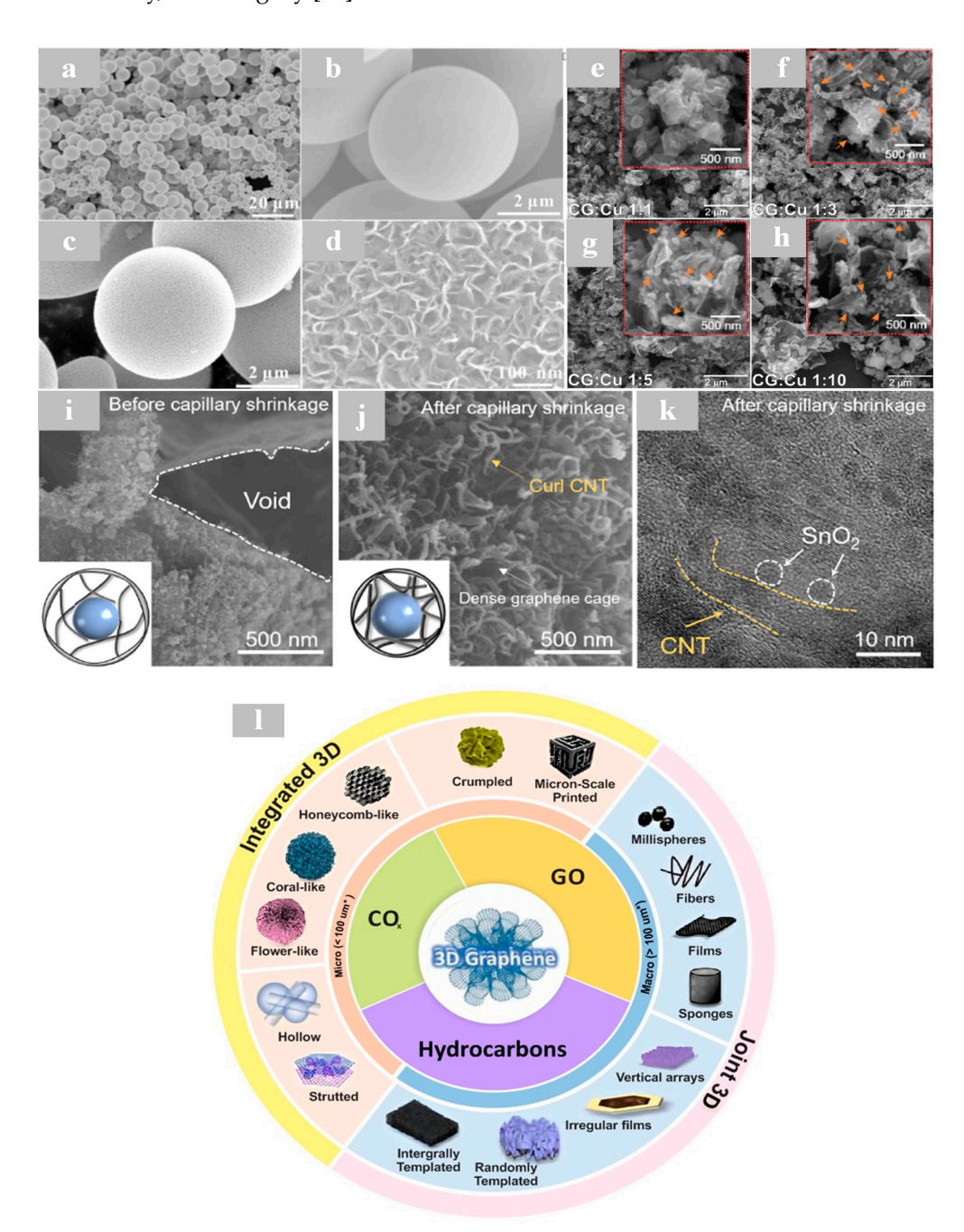


**Figure 1.** SEM images of  $SiO_x/NC$  (a,b) and  $VG@SiO_x/NC$  (c,d) show that the spherical morphology of the microspheres is characterized by well-dispersed, highly round, and smooth surfaces [63]; copper-based nanoparticles preferentially nucleate and grow on the crumpled graphene surface at a high CG:Cu ratio (e–g). In contrast, agglomeration of particles becomes more prominent at a 1:10 CG:Cu ratio (h) [64]; the  $SnO_2@CNT@GC$  (i) material exhibits a loose structure before capillary shrinkage. Following the shrinkage, (j) SEM and (k) TEM images reveal the condensed  $SnO_2@CNT@GC$  material [65]. (l) Representation of several 3D Graphene Materials at the micro and macro level [66]. \* signifies that materials with a length of 100 μm in single or multiple dimensions are identified as microscopic graphene materials.

J. Compos. Sci. 2025, 9, 18 7 of 53

#### 3.1. Three-Dimensional Graphene Spheres

The-dimensional graphene spheres, covering hierarchical, composite, doped, and functionalized forms, provide for a versatile and advanced class of nanomaterials. They have unique structural and functional properties that make them suitable for various applications related to energy storage, catalysis, environmental remediation, and biomedical engineering. Li et al. discussed the spherical nature of the 3D assembly of GO sheets, achieved through the flash-freezing of GO dispersion and the subsequent formation of hierarchical porous graphene networks via thermal-shock reduction, which enhances their performance by providing a gravimetric specific capacitance of around 306 F  $g^{-1}$  at 1.0 A  $g^{-1}$  and ensuring 93% capacitance retention after 10,000 cycles. This structure, due to its unique spherical architecture, results in a 30–50% capacitance improvement over GO powder, placing it among the top-performing GO-based structures developed through various chemical reduction processes [67]. Han et al. described a vertical graphene @SiO<sub>x</sub>/N-doped carbon (VG@SiO<sub>x</sub>/NC) 3D conductive network composite which is produced by CVD and exhibits a significantly enhancesd performance as a lithium-ion battery (LIB) anode. The uniform dispersion of SiO<sub>x</sub> and N-doped carbon at the sub-nanoscale within the spherical structure ensures consistent electrochemical behavior and prevents the aggregation of active materials. Overall, the spherical nature of the graphene in the VG@SiO<sub>x</sub>/NC composite significantly enhances its high reversible capacity of 1323.8 mA h g<sup>-1</sup>, excellent rate performance of 265.5 mA h  $g^{-1}$  at 20 A  $g^{-1}$ , and long cycling life, as it maintains 84.2% of its capacity after 500 cycles at 2 A  $g^{-1}$  (Figure 1a–d) [63].

Wen et al. reported on 3D hierarchical nitrogen-doped graphene/carbon nanotube (N-GCNT) microspheres prepared using a one-step ultrasonic spraying deposition method. The spherical architecture creates a 3D porous framework that greatly increases the sphere's BET specific surface area to  $575.8 \text{ m}^2\text{g}^{-1}$  and its pore volume to  $0.303568 \text{ cm}^3\text{g}^{-1}$ . The spherical shape maintains the characteristics of 1D and 2D nano-carbon materials, promoting efficient electron and ion transport pathways. This results in high initial discharge capacities of 1465.1 mAh  $g^{-1}$  at 0.1 °C, a good cycle stability of 1315.1 mAh  $g^{-1}$  after 200 cycles, and an outstanding long-term cycling performance of 849.1 mAh  $g^{-1}$  after 500 cycles at 2.0 °C. The uniform dispersion of nitrogen atoms within the spherical structure further enhances its electrochemical activity and stability, making N-GCNTs-2 microspheres highly effective in improving the performance of lithium-sulfur battery cathodes [68]. Zhang et al. reported a nitrogen-doped carbon microspheres/graphene aerogel (N-CMS/GA) composite achieved through a facile strategy involving spacer functionalization, lyophilization, and annealing treatment, resulting in a 3D hierarchical structure with high compressibility and excellent capacitive properties. Its spherical architecture increases the surface area and provides numerous active sites for electrochemical reactions, boosting its specific capacitance to  $346 \text{ F g}^{-1}$  at  $1 \text{ A g}^{-1}$ , with a superior rate capability (92% capacitance retention when the current density increases from 0.1 to 2.0 A g<sup>-1</sup>) and excellent cycle life (98.7% retention after 10,000 cycles in a 1.0 M KOH electrolyte) [69]. The use of advanced synthesis techniques to fine-tune these spheres for specific applications enriches their possibility of becoming key components in the next generation of advanced materials.

#### 3.2. Three-Dimensional Graphene Cages

In recent advancements, the design and construction of graphene cages with well-defined architectures have garnered significant attention due to the exceptional robustness, flexibility, and high electrical conductivity of graphene nanosheets, and these structures offer remarkable advantages for various applications [70]. Cao et al. have reported the fabrication of a 3D graphene-like structure coated on NVP nanoflake arrays through a one-pot, solid-state reaction in molten hydrocarbon. Three-dimensional graphene-like

J. Compos. Sci. 2025, 9, 18 8 of 53

cages serve as an excellent anode material, offering a dual functionality that simplifies the design of batteries and enhances their electrode compatibility. The uniform coating of NVP nanoflakes by graphene-like layers protects the active material from degradation and ensures consistent and efficient Na<sup>+</sup> ion diffusion, thereby maximizing the utilization of NVP [71]. Nanocages, particularly graphene nanocages, play a crucial role in enhancing the performance of lithium-sulfur batteries by addressing several key challenges. Yuan et al. proposed hollow porous graphene nanocages that were synthesized through a textbook reaction combined with acid leaching. These encapsulate sulfur, providing a stable environment that prevents sulfur loss due to dissolution in the electrolyte. The unique structure of these nanocages, including a yolk-shell configuration, allows for the accommodation of the volume expansion and contraction of sulfur during the charge and discharge cycles, preventing mechanical degradation of the electrode. This innovative design offers a promising approach to maximizing the sulfur loading within carbon matrices while also addressing the issue of polysulfide dissolution, thereby advancing the commercialization potential of lithium–sulfur batteries [72]. Xiao et al. developed a self-adapting electrical and mechanical carbon network by embedding carbon nanotubes within a capillary-shrinking graphene hydrogel, creating "nano-springs" that robustly connect and cushion the active noncarbon nanoparticles (Figure 1i-k). This dense carbon cage effectively buffers the volume changes of the noncarbon materials while maintaining dynamic electrical connectivity with the expanding and contracting noncarbon nanoparticles throughout the charging and discharging cycles [65].

#### 3.3. Three-Dimensional Crumpled Graphene

The development of 3D GBCMs offers an effective way to preserve the intrinsic properties of 2D graphene while enhancing characteristics such as its specific surface area, porosity, and mechanical strength [73]. Alencar et al. demonstrated an efficient one-step method, for use in practical applications like in electrochemical sensors, to create crumpled graphene composites that are fully decorated with copper chloride hydroxide hydrate nanoparticles. The copper-based nanoparticles are directly anchored to the crumpled graphene, as the carbon nanostructure serves as a platform for their nucleation and growth (Figure 1e-h). Additionally, the quantity of nanoparticles is controlled through decorating the graphene by adjusting the amount of copper salt precursor, a crucial factor in optimizing the performance of  $H_2O_2$  sensors [64]. The presence of organic contaminants (OCs) in aquatic systems poses a significant threat to both ecological and human health, and adsorption using GBCMs has emerged as a promising method for the removal of OCs. Fu et al. synthesized a nanocomposite composed of metal oxide (iron oxide, Fe<sub>3</sub>O<sub>4</sub>; titanium dioxide, TiO2; silicon oxide, SiO2; fumed silicon oxide, F-SiO2) nanoparticles encapsulated within crumpled graphene oxide (MGC) fabricated via a novel nano-spray drying technique, demonstrating robust adsorptive performance. The incorporation of metal oxides reduces the stacking of GO, expands the internal adsorptive surface area, and significantly boosts the adsorptive capacity of the MGC. MGCs formed using fumed SiO<sub>2</sub> or SiO<sub>2</sub> exhibited an enhanced Langmuir adsorption capacity (q<sub>m</sub>, normalized by % carbon) for a model OC, methylene blue, showing improvements of 60–86% compared to CGBs, and that were 3–4 times higher than that of powder activated carbon (PAC) and 6–7 times greater than that of granular activated carbon (GAC) [74]. The accurate detection of trace analytes in biological samples is crucial for medical diagnostics but often necessitates the use of complex and costly instruments. Boruah et al. presented the synthesis of porous 3D nitrogen-doped crumpled graphene nanoparticles (CGNPs) and their application as a platform for the sensitive detection of dopamine in complex biological media, such as blood serum. The CGNPs were synthesized by doping GO with ammonium hydroxide through

a hydrothermal treatment, which resulted in the crumpling of GO sheets into porous, sphere-like nanoparticles with a diameter of  $34 \pm 10$  nm. These nanoparticles, featuring a high surface area and enhanced electronic properties, exhibited strong catalytic activity for the oxidation of the peroxidase substrate 3,3',5,5'-tetramethylbenzidine (TMB) [75]. This structure is instrumental in achieving a low detection limit, a wide linearity range, and good selectivity in complex biological media, making crumpled graphene a key component in the functionality and effectiveness of sensing devices.

An additional category is formed by precursors synthesized from inorganic carbon compounds (CO, CO<sub>2</sub>, and CS<sub>2</sub>), hydrocarbon-synthesized variants, and GO-derived 3D graphene materials (3D rGOs). Each class possesses unique attributes; for instance, materials derived from GO frequently aggregate into macro monoliths; structures synthesized from hydrocarbons provide the flexibility to acquire micro or macro configurations; and 3D graphene architectures composed of inorganic carbon compounds typically exist at the micrometer scale with integrated structures [76]. By providing insights for future research and development, this comprehensive categorization enables an understanding of the diverse varieties of 3D graphene materials, as illustrated in Figure 11.

## 3.4. Advanced 3D Graphene-Based Composites

Modified 3D GBCMs can be a very beneficial method for wastewater treatment because of their unique physical and chemical properties, combined with their capability to be applied in real-life conditions [77,78]. Due to their strong  $\pi$ - $\pi$  interactions with aromatic compounds, 3D GBCMs enable these compounds for various applications, such as the adsorption of dye and pesticides. To this end, Shaojun et al. developed a Ni<sub>3</sub>(HITP)<sub>2</sub>-/graphene-based composite aerogel particle electrode possessing excellent stability and performance for efficient phenol degradation in a 3D TPB (triple-phase boundary) electrode system. Through selective H<sub>2</sub>O<sub>2</sub> production and radical generation, this system achieved full phenol degradation in 15 min (decomposition rate constant: 0.3283 min<sup>-1</sup>), with an improved mechanism of degradation minimizing its dependence on acid conditions that enables its potential application in industrial wastewater treatment [79]. A 3D graphene-based TiO<sub>2</sub>/g-C<sub>3</sub>N<sub>4</sub> (TiO<sub>2</sub>/CN/3DG) composite with defect engineering for water treatment was reported by Xin et al., in which plasma-induced O-defects in TiO<sub>2</sub>, N-defects in CN, and C-defects in graphene were used to boost its performance. The tetracycline (TC) removal rate of D-TiO<sub>2</sub>/CN/3DG was 88.5%, compared to the non-defective composite which only had a removal rate of 75.2%, and the material exhibited a high capacity of Cu<sup>2+</sup> adsorption. Nevertheless, its TC degradation was markedly suppressed in the TC/Cu<sup>2+</sup> mixed systems. On the contrary, TiO<sub>2</sub>/CN/D-3DG exhibited inferior performance for TC degradation, but an outstanding cooperative removal ability for TC and Cu<sup>2+</sup>. These results illustrate that defect engineering via plasma treatment could be a promising approach to addressing issues of antibiotic and heavy metal contamination through the tuning of its photocatalytic activity and adsorption performance [80]. Hence, there is a need for functionalized materials that support 3D graphene structures, improving their structural properties and enhancing their application performances, and that are based on graphene-based nanocomposite materials, g-C<sub>3</sub>N<sub>4</sub>, and visible light-activated metal oxide photocatalyst, which has been partially studied in water treatment and has potential to contribute to the development of environmental water treatment applications. The 3D microstructure response times, as modalities toward an acoustic field with 100 milliseconds, could also be a temporal trait conserved in the third dimension by keeping materials' aspect ratio and material properties stable across sizes [81]. High-precision 3D printing [82] and other manufacturing techniques allow the high-aspect-ratio microstructure to be fabricated directly on a substrate and assembled as part of a membrane filtration module in the setup of on-demand acoustic membrane clean-

ing. Yue et al. reported a weighted mobility analysis of polycrystalline graphene/strontium titanate (G/STO) nanocomposites which clearly shows that graphene-based nanocomposites also behave as single crystals at low graphene concentrations (0.11 vol%), with their charge transport properties converging with the crystallite size, indicating a reduction in the grain boundary effect that is greater than 700 K. At higher loadings (0.22 vol%), the grain boundary effect is eliminated. This change indicates that acoustic phonon scattering dominates the charge transport, as opposed to composite materials free from graphene, as their mobility is limited by grain boundary scattering [83]. Likewise, in aluminumdoped zinc oxide and reduced GO (AZO/RGO) nanocomposites, it was demonstrated that the weakened grain boundary barriers facilitated the free conduction of electrons [84]. These advances in graphene nanocomposites can provide strong guidance for the design of graphene-based composites with enhanced acoustic support for water treatment scenarios. Gang et al. presented a graphene-like carbon-assembled layered double oxide (G@LDO) material that was developed for effective microplastic (MP) adsorption in wastewater at different pH levels (1–13). At pH levels of 3–11, the material removed ≥80% of polystyrene (PS), whereas, at pH levels of 1 and 13, the PS removal was close to 60%. Compared to pure graphene, LDO, and 2D G@LDO, the maximum adsorption capacity for the PS was increased by 100% to 130% (209.39 mg/g for PS when immersed in its saturated solution). PS removal has been performed and, based on kinetic and thermodynamic analyses, it was found to be an exothermic chemisorption reaction. The removal mechanism involves hydrogen bonding, LDH complexation,  $\pi$ - $\pi$  interaction from graphene, and p- $\pi$  interaction with S in the carbon matrix. With its high pH tolerance, the G@LDO material is ideally suited to treating industrial wastewater, which often contains acidic or alkaline effluents [85]. Practical challenges such as material regeneration, industrial scale-up, and environmental viability post-disposal require further investigation. Despite these limitations, G@LDO represents an economically feasible solution for the remediation of microplastic (especially in acid/alkaline effluents) with a huge potential in the wastewater treatment industry.

# 4. Architectural Engineering of 3D GBCMs

The development of simple and efficient preparation methods is essential to meeting the requirements for removing organic dye pollution from water [86]. The domain of 3D graphene-based structures has been the subject of an abundance of research terminology, including terms such as foam, network, hydrogel, aerogel, monolith, bead, and sponge [87]. The synthesis of 3D configurations can be broadly classified into two categories: solutionbased synthesis and direct synthesis from carbon sources [47]. Two distinct methodologies, template-assisted and template-free approaches, are utilized within each class to fabricate 3D structures composed of graphene. The currently investigated 3D graphene-based architectures mainly fall into the categories of gels and foams, and the gels can also be divided into aerogels and hydrogels. The fabrication methods of 3D graphene architectures are broadly summarized as assembly by physical/chemical interactions, template methods, electrochemical reduction, controlled filtration, sol-gel synthesis, and chemical foaming methods. A straightforward bubble template-based strategy was adapted to fabricate a 3D graphene network, in which the GO was used to promote the aggregation of graphene nanoplates into a 3D porous framework structure [88]. The bubble template method enables the self-assembly of GO under surfactants and via strong stirring that generates many air microbubbles which act as templates. With this technique, large isotropic porous structures are formed. After that, the ice crystals are used as secondary templates to pierce and extrude the graphene networks to form dense graphene walls and interconnected channels [89]. Zhang et al. presented that ultralight, superplastic, and fatigue-resistant graphene aerogels (SFGAs) can be fabricated through GO liquid crystal-stabilized air bubbles strengthened by

sodium dodecyl sulfate (SDS). This ultralow density is due to the "volume exclusion effect" of air "bubbles" and isotropic ice crystal formation during freezing. The regular alignment of graphene sheets and the uniform, closely packed pore structure provide SFGAs with good dynamic mechanical properties [90]. Yang et al. improved this method further by devising a surfactant-foaming sol-gel method where air bubbles and ice crystals function as dual templates. This strategy dares to crush and reconstitute GO liquid crystals in dispersion to manufacture large-scale graphene hydrogel bulks with preserved structures. The burnt-aged hydrogels retain their structure to yield a monolith reaching  $\sim 1$  m<sup>2</sup> in size, super elasticity up to 99% compressive strain, and ultralow density (2.8 mg cm<sup>-3</sup>) after freeze-drying [91]. One suitable carbonaceous material is GO; it possesses hydroxyl, carboxyl, and epoxy functional groups that can easily be used as a basic starting material to build a 3D framework by chemical cross-linking. Because of the formation of a chemical bond within GO sheets during the process, the 3D scaffold that is formed is relatively stable and stronger than those made by other approaches [92]. The 3D porous network structure is usually constructed by weak physical interactions between the GO nanosheets, including electrostatic forces, hydrogen bonding, and  $\pi$ - $\pi$  interactions loaded at points of connectivity of the porous structure, leading to poor mechanical properties. However, these weak bonds are a precursor to the permanent collapse or deformation of the porous structure. Here, an essential solution that can use the classic weak non-covalent bonds and strong covalent bonds is chemical cross-linking, which has become an effective way to improve the structural stability of GAs. Ye et al. exhibited the synthesis of thin, hydrophilicityadjustable, and form-reversible cross-linked GAs by chemically binding GO nanosheets and poly (vinyl alcohol) (PVA) through glutaraldehyde (G). This method involves the acetalization of glyceraldehyde groups on glutaraldehyde with hydroxyl groups on GO sheets and PVA chains through intermolecular acetalization. The GAs that are produced have favorable elasticity and mechanical integrity [93]. Worsley et al. used resorcinol and formaldehyde as organic cross-linking agents. As a result, thermally reduced, cross-linking carbon-based agents were formed in the GA rubber matrix [94]. Such a sol-gel chemistry approach, providing the mechanism for supplying optional chemical bonding, has made it possible to help control the bulk properties of graphene-based composites to obtain better mechanical stability and better bulk material properties.

The direct synthesis process permits accurate control of the pore size, density, and distribution within 3D structures; however, it involves a comparatively elevated manufacturing cost. Conversely, the solution-based synthesis approach presents several benefits, including cost-effectiveness, an enhanced production yield, scalability, and elemental functionalization [95].

Three-dimensional GBCMs are created to deal with the colloidal stability of two-dimensional (2D) graphene sheets in water, which restricts their recovery rate after decontamination [96]. Three-dimensional GBCMs are produced by self-assembling 2D graphene-based components characterized by a remarkable surface area and distinctive chemical properties, employing a deliberate design approach and using 3D materials that exhibit exceptional characteristics and exclusive architectures [97]. These materials, owing to their numerous advantages, are emerging as strong contenders in a range of applications, showcasing promising performance levels that distinguish them from conventional activated carbons, bio-chars, and hydro-chars [98]. The production of these 3D materials typically necessitates intricate and time-intensive procedures, posing a significant barrier to their widespread utilization. In contrast, incorporating graphene sheets into 3D GBCMs is comparatively straightforward, thanks to the presence of interplanar  $\pi$ - $\pi$  interactions and van der Waals forces [99]. As a result, the synthesis and utilization of 3D GBCMs

have received substantial attention and research focus in recent years. GO is the primary precursor used in the 3D stacking of 2D graphene nanomaterials [100].

The primary factor propelling GO nanosheets toward the formation of 3D structures is their organized liquid crystalline alignment in aqueous environments at low concentrations of even 0.1 mg/mL [101]. When GO is stably suspended and dispersed, it possesses the capability to undergo self-assembly into lightweight and highly porous sponges through various methods, including spinning into fibers, cross-linking with GO beads, membrane pressing, spraying to generate 3D particles, and even chemically depositing onto templates to produce foams using procedures like hydrothermal processes or CVD [102]. Light-based 3D printing has enabled the fabrication of complex graphene aerogels with fine spatial features and pore sizes as small as 10 microns and 60 nm, respectively (Figure 2) [103]. This technique overcomes the limitations of traditional methods, allowing for the fabrication of intricate structures that enhance the properties of graphene foam, even at low densities. By improving their mechanical stability through the use of micro-architectures, these aerogels offer broad application potential in areas like catalysis, separation, thermal conductivity, and fluid flow management. These synthesis methods offer relative simplicity and the potential for scalability in commercial use. The porosity and surface area of the resultant macrostructure can potentially be straightforwardly and precisely controlled, making it ideal for a variety of applications [40]. The self-assembly of 2D GO into 3D GBCMs has found applications in diverse fields, including air and water purification [41,104], batteries [105], supercapacitors [106], and sensors [60]. Of particular note is its uses in water remediation. Three-dimensional materials (3DMs) exhibit promise in various wastewater treatment technologies, such as deionization [107], adsorption [108], solar desalination [109,110], catalysis [111,112], and advanced oxidation processes [113].

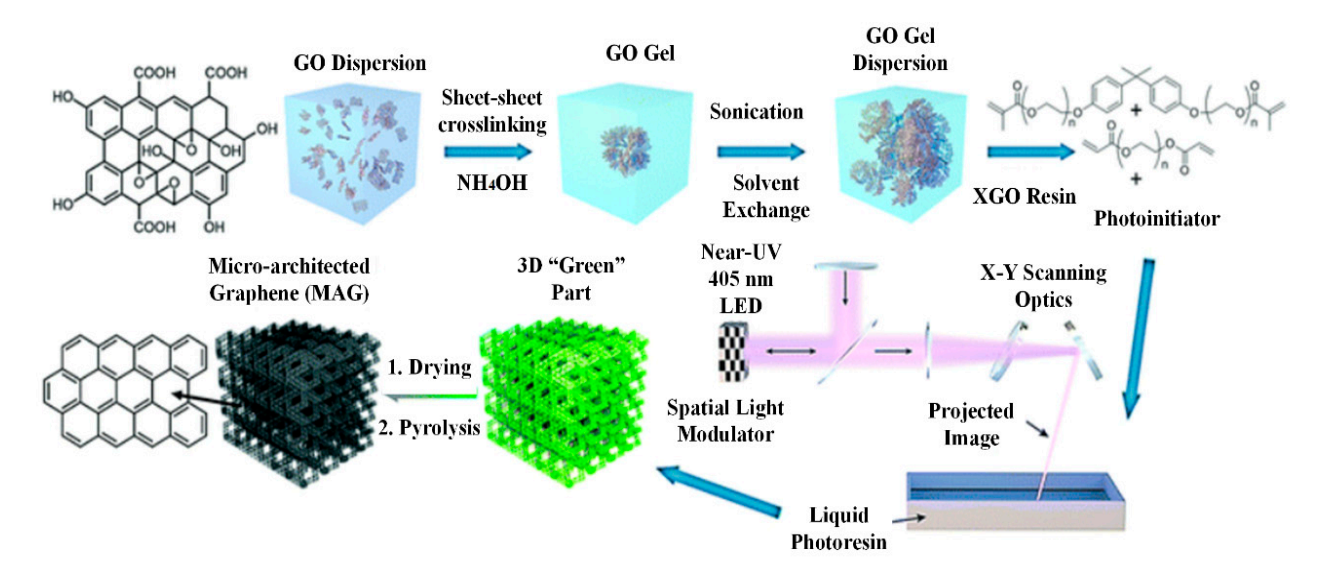


Figure 2. A light-based 3D printing process to create hierarchical graphene structures [103].

# 5. Structural Properties

Specifically, graphene-based adsorbents, especially 3D GBMs, have exhibited great interaction in the performance of pollutant removal due to their large specific surface areas and rich porosity. The developed materials efficiently absorb heavy metals, dyes, salts, and even broad ranges of organic pollutants like oils or pharmaceuticals [114]. Such unique structural features of 3D GBMs not only enhance their adsorption capacity but also render their easily separable from water during practical operations, thus making this kind of material an ideal choice for pollutant treatment. In most of the adsorption processes, the effectiveness of a 3D GBM is driven by its porosity [40]. This porosity

is influenced to a great extent by various factors such as the particle size, morphology, functional groups, and synthesis methods of the material. All of these factors can be controlled in order to fine-tune the performance of an adsorbent to effectively counter diversified environmental challenges.

#### 5.1. Role of Porosity

The effectiveness of wastewater pollutant removal is connected to the structural properties of the materials used. Important factors in this process are the surface area and the existence of active sites on these materials. The study of the particle size, pore size, and structure distribution of a porous material is also necessary as they have an inverse relation to the surface area and are directly associated with interconnectivity. This relationship is grounded in scientific principles. The interval of time that a material is in contact with wastewater contaminants directly affects its surface area [115]. Larger surface areas provide more opportunities for pollutants to come into contact with the material's active sites, thereby enhancing the pollutant removal capacity [116].

The presence of active sites, such as functional groups or specific chemical essentials, facilitates chemical interactions and adsorption processes, allowing pollutants to effectively bind to the material [117]. As such, binding is frequently the initial step in the process of cleaning wastewater of contaminants. Now, the pore structure and size are inversely related to surface area. Smaller pores generally result in a larger internal surface area, creating more internal surfaces for interaction with pollutants. This is due to the high surface-to-volume ratio inherent to smaller pore sizes [118,119]. Conversely, larger pores may have a smaller internal surface area, but they can accommodate larger pollutant molecules. Moreover, pore interconnectivity is vital. Well-connected pores ensure that pollutants can access the inner surfaces of the material effectively, further improving the material's pollutant removal efficiency [120]. Surface-functionalized 3D GBCMs showed strong adsorption interactions such as  $\pi$ - $\pi$  interaction, electrostatic interaction, hydrogen bonding interaction, and hydrophobic interactions with contaminants in water [121].

The intricate balance of the surface area and interconnectivity of pores is maintained by creating a multi-level pore system with both large and small pores that are intricately interconnected throughout the material's macrostructure [122]. Eliciting hierarchical porosity through the integration of micropores, mesopores, and macropores has become an important strategy in enhancing the adsorption performance of materials. In this regard, Jihun et al. proposed a hierarchical porous structure that effectively enhanced the adsorption ability of a material with three-level, micro-, meso-, and macro-porous 3D graphene. MMM-3DG exhibits a high surface area of 1492.8 m<sup>2</sup>/g and a substantial pore volume of 5.1198 cm<sup>3</sup>/g. MMM-3DG was prepared by a hard-template method using fumed silica as described schematically in Figure 3a. An  $8 \times 8$  cm<sup>2</sup> CDI electrode was fabricated using active MMM-3DG, which explains that MMM-3DG could be a suitable material for CDI with the capability to be mass produced. MMM-3DG exhibits a high adsorption rate constant value in comparison to activated carbon, and this result can be explained by the schematic in Figure 3b, which compares the ion transport paths based on the porosities of MMM-3DG and activated carbon. Figure 3c,d belongs to the domain of the pseudo-second-order kinetic model, which describes the electrosorption behaviors of activated carbon; the R<sup>2</sup> values obtained with the pseudo-first-order kinetic model were still surpassed by the MMM-3DG. The adsorption rate constants for activated carbon and MMM-3DG, according to the pseudo-second-order kinetic model, are 0.01350 and 0.07146, respectively. In the case of an MMM-3DG electrode in a 100 mg/L NaCl solution, it was found that the electrosorption capacity could reach up to 9.37 mg/g, which is excellent compared to the commercially available activated carbon, which has a capacity 9.25 mg/g. This effective ion transport

makes it even more energy-efficient, as only 33.17 kJ/mol was needed to desalinate the ions using MMM-3DG, compared to the 47.24 kJ/mol required for the same using activated carbon. Such hierarchic porosity, apart from enhancing the material's adsorption capacity and rate, improved other structural properties such as its electrical conductivity, wherein MMM-3DG performed with a better conductivity of 11.36 S/m compared to the activated carbon, which exhibited an electrical conductivity of 8.11 S/m. In turn, a well-balanced pore size combination in MMM-3DG leads to both mechanical stability and good surface chemistry, which enables fast and efficient ion removal in CDI applications [123].

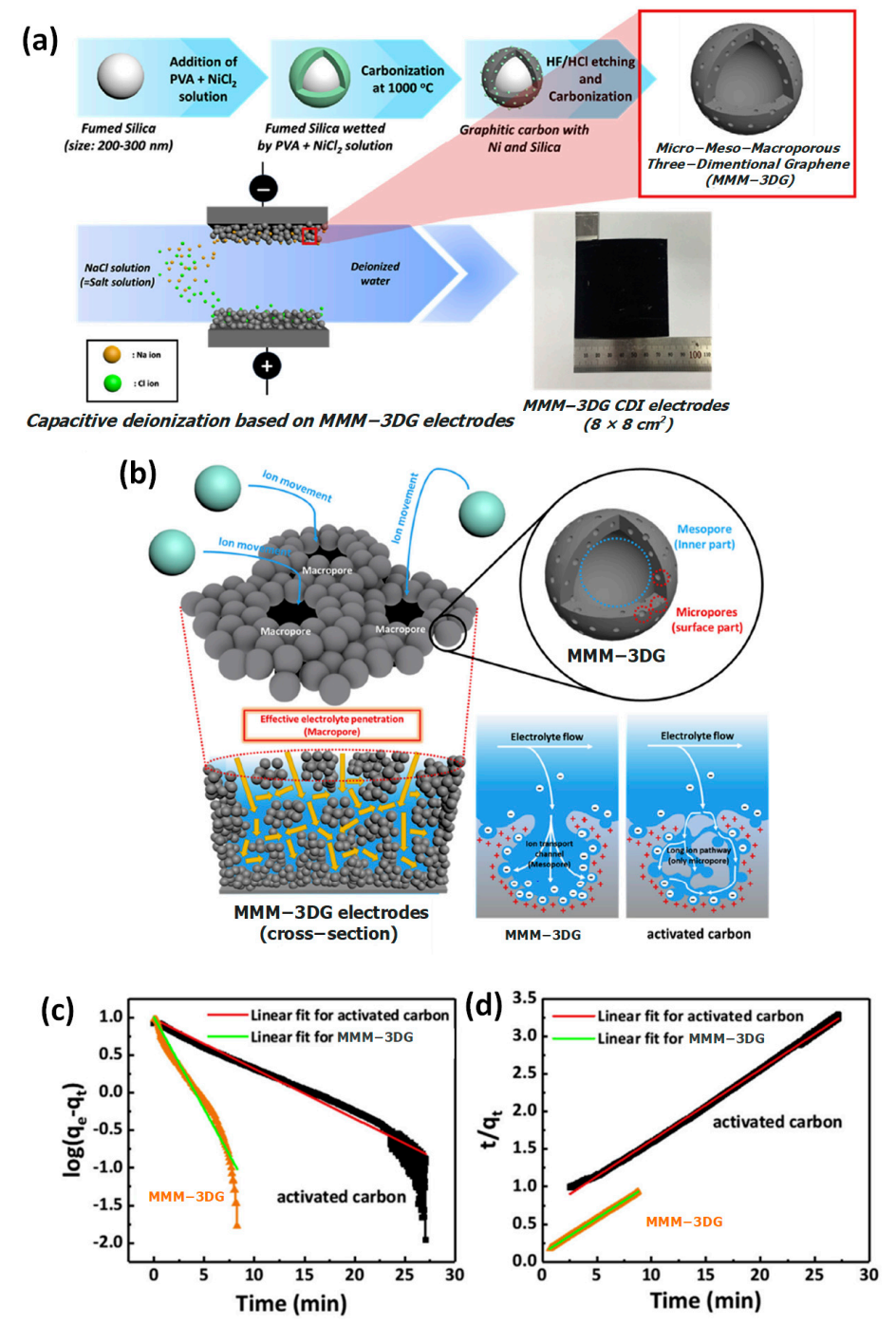


**Figure 3.** (a) Scheme representing MMM—3DG fabrication process and application to CDI, (b) scheme of the ion transport in the MMM—3DG electrode, linear fittings of electrosorption behaviors of NaCl by activated carbon and MMM—3DG electrodes according to kinetic models: (c) pseudo-first-order model and (d) pseudo-second-order model [123].

The dependency of the adsorption on the porosity is mainly attributed to the roles played by different pore sizes: whereas micropores provide a high surface area for adsorption, mesopores improve ion transport to the micropores, while macropores ensure accessibility and reduce diffusion paths. By introducing a hierarchical pore structure, a sacrificial template (e.g., polystyrene, cellulose fibers, polyvinyl alcohol, and silica nanoparticles) [124,125] or secondary material (e.g., inorganic salts, surfactants, metal nanoparticles, and activated carbon) [126,127] is incorporated during synthesis. These templates, essential for pore development, are subsequently removed using techniques like chemical etching [128], thermal treatment [129], and physical extraction [130], leaving behind voids and channels within the GO materials. Optionally, the resulting structure can undergo further functionalization, such as the addition of other materials, doping, or surface treatment, to customize its properties for specific applications, especially for the treatment polluted water through adsorption. Table 2 exhibits that pores are essential, as they help transfer molecules and ions to various pollutants during the adsorption process. Certain factors affect the porosity of the 3D GBM, and these are described in this review paper.

**Table 2.** Surface properties of 3D GBCMs.

3D GBM	Synthesis Route	Morphology	Pore Size Structure	Specific Surface Area (m <sup>2</sup> g <sup>-1</sup> )	Application Performance	References
3D COF/rGO	Hydrothermal method	3D sponge-like structure	Mesoporous	246	Higher adsorption capacity (98–240 g/g) towards organic solvents.	[131]
3D CF/N-RGO	Self-assembly method	Yarn-like structure	Mesoporous (3.716 nm)	329.6	Excellent superhydrophobicity and adsorption capacity (206.38 g/g).	[132]
3D TGAs-1	Hydrothermal method	Honeycomb- like 3D structures	Mesoporous	225.3	Remarkable 90% photocatalytic activity towards methylene blue.	[133]
3D GO-SS	Hydrothermal method	Curved or wrinkled surface	Micro-porous (1.78 nm)	303.5398	High adsorption capacities for metal ions (Pb(II) 108.68 mg/g, Cu(II) 32.12 mg/g, Cd(II) 46.28 mg/g, Yb(III) 41.76 mg/g and Nd(III) 38.168 mg/g).	[134]
3D MSG-1	Hydrothermal method	Flower-like structure	Mesoporous (21.283 nm)	28.746	CDI performance with a maximum desalination capacity of 16.82 mg/g at 1.0 V in 200 mg/L NaCl solution.	[135]
GO/Fe <sub>3</sub> O <sub>4</sub> / OPO <sub>3</sub> H <sub>2</sub> / PCN-222	Co- precipitation and pyrolysis methods	Spheres decorated rod like structures	Mesoporous	1350	Maximum adsorption capacity of uranium(VI) 416.7 mg/g in water	[136]

#### 5.2. Particle Size

Understanding the effect of the size of 3D GO nanosheets on their adsorption performance is very critical in designing highly effective GBAs for environmental cleanup. By controlling the sizes of 3D GO nanosheets, researchers could design adsorbents with their desired adsorption rates and capacities suitable for different scenarios of environmental remediation [137]. Shen et al. determined the effect of the particle size of 3D GO nanosheets by confirming the construction and adsorption efficiency of 3D GBCMs. The research found that the larger 3D GO nanosheets (~100  $\mu m$ ) are more porous, having a specific surface area of about 87.2  $m^2/g$ , than the smaller nanosheets (~5  $\mu m$  and ~30  $\mu m$ ), which have specific surface areas of about 50.2, 35.6  $m^2/g$ . The reason for this is that, with the increase in the size of the nanosheets, there will be reduced stacking accompanied by increased spacing between layers, hence increasing the overall porosity. The size of the 3D

GO nanosheets showed a proportional relation to the adsorption rate of pollutants. For example, the 3D GBCMs with the largest GO nanosheets had the highest adsorption rate for methylene blue and cadmium ions during the experiment; the values were found to be around 833.33 mg/g min<sup>-1</sup> for methylene blue and 500 mg/g min<sup>-1</sup> for Cd<sup>2+</sup> [138]. Larger nanosheets can provide more active sites and interspaces, thus increasing their adsorption capacities for pollutants.

The lateral sizes of GO nanosheets have a significant impact on the porosities of 3D graphene aerogels (GAs), which in turn affects their performance as electrocatalysts for CO<sub>2</sub> reduction reactions (CRRs). In the study by Shen et al., it was observed that GAs constructed from larger GO nanosheets (14  $\mu m$ ) resulted in structures with large pores and a low surface area (15  $m^2/g$ ). Conversely, smaller GO nanosheets (1.5  $\mu m$ ) produced GAs with thicker walls and isolated pores, leading to a higher surface area (45  $m^2/g$ ) but poor mass transfer properties for CO<sub>2</sub>. The most effective porosity was achieved with medium-sized GO nanosheets (5  $\mu m$ ), which formed GAs with a hierarchical porous network and the highest surface area (98  $m^2/g$ ). This structure enhanced both the adsorption and diffusion of CO<sub>2</sub> molecules, resulting in superior Faradaic efficiency (FE) for CO (FECO = 81%) and a favorable CO/H<sub>2</sub> ratio at -0.82 V versus RHE [139]. Thus, the size of the GO nanosheets used directly influences the pore structure, surface area, and overall effectiveness of 3D GBCMs in practical applications.

# 5.3. Morphology

The arrangement and size distribution of pores within a material are crucial to the process of adsorption. A well-developed porous network allows easier access of adsorbate molecules to the interior surfaces of the adsorbent. The morphology of the material determines the accessibility of its adsorptive sites, and the use of materials with hierarchical or interconnected pore structures ensures that adsorbates can quickly reach the adsorption sites, thereby improving the material's adsorption kinetics [140]. Specific surface characteristics, such as roughness and the presence of functional groups, influence the interaction mechanisms (e.g., van der Waals forces, hydrogen bonding, electrostatic interactions) between the adsorbent and adsorbate.

The morphologies of 3D graphene spheres play a crucial role in determining their physical, chemical, and electrochemical properties, which in turn affect their suitability for various applications. Haghighi Poudeh et al. demonstrated that controlled synthesis methods, such as core-shell electrospinning/electrospraying, can tailor the morphologies of graphene-based structures into forms like fibers, spheres, and foams by adjusting the polymer concentration, molecular weight, and applied voltage (Figure 4a–m). The morphology affects the electrochemical performance of the material, with Pt-decorated 3D graphene spheres showing the highest specific capacitance (118 F/g) due to their uniform decoration of small Pt nanoparticles, which enhance the spheres' electrochemical activity [141].

Tao et al. showed that the morphology of GO-MMT/SA aerogel beads results in a 3D porous network. This structure, formed through cross-linking and hydrogen bonding among GO, MMT, and SA, significantly enhances the material's porosity and specific surface area. The introduction of MMT increases the thickness of the spherical walls and improves the pore structure, leading to a higher specific surface area and more active sites for adsorption. Specifically, the introduction of MMT into the aerogel beads increases the specific surface area from  $85.18 \text{ m}^2/\text{g}$  to  $266.30 \text{ m}^2/\text{g}$  [142]. This increase in surface area is due to the improved pore architecture and porosity resulting from the material's morphology. This interconnectivity is crucial for maximizing the utilization of the entire surface of the adsorbent for adsorption. Wu et al. presented a graphene oxide/alkali lignin (GO-AL) aerogel composite with a 3D porous structure formed by the layer-by-

layer assembly of GO and AL. The overlapping GO slices create a layered structure in the GO-AL aerogel, resulting in a significantly larger surface area (41.5 m<sup>2</sup>/g) compared to that of GO alone (24.8 m<sup>2</sup>/g). SEM images reveal the rough and wrinkled surface of the GO-AL aerogel, indicating a high degree of porosity. This morphology is responsible for providing a large specific surface area and numerous active sites for adsorption. The maximum adsorption capacity of methylene blue on the GO-AL aerogel was 1185.98 mg/g at 303 K. The primary adsorption mechanisms of this material are hydrogen bonding and  $\pi$ - $\pi$  interactions, rather than electrostatic attractions [143]. This increase in surface area is attributed to the improved pore architecture and morphology of the aerogel, which enhance its adsorption capacity.

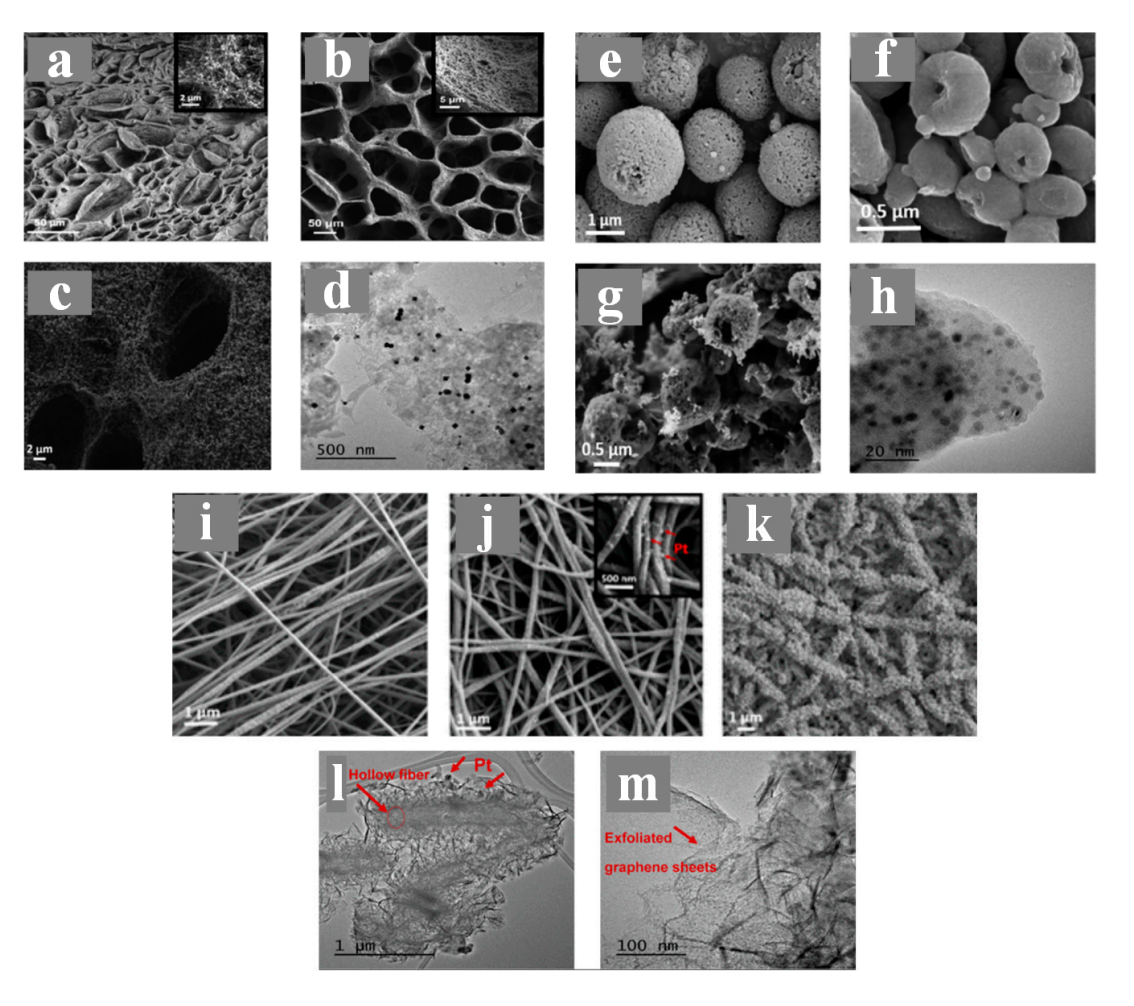


**Figure 4.** The SEM images illustrate various stages of Pt-decorated graphene-based materials: (a) electrosprayed, (b) reduced, and (c) carbonized foam, along with (d) TEM image showcasing the Pt-decorated foam at a finer scale. Additionally, SEM images depict (i) electrospun, (j) reduced, and (k) carbonized Pt-decorated graphene-based fibers, accompanied by (l,m) TEM images at different magnifications to highlight the Pt distribution within the fibers. Furthermore, the sequence includes SEM images of (e) electrosprayed, (f) reduced, and (g) carbonized Pt-decorated graphene-based spheres, with (h) a TEM image providing a detailed view of the Pt-decorated spheres [141].

## 6. Mechanisms Employed by 3D GBCMs in Wastewater Treatment

Rapid urbanization causes considerable wastewater production from industries such as the manufacturing, mining, and power generation unit [144,145] industries, which release pollutants such as heavy metals [146], dyes [147], particulate matter [148], and other toxins that carry substantial health and environmental threats. Industrial pollution is threatening water bodies and deteriorating the quality of air and soil by releasing active

sulfur nitrogen oxides [149] and other volatile organic compounds [150]. The resulting contamination can disrupt the balance of the ecosystem, leading to the loss of biodiversity and habitat degradation [151,152]. This review explores the diverse applications of 3D graphene within the realm of water remediation, providing insights into the intricate mechanisms that underlie its efficacy in purifying water sources. From the removal of heavy metal ions to the degradation of organic pollutants, the potential of 3D graphene materials in probing the rejuvenation of water resources presents a promising and transformative frontier.

#### 6.1. Adsorption

Adsorption is an efficient, simple, and versatile technique for treating wastewater containing hazardous contaminants [153]. Of the various treatment methods available, adsorption is the most energy-efficient, cost-effective, relatively simple in design, easy to operate, and available for application [154]. Solid materials, known as adsorbents, work as sponges to adsorb and immobilize the pollutants in wastewater streams. This process has all the specificity and selectivity needed to effectively remove contaminates such as heavy metals, dyes, organic compounds, and microplastics [155]. Adsorption comprises two fundamental mechanisms: chemisorption (including chemical coordination, ion exchange, and complexation) and physisorption (including electrostatic interaction, van der Waals, hydrogen bond, and  $\pi$ - $\pi$  interactions) [156]. By selecting suitable adsorbent materials, synthetic drugs and industrial dyes can be removed from the environment simply and effectively [157]. One innovative approach to promoting the adsorption process's efficiency and practical applicability is to use GBCMs, especially 3D macroscopic devices [158]. Of them, 3D graphene aerogels have been proven as the adsorbents with the most potential for water purification owing to their unique properties, such as their high specific surface area, low density, large pore volume, and high porosity. These factors lead to their remarkable adsorption efficiencies and environmental applicability.

Khan et al. reported a significant advance in this area comprising the design of a graphene sand hybrid (D-GSH) derived from the pyrolysis of date syrup, a sustainable, one-step route method (Figure 5a) [159]. The D-GSH showed an excellent absorption capability when tested in a batch mode, with maximum adsorption capacities of 2564 mg/g (MV), 781 mg/g (Pb<sup>2+</sup>), and 793 mg/g (Cd<sup>2+</sup>) at 25 °C; among the tested heavy metals, the D-GSH also had a high absorption capacity (333 mg/g) toward Congo red. Kinetic studies have shown that the adsorptions of MV and CR were fast, occurring within about 0.5 and 2 h, respectively (Figure 5c,d). At the same time, the isotherm and thermodynamic analyses indicated that the material's high efficiency of adsorption is due to its strong electrostatic interactions and hydrophobic effects (Figure 5b). Furthermore, in studies using multi-component systems, 99.87% of Pb<sup>2+</sup>, 99.62% of Cd<sup>2+</sup>, 97.35% of Zn<sup>2+</sup>, and 95.38% of Cu<sup>2+</sup> was removed by the D-GSH (Figure 5e) [159]. These results highlight its versatility in tackling multidimensional wastewater issues that involve multiple pollutants in the same system [160].

The hierarchical porous structures and design of 3D GBCMs considerably promote their adaptability through fast mass transport and convenient processing. They effectively target adsorption because of their inherent hydrophobic characteristics and large  $\pi$ -conjugated system that facilitates molecular interaction with aromatic organic pollutants [161]. They are also macroscopic, mechanically rigid, and easily recoverable for reuse, which solves some major bottlenecks that exist for real-world wastewater treatment applications. In addition to adsorption, coupling adsorption with photocatalytic degradation is another efficient approach for removing dyes. It takes advantage of the highly adsorbent properties of 3D graphene aerogels and the photocatalytic activities of transition metal-based materials (like MnO<sub>2</sub>, TiO<sub>2</sub>, ZnO, and CdS) [162]. For example, Mei et al. produced

GA-ZnO hybrids by embedding ZnO nanoparticles on graphene aerogel, resulting in the removal methylene blue at 94.2% adsorptive efficiency and 97.6% total dye removal efficiency [163]. Additionally, Liu et al. developed Bi<sub>2</sub>MoO<sub>6</sub>/reduced graphene oxide aerogel (BMO/GA) composites for MB removal, the performance of which was 2.1 times higher than that of pure BMO, which removed 98.3% within 100 min [164]. The results further illustrate the synergistic roles of graphene aerogels and photocatalysts in the adsorption and photocatalytic degradation of dye pollutants. These properties, when combined, render 3D GBCMs scalable and sustainable solutions for environmental remediation with great promise for field applications.

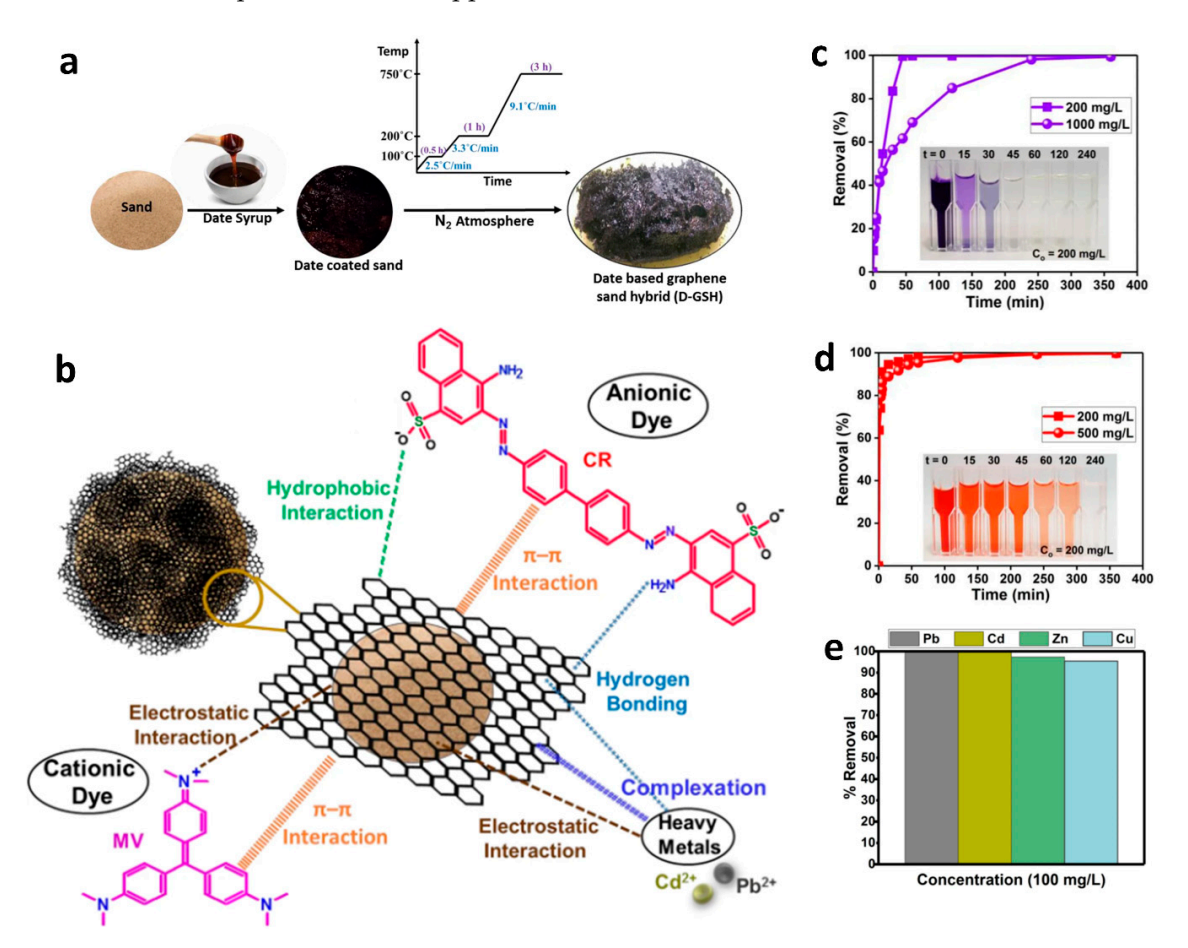


**Figure 5.** (a) Method for producing a graphene sand hybrid using date syrup as a carbon source, (b,c) analysis of how varying contact time influences the adsorption efficiency of methyl violet and Congo red onto D-GSH, (d) D-GSH's effectiveness in adsorbing heavy metals, specifically  $Pb^{2+}$ ,  $Cd^{2+}$ ,  $Zn^{2+}$ , and  $Cu^{2+}$  ions, (e) proposed adsorption mechanism of D-GSH for cationic and anionic contaminants [159].

# 6.2. Catalysis

Photocatalytic degradation is a key technology within advanced oxidation processes (AOPs) for breaking down organic pollutants [165]. During this process, organic contaminants are decomposed by reactive species like hydroxyl radicals (HO●) and photogenerated holes (h⁺). These reactive species are produced through a series of steps involving the interaction of a photocatalyst, an energetic light source, and an oxidizing agent such as oxygen or air. This method has proven to be highly effective in addressing various environmental pollutants [166]. Graphene-based nanomaterials (GBNs) have exhibited exceptional results in their use in heterogeneous photocatalysis [163] and Fenton-like reactions [167] for pollutant removal, holding promise for advanced water treatment applications. Nonetheless, there are two key impediments to their direct use in water treatment. Firstly, graphene nanosheets

tend to agglomerate due to strong  $\pi$ - $\pi$  interactions between adjacent layers [168]. Secondly, recycling GBNs at the nanoscale presents challenges, and the potential environmental hazards of their release raise concerns regarding human health [169].

Developing monolithic graphene materials that have a 3D cross-linked structure, in particular 3D gels such as aerogels and hydrogels [170], presents a promising approach to mitigating the limitations associated with the large-scale application of graphene [171]. Recent research has developed spent N-doped graphene oxide (SNGO) for environmental remediation, focusing on the catalytic degradation of organic pollutants. Using a modified Hummers method, GO and a variant derived from spent graphite (SG), spent graphene oxide (SGO), were synthesized and N-doped via hydrothermal treatment with NH<sub>3</sub>·H<sub>2</sub>O (Figure 6a), and corresponding SEM images of SG, SGO, and SNGO-x, respectively, were obtained (Figure 6b–d). Among the variants, SNGO-2 demonstrated exceptional reactivity in activating peroxymonosulfate (PMS), leading to near-complete (~100%) Rhodamine B degradation within 60 min and a 60% reduction in the total organic carbon (TOC) within 40 min (Figure 6e). XRD confirmed the stability of the crystal structure, despite the SEM images showing some morphological damage (Figure 6f). The SNGO-2/PMS system effectively removes Rhodamine B through a multifaceted mechanism involving singlet oxygen production, free radical generation, and electron transfer, all enhanced by nitrogen doping in the catalyst (Figure 6g). The catalyst's strong performance is attributed to the synergistic effects of the nitrogen dopants and structural defects, with singlet oxygen (<sup>1</sup>O<sub>2</sub>) being the key reactive species, underscoring SNGO-2's potential as an effective and durable catalyst for environmental remediation [172]. Three-dimensional networked graphene gels possess a massive framework structure consisting of linked micro-/nano-sheets. In contrast to the 2D films, these gels have a multi-porous system that extends over the micro, meso, and macro scales. This hierarchical porous structure found in 3D GBGs functions as an ideal scaffold, preventing the aggregation or stacking of graphene subunits and consequently maintaining high structural stability. Furthermore, it enhances the exposure of active sites to photocatalytic reactions [173].

## 6.3. Capacitive Deionization

GBMs, including 3D graphene, have become promising candidates in water deionization to remove ions (cations and anions) and thus obtain deionized or purified water [174]. GBMs are used in the reversible adsorption of ions to the surface of porous electrodes under an applied voltage in a CDI process due to their high surface area and electrical conductivity. When the electrodes reach saturation, a reverse in the voltage regenerates the electrodes by releasing the ions again, yielding deionized water [175]. A more sophisticated system, MCDI, adds ion-selective membranes interposed between the electrodes to enhance the separation efficiency of the ions drawn from the feed water from the electrodes under the influence of a given voltage [176]. The performance of CDI is closely correlated with the type of electrodes utilized, and the ideal electrodes are characterized by a high specific surface area, high conductivity, good wettability, and an interconnected porous structure [177].

Three-dimensional GBMs such as graphene aerogels, GO aerogels, and GBCMs have been investigated for use in CDI and MCDI systems [178,179]. These materials are typically combined with porous scaffolds, carbon nanotubes, or activated carbon to form highly porous 3D structures that effectively improve their ion adsorption [180] and electronic conductivity [181]. In the first study that used GAs as electrodes for CDI, Wang et al. achieved a sorption capacity of 5.39 mg/g for NaCl at 2.0 V [182], and strategies for further improvement of the performance of GAs and GHs have since been proposed, including increasing the surface areas of GAs and GHs or blending them with metal oxides. Finally,

J. Compos. Sci. 2025, 9, 18 21 of 53

3D holey graphene hydrogel (GH) electrodes with plenty of in-plane pores were constructed for NaCl electrosorption. These electrodes were prepared by compressing the 3D holey GH onto a graphite film. It was easily observed that the as-prepared electrodes delivered a high electrosorptive capacity of 17.1 mg/g at 1.6 V due to their large specific surface area (445 m²/g) and abundant pores that accelerated the transfer of ions [183]. The use of 3D graphene-based asymmetric electrodes in CDI for the selective separation and recovery of heavy metals and salty ions from wastewater is important. One innovative design used a hydrothermal method with subsequent freeze-drying drop casting onto a carbon fiber paper (CFP) substrate, utilizing CFP/3DG/MnO<sub>2</sub> as the cathode and CFP/3DG/NiO as the anode. The 3D graphene structure significantly enhances the conductivity and surface area of electrodes, while MnO<sub>2</sub> and NiO nanoparticles improve their porosity and deionization capacitance. The distinct isoelectric points of MnO<sub>2</sub> and NiO optimize the adsorption of cations and anions in brackish water. One CDI cell showed a desalination capacity of 21.01 mg/g at 1.2 V and a good regeneration electrochemical performance, indicating a real potential application for CDI cells in the treatment of brackish water (Figure 7c) [184].

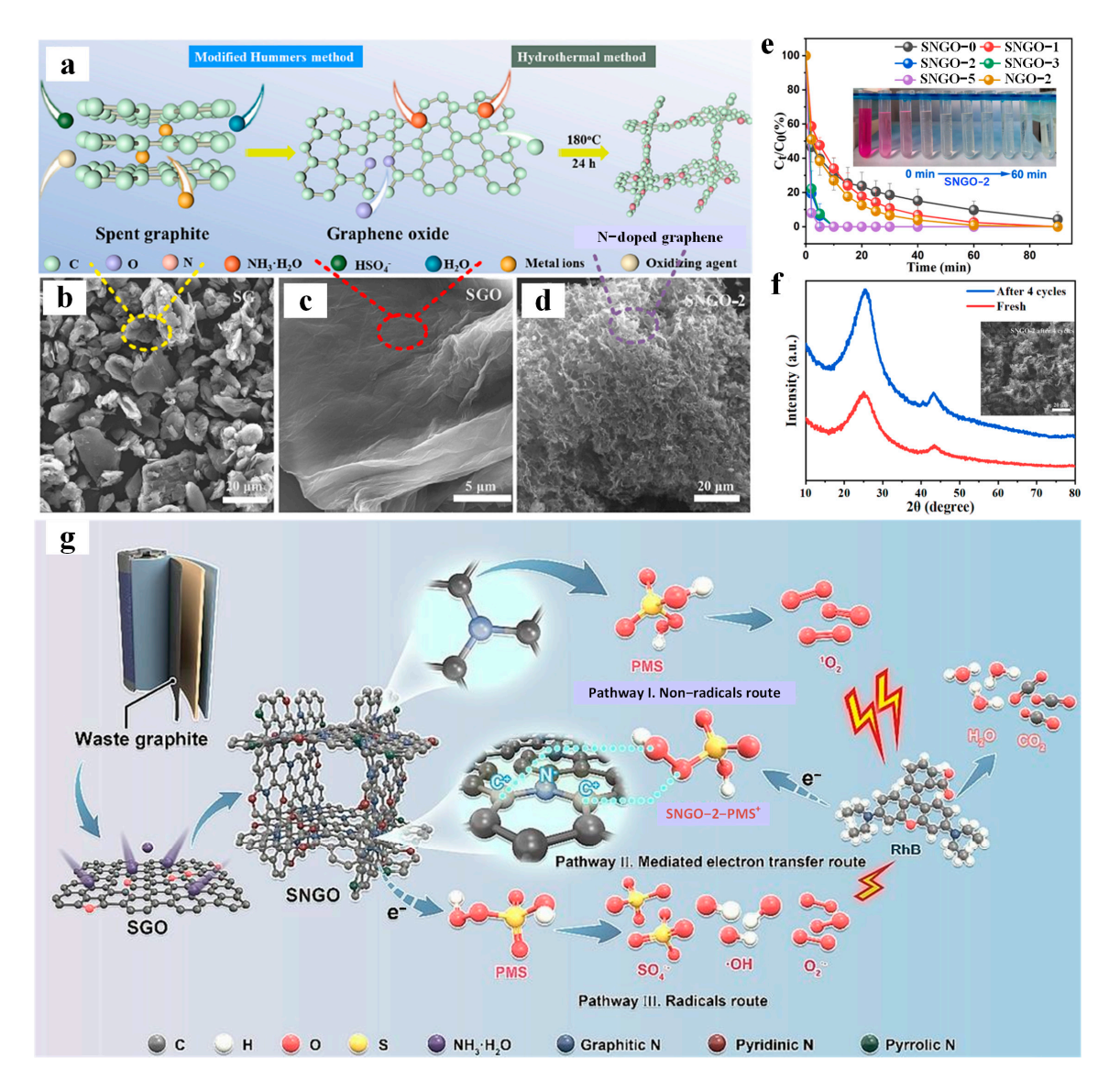


**Figure 6.** (a) Synthesis of N—doped graphene, SEM images of (b) spent graphite, (c) spent graphene oxide, (d) spent N—doped graphene oxide—2, (e) efficiencies of different SNGO—x systems for Rhodamine B removal, (f) XRD and SEM images after four cycles. (g) The proposed mechanism of peroxymonosulfate (PMS) activation and the subsequent oxidation of Rhodamine B by SNGO—2 [172].

J. Compos. Sci. 2025, 9, 18 22 of 53

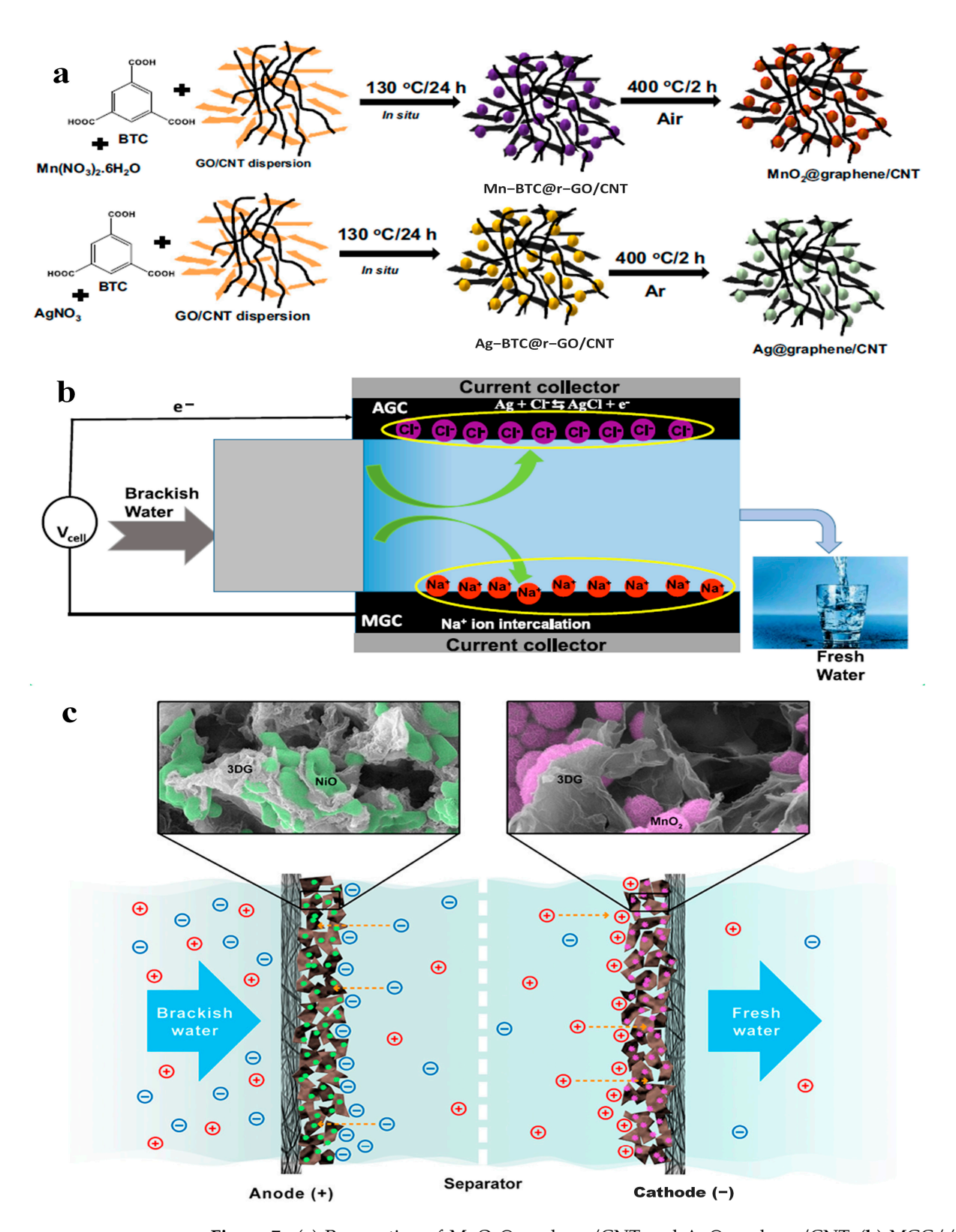


**Figure 7.** (a) Preparation of MnO<sub>2</sub>@graphene/CNT and Ag@graphene/CNT, (b) MGC//AGC electrode-based pseudocapacitive deionization system [185], (c) CFP/3DG/NiO | CFP/3DG/MnO<sub>2</sub>-based ion removal behaviour of CDI systems [184].

Recent progress in CDI has been made using 3D GBCMs, which have also been successfully applied in asymmetric pseudocapacitive deionization (PCDI) systems. Rangaraj et al. synthesized  $MnO_2$  and Ag-doped graphene/CNT composite redox-active electrodes via a simple two-step method (Figure 7a). An MGC cathode and an AGC-anode enabled the

formation of a 3D MnO<sub>2</sub>@graphene/CNT (MGC) and Ag@graphene/CNT (AGC) valve, which showed high specific capacitances and an enhanced dual-ion capture mechanism. The salt adsorption capacity of this system was 62.4 mg/g and its charge efficiency was 95% in 1000 ppm NaCl solution with a voltage of 1.2 V (Figure 7b), which was also attributable to the utilization of redox-active MnO<sub>2</sub> combined with the conductive graphene/CNT structure, demonstrating an effective desalination capability and a potential method for further development of CDI [185].

Another contentious subject is the coupling of GBMs with transition metal oxides or carbon nanotubes. The exact reason for the resulting higher adsorption capacities, potentially involving the effect of the pore size distribution and electrode conductivity, is still unclear, and the discrepancies in the performance metrics reported in the literature can typically be attributed to different experimental setups and operational conditions. While most studies to date have centered on the electrosorption of NaCl, CDI has considerable promise for the removal of heavy metal ions and radionuclides from water. Considering that 3D GBCMs have been shown to be effective at adsorbing such contaminants, thus enabling their application as CDI electrodes for water purification, may create more avenues for the development of advanced environmental remediation technologies.

The key advantages of CDI and MCDI include their energy efficiency, low maintenance requirements, and ability to remove a wide range of ions, including ions that are challenging to remove through conventional methods. They are used in applications such as producing high-purity water, desalination, and removing contaminants from industrial wastewater. CDI and MCDI are often considered promising technology for sustainable and cost-effective water treatment, particularly in areas where access to fresh water is limited or where traditional purification methods are energy-intensive [186].

#### 6.4. Solar Desalination

Solar desalination, powered solely by clean, renewable, and abundant sun energy, has recently emerged as a means to provide a sustainable solution to the global crisis of freshwater scarcity [187]. The performance of this category of solar-driven interfacial desalination systems is heavily dependent on the type of photothermal materials used therein, which should ideally possess a wide-spectrum absorption for solar radiation and high efficiency in converting this radiation into heat. This heat is then localized in the system, assisted by a thermal insulation layer that reduces heat loss. At the same time, water transfer channels guarantee a constant water supply to the evaporative surface, improving the overall system efficiency [188]. The photothermal material, or solar absorber, is these systems' most important component. The ideal materials for this component should have a capacity for high solar absorption, a high photothermal conversion efficiency, adequate porosity, and be scalable [189]. Three-dimensional GBCMs have emerged as one of the most promising candidates, as they can provide practical advantages like a larger evaporation surface area, which gives the evaporator multiple evaporative interfaces per small area, enhancing the overall desalination efficiency [190].

For example, Li et al. developed a low-cost lamella network of graphene/cellulose nanocrystals (CNCs) (GCLNs) with melamine foam (MF) as the matrix. Relying on the light-absorption capability of graphene and the hydrophilalaoprotein of CNCs, a 3D GCLN system was created which achieved an evaporation rate of 1.66 kg m<sup>-2</sup> h<sup>-1</sup> at 97.5% efficiency under sunlight. The durability of the design enables its operation under harsh conditions. It can be easily adapted for basic performance enhancement, making it a scalable and low-cost solution, which is particularly advantageous in remote regions where conventional water treatment methods are limited [110]. Further, super elastic 3D clay/graphene aerogels (CGAs) were prepared based on a commercial foam, exhibiting

50% decrease in graphene consumption while preserving a strong solvent absorption ability. The salt collection-aided 3D hydrophilic CGA device displayed a high solar desalinization evaporation rate of  $4.11 \text{ kg m}^{-2} \text{ h}^{-1}$  and a remarkable salt resistance. It can operate for 36 h in 20 wt% brine without salt accretion. This design allows for a simple collection of salt, representing a breakthrough in solar desalination and solvent adsorption [191]. Meanwhile, a 3D Ag-doped rGO network is being synthesized to allow for more efficient photothermic applications. In experiments, this material had a photothermal conversion efficiency of 97.54% and produced a water evaporation rate of 1.40 kg m<sup>-2</sup> h<sup>-1</sup> under simulated sunlight and 1.50 kg m<sup>-2</sup> h<sup>-1</sup> in the real world. Even after 54 h of operation, the system lacked salt accumulation, demonstrating its effectiveness and potential for salt-free, long-term solar desalination systems [192].

While great strides have been made, solar desalination systems still struggle with issues like lost heat, dead-end water transport, and internal salt accumulation. Yet, new ideas keep coming up. For instance, Wang et al. used a two-step dipping process to establish a Janus evaporator with dual layers, resulting in a significant performance enhancement in solar interfacial evaporation desalination systems. The upper hydrophobic layer can convert solar energy to heat while repelling salt; the lower hydrophilic layer allows for continuous and capillary water migration (Figure 8a). This design promotes salt redistribution and dissolution due to concentration and thermal gradients (Figure 8b). Under low solar irradiance, the Janus evaporator produced 1.2–3.1 kg/m²/h of freshwater output and exhibited a solar conversion efficiency from 90.67% to 94.62%. This evaporator configuration holds great promise for solar-driven water purification in various environmental conditions, owing to its remarkable flexibility, stability, and long-term salt resistance [193].

Another step forward by Yang et al. included the construction of a free-standing 3D graphene-based Janus evaporator by surface treatment with UV-O<sub>3</sub> to achieve wettability control (Figure 8c). The top hydrophilic layer guarantees that water is continually available to evaporate. In contrast, the bottom hydrophobic layer enables the material to float, which improves light capture and minimizes heat waste (Figure 8d). Under the irradiation intensity of 1 kW m $^{-2}$ , the stable evaporation rate of this integrated design reached 1.71 kg m $^{-2}$  h $^{-1}$ , with a high conversion efficiency up to 94.1% and a good salt resistance even in 10 wt% simulated seawater. When the treated water salinity was measured using inductively coupled plasma mass spectrometry (ICP-MS), the results showed that the salinity decreased to meet the WHO criteria for potable water. The same method was used for wastewater purification containing dyes such as methyl orange, rhodamine B, and methylene blue at different pH levels [15,23,26]. The resulting condensed water was transparent, with no detectable absorption of UV-Vis by the dyes, suggesting the complete removal of contaminations from the wastewater [194].

Further, Jiao et al., using polypyrrole-, reduced GO (RGO)-, and cobalt phosphate-decorated nickel foam (PGCN), developed a PGCN hybrid system to facilitate the taper of water in the submerged system and generate active singlet oxygen for the purpose of efficient contaminant degradation. Under one sun, this solar-absorbing and thermal transferring hybrid system achieved a water evaporation rate of 2.08 kg m $^{-2}$  h $^{-1}$  and the 100% degradation of Norfloxacin and dyes. Thus, it suits solar desalination and water purification in high-salinity environments [195].

Such advances are a testament to the immense potential of solar-driven interfacial desalination systems. They provide potential solutions to water scarcity and contamination challenges by integrating high-efficiency materials with cutting-edge designs. However, while these systems have great potential, we still need more research to ascertain the true implications of their practical use, regarding how durable the materials will be when exposed to real-world conditions and how scalable these methods will be for larger op-

J. Compos. Sci. 2025, 9, 18 25 of 53

erations. However, driven by the ongoing development of materials design and system integration, solar desalination has a strong potential to be at the frontline of designs leading to commoditized products in sustainable desalination technologies.

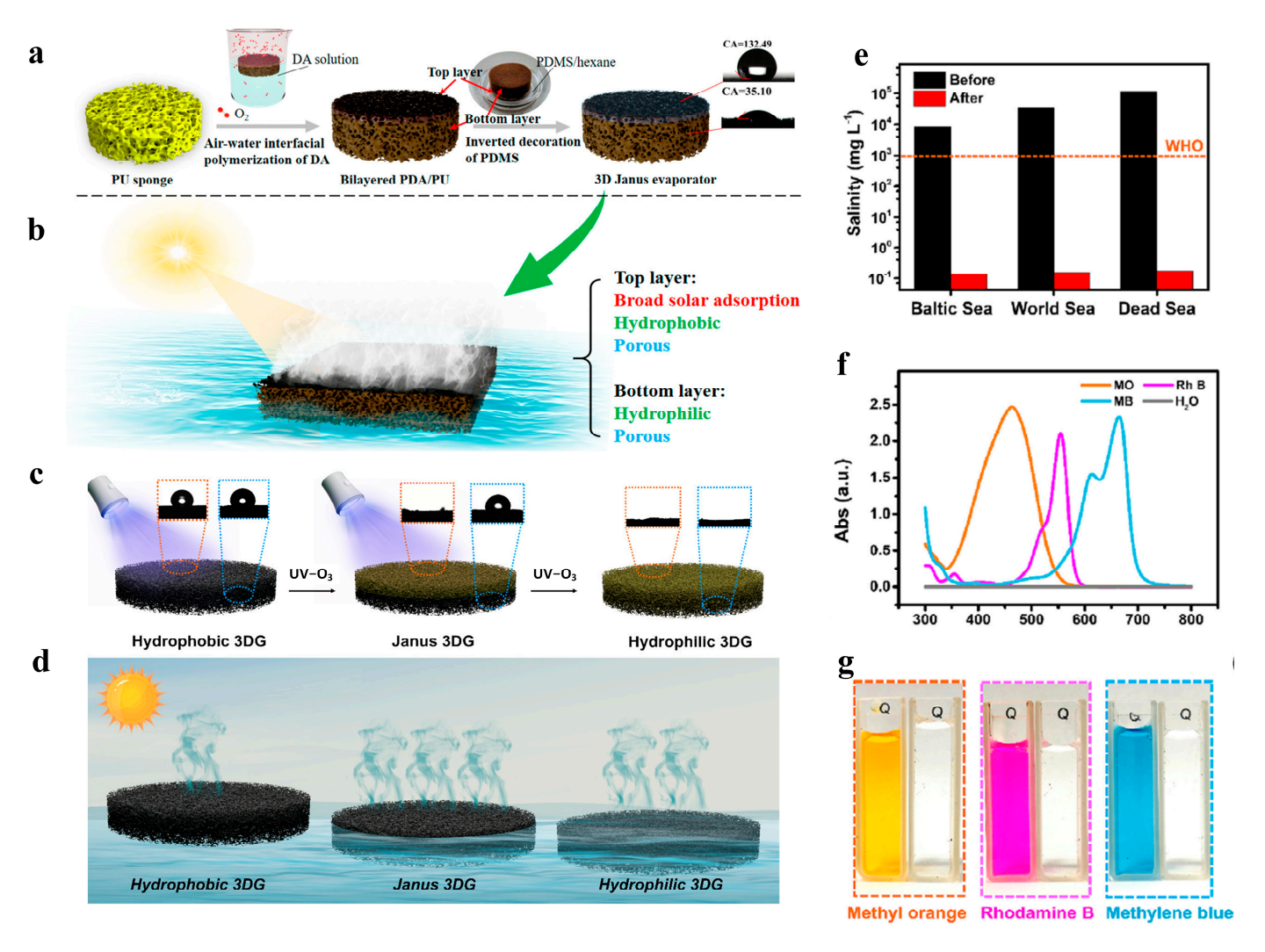


**Figure 8.** (a) The manufacturing process of the Janus evaporator, (b) diagram of continuous solar evaporation and salt rejection [193], (c) the fabrication process of 3D graphene at different times, (d) the optical image of 3DG-0, 3DG-30, and 3DG-900 floating on the water, (e) the three simulated seawater samples of salinity before and after desalination, (f) pictures (g) and UV Vis spectra of methyl orange, rhodamine B, and methylene blue aqueous before and after wastewater purification [194].

# 7. Three-Dimensional Graphene-Based Composite Materials Applications in Wastewater Treatment

Polluted water has an inimical effect on public health and aquatic life equally. The roots of contamination stem from both point sources and nonpoint sources [196]. Water contamination disrupts the spontaneity of chemical processes in living cells, resulting in long-/short-term diseases because the synthesis of cell constituents, the transport of nutrients, and body metabolism occur in aqueous media. Natural water channels serving as sewerage for domestic, pharmaceutical, and industrial waste are the leading cause of water pollution [197,198].

The impact of sewage and industrial wastewater on the quality of groundwater is well-documented as a major concern globally. According to reports, developed nations have more issues with chemical seepage, whereas underdeveloped nations have more issues with agricultural waste [199,200]. This adulteration through organic, inorganic, and biolog-

J. Compos. Sci. 2025, 9, 18 26 of 53

ical impurities can cause serious ailments like nervous disorders, cancer, and hormonal imbalance. The removal of these detrimental compounds, knowingly or unknowingly discharged into the aquatic system, is a prerequisite for mankind's survival [201,202].

#### 7.1. Removal of Heavy Metals

Heavy metal pollution in water is a growing environmental concern, stemming from multiple sources and posing significant threats to aquatic ecosystems and human health [203]. One of the primary contributors is industrial activities, such as mining, manufacturing, and the disposal of industrial waste [204]. These processes release heavy metals like lead, mercury, and cadmium into water bodies, contaminating them over time [205]. Tunable GO, a derivative of graphene with ion-chelating negatively charged functional groups, exhibits promising potential for removing heavy metal ions from water [206–208]. This effectiveness is primarily attributed to the large surface area and interconnected porous structure of GO-based 3D materials, providing abundant binding sites for metals [209]. Three-dimensional graphene/δ-MnO<sub>2</sub> aerogels were created, featuring an interconnected network of ultrathin  $\delta$ -MnO<sub>2</sub> nanosheets on a graphene framework [210]. These aerogels exhibited rapid adsorption kinetics and high adsorption capacities for heavy metal ions like  $Pb^{2+}$  (643.6 mg/g),  $Cd^{2+}$  (250.3 mg/g), and  $Cu^{2+}$  (228.5 mg/g), exceeding those of pristine 3D graphene and  $\delta$ -MnO<sub>2</sub> nanosheets. The synergistic effects of electrical attraction, surface complexation, and ion exchange were observed during the adsorption process. Notably, these aerogels maintained their performance even after multiple regeneration cycles, offering sustainable absorbents. Furthermore, GO's exceptional dispersibility ensures that it maintains an extremely large specific surface area, making it an outstanding choice for water remediation. This indicates that GO exhibits promise as a highly efficient adsorbent for effectively removing various heavy metal ions from water. GO macrostructures also exhibit partial electrical conductivity, which can be harnessed using advanced techniques to effectively remove heavy metals from wastewater by applying external energy extending beyond adsorption. Table 3 presents a range of adsorbents, each with unique affinities for different pollutants, allowing for targeted and customized treatment solutions.

Peng et al. have reported that hollow 3D graphene oxide/MnFe<sub>2</sub>O<sub>4</sub> motors, achieved through the combination of shear force and capillarity in GO suspension, effectively removed heavy metals (Pb<sup>2+</sup> and Cd<sup>2+</sup>) due to GO's oxygen-containing groups, while MnFe<sub>2</sub>O<sub>4</sub> allows for external magnetic control and bubble-driven movement powered by H<sub>2</sub>O<sub>2</sub> decomposition, A 20 mg GO/MnFe<sub>2</sub>O<sub>4</sub> motor eliminates 100 mg/L of Pb<sup>2+</sup> and Cd<sup>2+</sup> in 150 and 180 min, respectively, with high reusability and a 99.8% adsorption efficiency in the fifth cycle after chemical detachment with 0.2 M (HCl) [211]. Tan and his coworkers grafted graphene macrostructures with the aid of phytic acid and studied their mercury sorption abilities. These graphene foams boasted significant surface area and amphiphilic properties. The primary mechanisms involved ion exchange and surface complexation, highlighting the potential of these foams for purifying both river and seawater [212]. Notably, a rich variety of heavy metals has been efficiently disposed of, including Hg(II), Cu(II), Cd(II), Pb(II), Zn(II), Co(II), Ni(II), Cr(VI), Fe(II), Fe(III), Ag(I), and so on [61]. The adsorption capacities of these 3D GBMs are generally either comparable or superior to those of other ordinary materials [213]. Using a one-step chemical method and changing the 3D GO-ZG mass ratio and conditions, a group of 3D GO-ZG<sub>x:v</sub> composites with great stability showed an impressive ability to absorb REEs. Figure 9a shows that 3D GO-ZG<sub>2:1/6 h/120 °C</sub> had a specific adsorption value of 44.56 mg/g for La<sup>3+</sup>, 53.64 mg/g for Yb<sup>3+</sup>, 45.96 mg/g for  $Nd^{3+}$ , 50.48 mg/g for  $Er^{3+}$ , and 30.63 mg/g for  $Y^{3+}$ . Rare earth elements attach to surfaces through ion exchange, surface complexation, and electrostatic binding. Notably, the compound showed excellent stability and recoverability over 10 cycles of adsorption

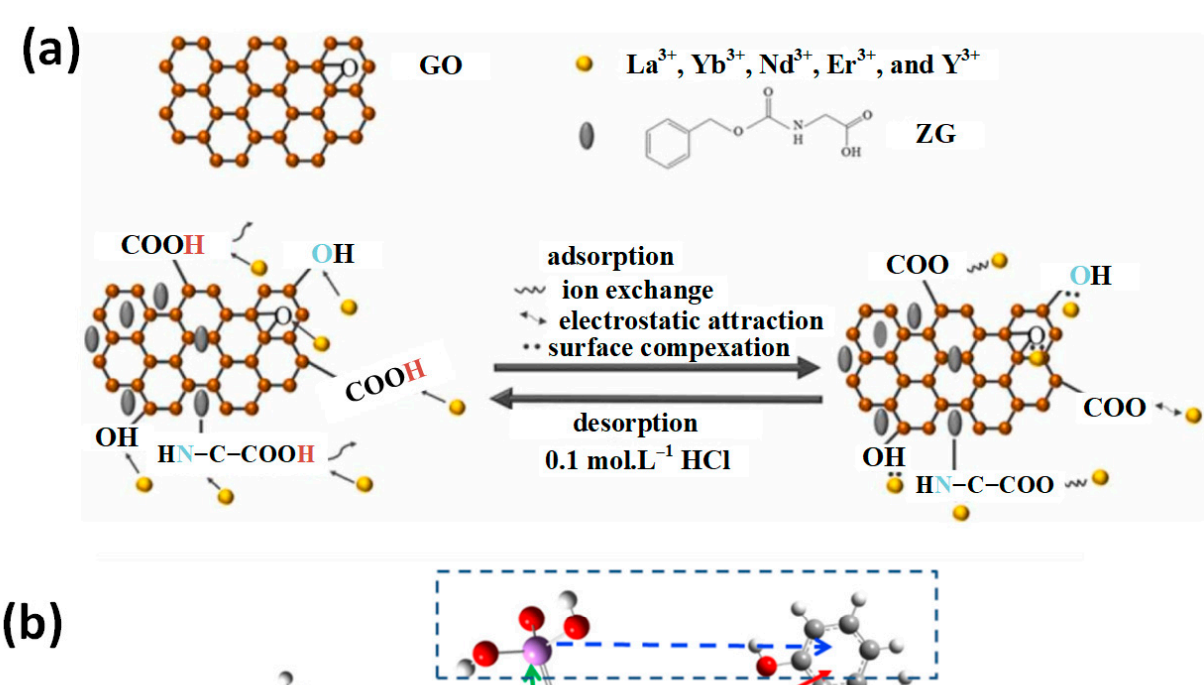
J. Compos. Sci. 2025, 9, 18 27 of 53

and discharge. To assess the reusability of the 3D GO-ZG  $_{2:1/6\,h/120\,^{\circ}C}$  composite, the adsorbent was desorbed with a 0.1 mol/L HCl solution after REEs adsorption, rinsed with deionized water, and subsequently employed in the next adsorption experiment [214]. He et al. represented the application of a new composite based on immobilized yttrium on graphene oxide-alginate hydrogel (Y-GO-SA) to the adsorption of arsenic (As(V)) and tetracycline (TC) from aqueous solution and wastewater coming from livestock farms [215]. In this study, the highest adsorption capacity values obtained reached 273.39 mg/g for arsenic and 477.9 mg/g for tetracycline. The adsorption mechanisms of arsenic include chemisorption via ion exchange and surface complexation with yttrium ions and hydrogen bonds with oxygen-containing groups on the hydrogel. Tetracycline adsorption combines electrostatic interactions via hydrogen bonds with different  $\pi$  interactions, which contribute to its high adsorption capacity. Figure 9b depict the possible co-adsorption mechanisms of As(V) and TC by Y-GO-SA gel. From the perspective of macroscopic structure, its unique macrostructures with large surface areas and continuous pores are favorable for the diffusion of metal ions. Due to its high adsorption capacity and expanded surface area, it shows potential for mass production and industrial-scale applications.

**Table 3.** Various reported 3D GBCMs for heavy metal adsorption.

3D GBCMs	<b>Heavy Metals</b>	pН	Adsorption mg/g	<b>Underlying Mechanism</b>	References
	Yb (III)		30.88		
	Er (III)		26.52	Ion exchange/	
3DGO-TAPA	Nd (III)	6	20.60		[216]
	La (III)		11.24	Surface complexation	
	Y (III)		10.52		
3D GA/TiO <sub>2</sub>	U (VI)	5	441.3	Surface complexation or ion exchange Electrostatic attraction/	[217]
BD G/TiO <sub>2</sub> /Xanthan Composite	Pb (II)	5.2	199.2	Surface complexation/ Ion exchange	[218]
3D OGRs	Cr (VI)	3	687.8	Electrostatic attractions	[219]
3D rGO/PBAs	Cs (I)	5	204.9	Ion-exchange, ion trapping, complexation interaction	[220]
$3D (GOF/Fe_3O_4)$	Cr (IV)	2	258.6	Ion exchange	[221]
	Pb (II)	-	358.9	<u>g</u>	
3D G/MgO	Cd (II)	-	388.4	Electrostatic attraction/	[222]
Composite	Cu (II)	-	169.8	Surface complexation	
3D rGO	Cu (II)	-	18.1	Electrodeposition	[223]
	Pb (II)		84.76	Hydrogen bonding interaction, $\pi$ - $\pi$ stacking interactions, electrostatic interactions, Lewis acid-base interactions	[224]
	Mn (II)		7.92		
	$Cr_2O_7^{2-}$		13.6		
	Cd (II)	5	17.64		
3D GO-MA	Cu (II)		30.56		
3D GO-MA	Nd (III)	3	25.52		
	La (III)		12.48		
	Y (III)		16.96		
	Yb (III)		23.32		
	Er (III)		30.32		
	Y (III)		42.8		
3D CEG	La (III)		32.16	Electrostatic interactions and coordination	
composites	Er (III)	7	56.44	interactions	[225]
composites	Yb (III)		1.44	interactions	
	Nd (III)		50.16		
3DGF-MnO <sub>2</sub>	Sr (II)	-	47.39	Electrostatic attraction	[226]
MCF3DG	Pb (II)	8.5	957	Electrostatic attraction/	[227]
	` '			Surface complexation	
3DG	Cr (VI)	6	107	Electrostatic attraction	[228]
3D GOCS	EU (III)	6	150	Surface complexation	[229]
22 00 00	Th (IV)	3	220	r	[ ]
3D PG/L/SA	Cd (II)	6	79.88	Ion exchange	[230]
	Pb (II)		226.24	· ·	
3D PA-Gr	Hg (II)	7.2	361.01	Ion exchange, hydrogen bonding	[212]

J. Compos. Sci. 2025, 9, 18 28 of 53



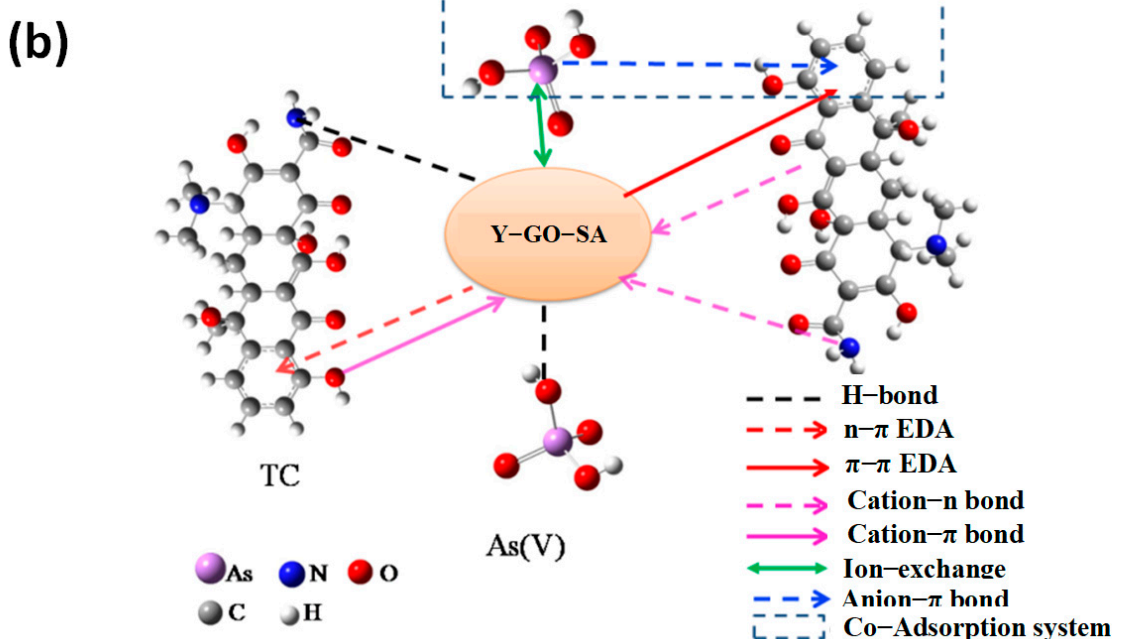


**Figure 9.** (a) 3D GO-ZG composites showed strong adsorption capabilities for La<sup>3+</sup>, Yb<sup>3+</sup>, Nd<sup>3+</sup>, Er<sup>3+</sup>, and Y<sup>3+</sup>; ion exchange, electrostatic attraction, and surface complexation were the adsorption mechanisms for rare earth elements (REEs) [214]. (b) Co-adsorption mechanism of As (V) and TC onto Y–GO–SA [215].

## 7.2. Removal of Dyes

Water pollution is a pressing global concern, and one of its lesser-known but significant contributors is the discharge of dyes from various industrial processes [231]. A multitude of techniques exist in the water treatment process for tackling the removal of dye and heavy metal pollutants, encompassing a spectrum of physical and chemical methods, but these methods often present limitations such as excessive sludge generation [232], high costs, a limited lifespan [233], and demanding oxygen requirements as in the case of flocculation, active oxidation, and biological degradation [234]. Table 4 illustrates the prominence of graphene in wastewater treatment. Graphene, with its hexagonal lattice of carbon atoms forming a single layer, has gained substantial attention as a prime candidate for wastewater treatment. These 3D carbon-based architectures not only inherit the advantageous properties of 2D graphene, including a large specific surface area, but also surmount its drawbacks

through the creation of stable, interconnected porous frameworks [235]. Three-dimensional graphene gels, sponges, ribbons, and films utilize both adsorption and photocatalytic degradation to remove dyes and other organic contaminants from wastewater [236].

**Table 4.** Organic dye adsorption capacity and mechanism analysis of 3D GBCMs.

3D Graphene/Composite Materials	Organic Dyes	pН	Adsorption mg/g	Underlying Mechanism	References
3D GO	MB	6.5	86%-one ton	Electrostatic interaction, $\pi/n-\pi$ interaction and hydrogen bonding	[74]
3D-CTG	MG CV	4 6.5	334.8 583.6	Electrostatic attraction	[237]
3D G/Chitosan Composite	Black 5	10	638.9	Electrostatic attraction/ Hydrogen bonding/ $\pi$ - $\pi$ interactions	[238]
3D-G aerogel/CaCO <sub>3</sub> Composite	AR 88	6	1000	Electrostatic attraction	[158]
3D-GO/CS/β-CD	MB	12	1134	Strong electrostatic interaction, $\pi$ - $\pi$ interaction, hydrogen bonding	[239]
3D G/C <sub>3</sub> N <sub>4</sub> /TiO <sub>2</sub> Aerogel	Rh B	-	984	Electrostatic interaction	[240]
Ag/ZnO/3D graphene	MB	7	300	Electrostatic attraction/ Hydrogen bonding/ $\pi$ - $\pi$ interactions	[162]
3D rGO/ZIF-67 aerogel	CV MO	6	1714.2 426.3	π- $π$ interactions and electrostatic interactions	[241]
MCF3DG	CV	7.5	827.15	Electrostatic interactions	[242]
GO/PEI (GP) 3D aerogels	MO MB	2 10.5	331.0 249.6	Electrostatic attraction force and $\pi$ - $\pi$ interaction	[243]
3D graphene nanoedges	MO	2	27.932	Electrostatic attraction/ Hydrogen bonding/ $\pi$ - $\pi$ interactions	[244]
3D-GA	Rh B	8	280.8	Electrostatic attraction/ Hydrogen bonding/ $\pi$ - $\pi$ interactions	[245]

The adsorption of dyes onto these 3D macrostructures is facilitated by several factors. Firstly, electrostatic forces and  $\pi$ - $\pi$  interactions play a significant role in attracting and binding the dye molecules to the macrostructure's surface. Additionally, these macrostructures possess chemically active functional groups that further enhance their affinity for organic contaminants [121]. Furthermore, when graphene hydrogel is combined with photocatalysts, a synergistic effect emerges, combining adsorption and photocatalytic activities for the effective removal of organic contaminants from the environment. In this process, the pollutant molecules are initially adsorbed onto the surface of the 3D graphene network. Subsequently, when exposed to light, the photogenerated charge carriers participate in chemical reactions that lead to the decomposition of these pollutants. Moreover, the interconnected network of the 3D graphene structure provides efficient pathways for the transfer of photogenerated electrons and holes [246]. This characteristic significantly enhances the photocatalytic performance of composites composed of a graphene 3D macrobody and semiconductor materials. One recent paper describes a metal oxide nanoparticle-encapsulated crushed graphene oxide (MGC) nanocomposite that dramatically increases the adsorption capacity of organic pollutants such as methylene blue [74]. The MGC nanocomposite has a Langmuir adsorption capacity (q<sub>m</sub>, normalized by carbon) that is improved by 60-86% compared crumpled graphene balls (CGB), is from three to four times more efficient than powdered activated carbon (PAC), and is from 6 to seven times more effective than GAC. These findings emphasize MGC's potential for effective and quick water treatment. Furthermore, the MGC nanocomposite improves industrial-scale water treatment due to its larger adsorption capacity, achievement of quick equilibrium, and ability to maintain stability in wastewater, making it a scalable and cost-effective alternative

for large-scale organic pollutant removal [74]. Notably, composite materials have shown promising results in the removal of water pollutants. The adsorption of methylene blue using Ag/ZnO/3DG, a hybrid photocatalytic adsorbent, has already been studied [162]. A wide range of dyes have successfully been removed from aqueous media using tuneable 3D graphene microbodies and their composites, such as Rhodamine B dye in water using g-C<sub>3</sub>N<sub>4</sub> and TiO<sub>2</sub> co-hybridized 3D graphene aerogel composites [240], Crystal Violet dye by magnetic citric acid-functionalized 3D graphene nanocomposite [242], Acid Red 88 dye by 3D graphene aerogel/CaCO<sub>3</sub> nanocomposite [158], and Reactive Black 5 dye by 3D GO/high molecular weight chitosan (GO/HCS) composite [238]. One possible explanation for the pH-dependent adsorption capacity variation of these materials is that the charged groups of MCF3DG undergo reversal in acidic and basic mediums. Therefore, their CV removal efficacy varies across pH ranges due to unique electrostatic interactions between the CV molecules and MCF3DG [242]. While there have been limited studies on 3D graphene-based photocatalysts with high pollutant elimination rates, further research is needed to improve their efficiency. Various composite materials, such as 3DG/TiO<sub>2</sub> [80], 3DG/Fe<sub>3</sub>O<sub>4</sub> [247], and 3DG/g-C<sub>3</sub>N<sub>4</sub> [248], have been investigated for their potential in both dye adsorption and photocatalytic degradation, demonstrating the potential of 3D GBCMs in environmental remediation efforts. Recent advances in wastewater treatment have led to the development of 3D Co/Mo co-catalyzed graphene sponges (SCMG) as highly efficient catalysts, which were created through a simple impregnation pyrolysis method (Figure 10a).

SCMG rapidly degrades rhodamine B within 2 min by activating peroxymonosulfate (PMS). Enhanced by GO and MoS<sub>2</sub> co-catalysis, SCMG shows high reactivity across a broad pH range (3-9), resistance to common anions and humic acid, and excellent reusability with minimal metal leaching. Both free radical and non-radical pathways are involved, with  ${}^{1}O_{2}$  and  $SO_{4} \bullet^{-}$  being the main active species (Figure 10b). This study underscores the potential of SCMGs in sustainable, industrial-scale wastewater treatment [249]. Their heterogeneous catalysis has led to the development of CoFe<sub>2</sub>O<sub>4</sub> supported on 3D graphene aerogels (CoFe<sub>2</sub>O<sub>4</sub>@3DG) as an effective catalyst for peroxymonosulfate (PMS) activation, especially for degrading recalcitrant pollutants like Benzotriazole (BTA). In comparison, the CoFe<sub>2</sub>O<sub>4</sub>/PMS system degraded only 26.7% of BTA in 3 h, and the 3DG/PMS system achieved 16.7% degradation due to the hydrophilic nature of BTA and the hydrophobic surface of 3DG. However, the CoFe<sub>2</sub>O<sub>4</sub>@3DG/PMS system achieved 100% degradation within 2.5 h, outperforming the CoFe<sub>2</sub>O<sub>4</sub>@RGO/PMS system and showcasing the superior catalytic performance of the 3D graphene aerogel structure (Figure 10e,f). Stability tests over seven cycles revealed that the CoFe<sub>2</sub>O<sub>4</sub>@3DG/PMS system maintained a 90% BTA degradation efficiency, with only a 10% reduction, indicating excellent durability (Figure 10d). This superior performance results from the comprehensive effect of multiple oxidation pathways and the synergistic activation of PMS by CoFe<sub>2</sub>O<sub>4</sub> and 3DG, which generates multiple reactive oxygen species ( $\bullet$ OH,  $SO_4\bullet^-$ ,  $O_2\bullet^-$ , and  $^1O_2$ ) and enhances the electron transfer (Figure 10c). Additionally, CoFe<sub>2</sub>O<sub>4</sub>@3DG offers superior stability and recyclability, and reduced metal leaching, making it a highly promising catalyst for wastewater treatment applications [250].

J. Compos. Sci. 2025, 9, 18 31 of 53

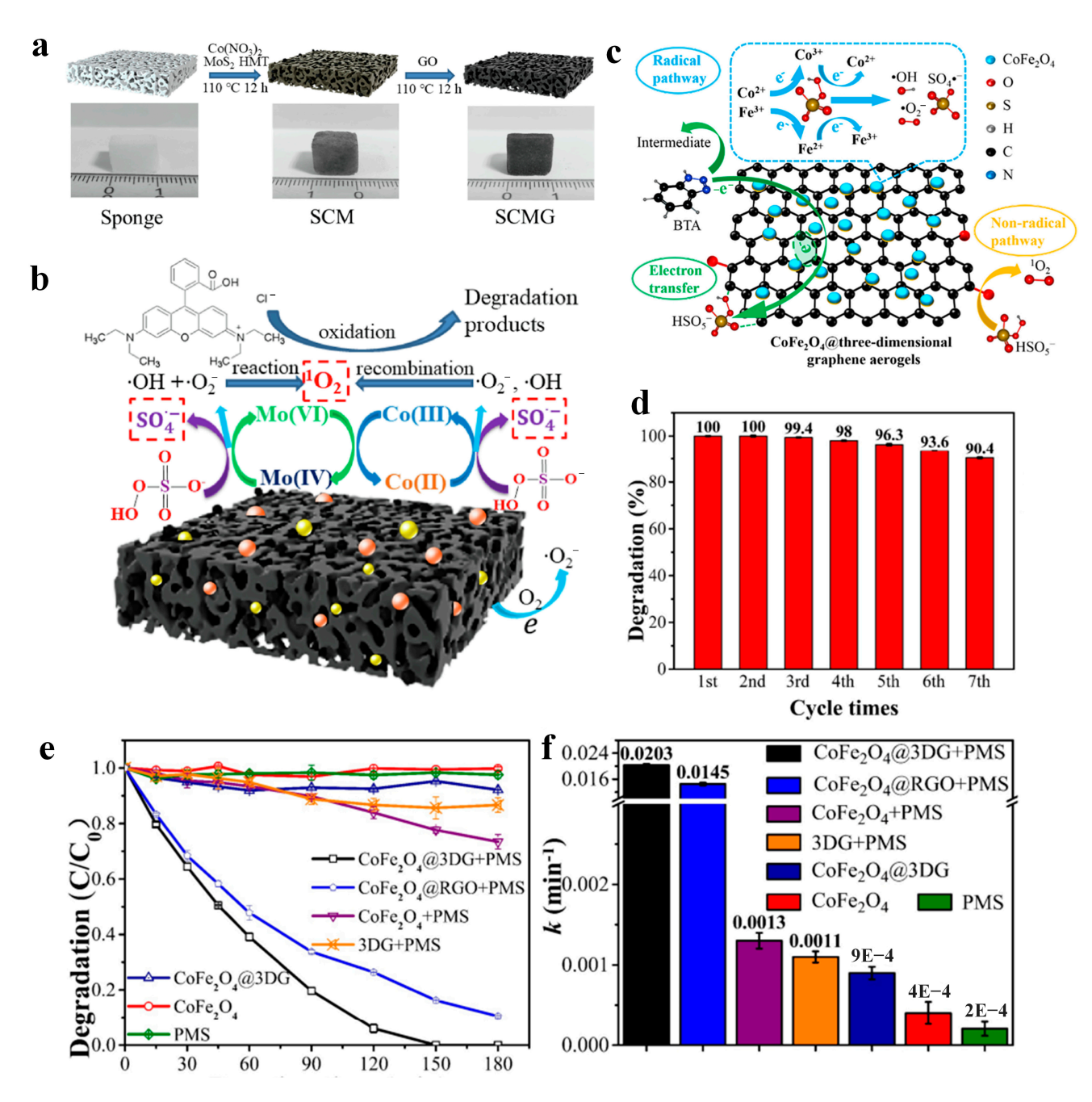


**Figure 10.** (a) Synthesis scheme of SCMG, (b) probable catalytic oxidation mechanism of Rhodamine B in SFMG/PMS system [249], (c) activation mechanism of PMS by CoFe<sub>2</sub>O<sub>4</sub>@3DG, (d) the BTA degradation rate in the CoFe<sub>2</sub>O<sub>4</sub>@3DG/PMS system in seven cycles, (e) degradation performance and (f) reaction rate constant in different catalytic systems of BTA [250].

# 7.3. Removal of Salts

The process of desalination, in which salt and other impurities are removed from saltwater or brackish water to produce drinking water [251], is crucial for solving the world's water shortage problems. This growing concern regarding water pollution has spurred extensive research into the purification of contaminated water using advanced functional nanomaterials. One intriguing approach is the development of catalytic membranes, which offer both filtration and catalytic capabilities [252], showing promise for sewage treatment. Among the array of materials considered for this application, GO membranes have attracted substantial attention from materials scientists due to their exceptional attributes [253]. These include a remarkable structural stability, outstanding water

permeation characteristics, and molecular sieving properties [254]. In the construction of efficient systems for producing clean water from sources like wastewater and saline water, GO nanosheets play a pivotal role as building blocks [255]. These nanosheets are used to create layered 3D porous membranes, setting them apart from conventional polymeric membranes. In contrast to conventional polymeric membranes, 3D GBCMs offer several distinct advantages [194]. Table 5 lists various GBCMs that are suitable for use as electrode materials.

**Table 5.** Adsorption performances of salt ions and mechanism analysis of their deposition onto 3D GBCMs.

3D Graphene/Composite Materials	Salty Ions	Adsorption mg/g	Underlying Mechanism	References
3DMG	Na <sup>+</sup> Cl <sup>-</sup>	32.08	Electrodeposition	[256]
3D-G/MnO <sub>2</sub> Electrode 3D-G/NiO Electrode	Na <sup>+</sup> Cl <sup>-</sup>	21.0	Electrodeposition	[184]
3D G nanostructures on Ni foam substrate	Na <sup>+</sup> Cl <sup>-</sup>	22.3	Electrodeposition	[257]
3D G	Na <sup>+</sup> Cl <sup>-</sup>	21.6	Electrodeposition	[258]
3D G Nanopores	Na <sup>+</sup> Cl <sup>-</sup>	17.1	Electrodeposition	[183]
3D G	Na <sup>+</sup> Pb <sup>+2</sup>	987	Electrodeposition	[174]
3D G nanocomposite	Na <sup>+</sup> Cl <sup>-</sup>	22.09	Electrodeposition	[259]
3D G	Na <sup>+</sup> Cl <sup>-</sup>	9.86	Electrodeposition	[260]
3D (CSG)	Na <sup>+</sup> Cl <sup>-</sup>	9.60	Electrodeposition	[261]
3D G	Na <sup>+</sup> Cl <sup>-</sup>	14.08	Electrodeposition	[262]
3DHGR	Na <sup>+</sup> Cl <sup>-</sup>	14.7	Electrodeposition	[263]
3D G	Na <sup>+</sup> Cl <sup>-</sup>	21.58	Electrodeposition	[258]
3D G Nanopores	Na <sup>+</sup> Cl <sup>-</sup>	18.43	Electrodeposition	[262]
3D graphene	Na <sup>+</sup> Cl <sup>-</sup>	13.72	Electrodeposition	[264]
3D rGO composites	Na <sup>+</sup> Cl <sup>-</sup>	21.9	Electrodeposition	[265]

Three-dimensional GBCMs facilitate the swift movement of water through defects or nanochannels formed between individual GO nanosheets. These membranes are characterized by narrow interlayer spacings and expansive specific surface areas and exhibit remarkable effectiveness in eliminating a broad spectrum of organic compounds and soluble metal ions through processes such as rejection or adsorption [259]. Traditional membranes often exhibit a tradeoff between permeation fluxes (the rate of water flow) and intercept precision (the ability to separate specific contaminants). Three-dimensional GMs adeptly surmount this challenge, exhibiting both high permeation rates and superior contaminant removal capabilities [258]. CDI has emerged as another notable desalination technology. This process hinges upon the application of an external voltage across a pair of carbon electrodes, distinguished by opposing charges, which are immersed within a saline solution. However, the pivotal desalination process occurs within the intricate porous matrix of these electrodes. This process, termed electrosorption, entails the organized retention of salt ions within the electric double layer at the electrode-electrolyte interface. This double layer, comprising a positively ion-enriched region and a negatively ion-enriched counterpart, serves as the locus for ion separation, ultimately leading to the removal of salt species from the solution [266]. Three-dimensional carbon electrodes, lauded for their exceptional porosity and low-density characteristics, have been established as formidable contenders in CDI applications [267]. These electrodes can be made ion-selective by grafting desired functional groups on the surface of GO microbodies. These groups serve a dual purpose, the first part of which is that they function as specialized coatings that selectively interact with ions, effectively reducing the undesired expulsion of co-ions during the electrochemical process. Secondly, these grafted groups play a role in altering the properties of the electrode's surface. They increase its hydrophilicity, making it more inclined to interact with water molecules, and enhance its wettability, which means that it becomes more capable of

efficiently facilitating the transmission of ions from the surrounding solution to the electrode. This selective interaction enhances the overall efficiency of the charge transfer within the system [268]. Introducing sulfonic and amino functional groups elicited significant enhancements in the salt adsorption capacity and charge efficiency of this material. Using a 500 mg/L NaCl aqueous solution, the 3D graphene rode flow-through capacitor showed an outstanding salt adsorption capacity of 13.72 mg/g and an exceptional charge efficiency of 0.85 by reducing the co-ion expulsion effect [264]. Three-dimensional graphene has a higher specific surface area and is capable of handling different concentrations of salt. It has more active edge sites and ion channels because of the hierarchical holes in the 3D graphene sheet, which each have a distinct array of benefits. This improvement eventually improves the material's electrochemical performance. Its electrosorption capacity of 29.6 mg/g and specific capacitance of 219.6 F/g when exposed to a 1 mol/L NaCl solution at 1 A/g are clearly outperformed by a monolithic HGF with an effectively distributed pore size [107]. Recent progress in CDI has resulted in the creation of a hole-rich graphene framework (HGF) fabricated through lyophilization and thermal treatment. This 3D graphene mesh, used as a binder-free CDI electrode, preserves its structure, enhancing its performance. The core of a CDI unit consists of self-supporting electrodes in a sandwich structure. When voltage is applied, the electrodes create an electric field that attracts Na<sup>+</sup> and Cl<sup>-</sup> ions, achieving deionization. The key factors that affect electrosorption are the applied voltage, which determines the ion force, and the initial salt concentration, which influences the diffusion pathway and resistance (Figure 11a). The desalination capacities of this material were measured as 29.6 mg/g, 8.0 mg/g, and 16.9 mg/g (Figure 11b). A lower salinity results in a higher resistance, longer diffusion pathways, and longer adsorption times, while a higher initial current reflects a lower resistance and faster ion movement (Figure 11c). This highlights HGF's potential to advance CDI technology through innovative material design [107].

CDI is a promising method for water purification, but developing efficient electrode materials remains a challenge. A recent study synthesized N- and P-doped 3D graphene with tunable pore sizes, yielding a high specific surface area (567.14 m<sup>2</sup>/g) and specific capacitance (177.19 F/g) [269]. When tested in a NaCl solution (100 mg/L) at 1.6 V, the conductivity of the NGA and PGA electrodes was quickly reduced within 20 min, stabilizing after 80 min, while the GA electrodes took 100 min to reach equilibrium (Figure 11d). This demonstrates that PGA and NGA outperform GA in desalination. The adsorption capacities showed that PGA had the highest desalination rate at 20.69 mg/g, compared to those of GA (9.55 mg/g) and NGA (13.52 mg/g) (Figure 11e). The superior performance of PGA is attributed to its higher pore volume (0.504 cm<sup>3</sup>/g) and larger pore sizes (0.7–1 nm and 2–6 nm), created through H<sub>3</sub>PO<sub>4</sub> activation and annealing, and providing a hybrid micropore–mesopore structure (Figure 11f). This study highlights the potential of N- and Pdoped 3D graphene for use in CDI and other applications in industrial water treatment and energy storage due to its high surface area, capacitance, and optimized pore structure [269]. CDI offers a compelling array of advantages, including remarkable energy efficiency, cost-effectiveness, environmental sustainability, and suitability for applications requiring small-scale, portable implementation [270].

J. Compos. Sci. 2025, 9, 18 34 of 53

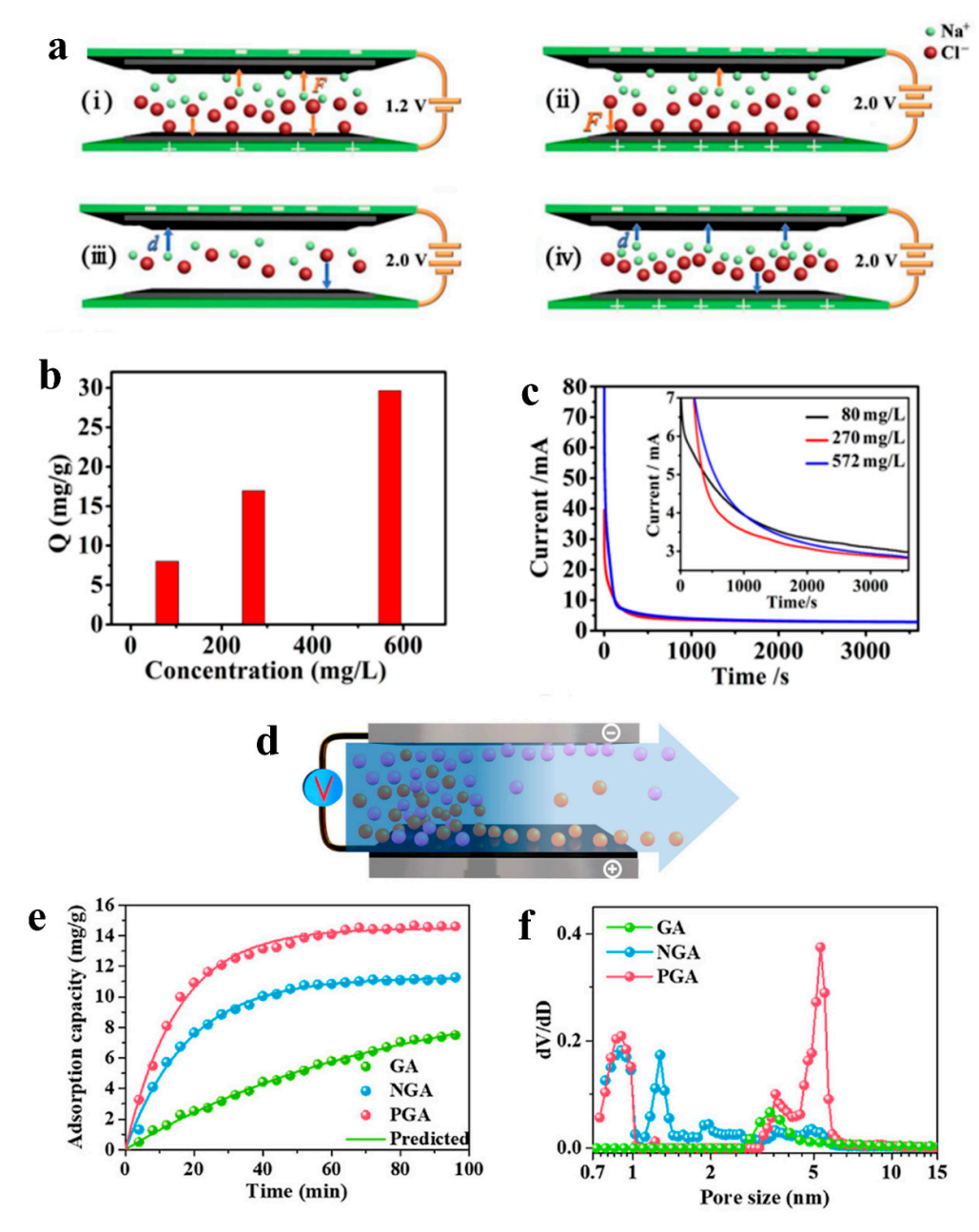


**Figure 11.** (a) The CDI mechanism at different applied voltages and initial salt concentrations, illustrating the variations in electric force on salt ions between low (i) and high (ii) voltages at the same concentration, and the difference in diffusion pathway length at low (iii) versus high (iv) salt concentrations at a fixed voltage, (b) the electrosorption capacity and (c) corresponding current of HGF in NaCl solutions at concentrations of 80 mg/L, 270 mg/L, and 572 mg/L at 2.0 V, with an inset showing a detailed view of the current–time relationship [107], (d) the CDI desalination process, (e) pore size distribution, and (f) Langmuir adsorption isotherms at an applied potential of 1.6 V [269].

#### 7.4. Pharmaceutical

The continual consumption of pharmaceutical compounds around the world in medicine, aquaculture, livestock production, and everyday life has created an enormous issue for the environment [271]. Pharmaceutical residues have turned into widespread pollutants that get into people's and animals' bodies and spread through the environment [272]. Their annual production has surpassed 20 million tons and is slowly rising to meet the demand for medical drugs. Pharmaceutical compounds, which are grouped by their specific uses, are a growing group of man-made pollutants. They are full of

J. Compos. Sci. **2025**, 9, 18 35 of 53

biologically active substances that are commonly found in medicines and personal care items [273].

Pharmaceutical residues get into the environment through effluent discharge from many places, such as hospitals, veterinary facilities, wastewater treatment plants, pharmaceutical industries, and residential areas [274]. They have been found in surface waters, groundwater, soil, and even drinking water. Pharmaceutical residues are very harmful to water quality and environments, even though they are only found in very small amounts (ng/L to mg/L) in bodies of water. This is because they do not break down easily and build up over time. To lessen the damage they do to the environment, it is now necessary to control the amount of medication residues in water sources [275]. Implementing 3D GBCMs appears to be a revolutionary way to effectively remove pharmaceutical contaminants from water, which presents a solution to this urgent global issue. Many variables contribute to the enhanced pharmacological adsorption onto these 3D macrostructures. Primarily, the surfaces of these macrostructures engage electrostatic forces,  $\pi$ - $\pi$  interactions, hydrogen bonding, and hydrophobic interactions, all of which play a considerable role in attracting and binding pharmaceutical compounds [276]. The naturally porous and networked shapes of these structures allow for faster mass movement, which makes decontamination processes very effective. The World Health Organization says that the problem of pharmaceutical garbage discharge is getting worse, so new ways of dealing with it are needed in the 21st century [277]. A significant step forward is represented by a 3D graphene aerogel loaded with soy protein (SP), which shows great adsorption effectiveness for drugs like tetracycline and ciprofloxacin. It works well because it has a large amount of microspores, a large specific surface area (SSA), and good hydrophilic features [278]. Another approach looks into how to make a honeycomb-like structure out of 3D graphene by magnetically adding N-doping within a 3D graphene framework, examples of which have shown a strong attraction to cephalosporin antibiotics [279]. In the area of combined reduction and assembly, treating a 3D reduced GO aerogel with Lewis-ascorbic acid achieves a high level of diclofenac removal efficiency [198]. Another thing is that a 3D binary carbon materialbased design made from carbon nanotubes and GO has been shown to be better than traditional methods at absorbing drugs, especially oxytetracycline [280]. Pharmaceutical waste negatively influences marine biodiversity because it is toxic and has the potential to bioaccumulate. In a recent study, a novel phosphorus-doped 3D graphene oxide with bentonite and carboxymethyl cellulose cross-linking (PG/BCC) that exhibited outstanding imipramine adsorption was successfully created employing an environmentally benign ice-templating method [49]. The PG/BCC adsorbent showed a high imipramine adsorption capability and stability in the pH range of 4–9. The adsorption equilibrium and kinetic modeling of the material revealed monolayer adsorption on homogenous sites that was governed by chemisorption. The ideal parameters were 10 mg PG/BCC, a 250 ppm initial concentration, a 34 min contact duration, and a temperature of 321 K temperature, which resulted in the maximum adsorption capacity of 458.95 mg/g. This work provides a new approach to solving real-world environmental issues and marks a big step towards industrial-scale wastewater treatment. Table 6 provides the adsorption performances of various 3D GBCMs on pharmaceuticals.

J. Compos. Sci. 2025, 9, 18 36 of 53

Table 6. Pharmaceutical adsorption capacity and mechanism analysis onto 3D GBCMs.

3D Graphene/Composite Materials	Pharmaceuticals	pН	Adsorption Performances	Mechanism	References
	Naproxen	3.5	357 mg/g	Hydrophobic	
3D rGO-based hydrogel	Ibuprofen Diclofenc	3.3 3	500 mg/g 526 mg/g	interactions, $\pi$ -hydrogen bonding	[281]
3D-rGO/Fe <sub>3</sub> O <sub>4</sub> hybrid hydrogel	Ciprofloxacin Tetracycline	6	2.78 mmol/g 4.76 mmol/g,	Hydrophobic and $\pi$ - $\pi$ stacking interactions	[282]
3DG- hydrogels	Ofloxacin	-	134 mg/g	$\pi$ - $\pi$ interaction, hydrogen bonding, and hydrophobic interaction	[283]
3D CGO	Tetracycline		163.4 mg/g	Electrostatic interaction	[284]
3D rGO and CN	Naproxen	6	132.09 mg/g	Hydrophobic interaction, electrostatic interaction, $\pi/n$ - $\pi$ interaction and hydrogen bonding	[285]
3D/GO-HPEDr-G5-PAH	Donepezil hydrochloride	7	98.76%	Strong hydrogen bond	[286]
FeNi <sub>3</sub> @3DGr	Ibuprofen Diclofenac	7.1	91% 100%	Electrostatic interaction and $\pi$ - $\pi$ stacking	[287]
3D (rGOA)	Diclofenac	9	596.71 mg/g	Hydrogen bonding, hydrophobic attraction, $\pi$ - $\pi$ EDA	[198]
3D Gr-SP	Tetracycline and Ciprofloxacin	-	500.0 mg/g for both antibiotics	Electrostatic interaction and $\pi$ - $\pi$ stacking	[278]

To get around the problems with single adsorption methods, a method that uses both photodegradation and adsorption has been created to get rid of drugs. A new threepart composite called 3D CeVO<sub>4</sub>/rGO/BiVO<sub>4</sub> was carefully created based on the idea of efficient electron-hole separation and charge transfer. This mixture works well to get rid of tetracycline in water, showing both effective adsorption and synergic breakdown driven by visible light. This new method greatly improves the removal process and encourages the cleanup of antibiotic-contaminated water in an environmentally friendly way [276]. Further, in one reported work [277], the adsorption potentials of magnetic reduced graphene oxide (MrGO) nanocomposites, especially MrGO-2 (5.31 µg/mg), were enhanced by their unique 3D-interconnected structure, as compared to pristine Fe<sub>3</sub>O<sub>4</sub> (2.13 μg/mg) and rGO (4.51 µg/mg). A better match was seen for the pseudo-second-order model, which represents a combination of physical and chemical adsorption processes, when comparing the data fitted to the pseudo-first-order model (Figure 12a). Particularly, the rate constant for SDZ adsorption was greatest in MrGO-2 (5.79 mg/(µg/h)), demonstrating that the efficiency of magnetic materials might vary considering the extensive use of SDZ and its aromatic ring structure, and it was found that the  $\pi$ - $\pi$  electron interaction with rGO was crucial to the adsorption procedure (Figure 12b). After five repeated adsorption cycles, the removal efficiency remained at 89.3%. This represents only a 3% decrease compared to the efficiency observed during the initial adsorption (Figure 12c). The use of 3D graphenebased structures is a ray of hope regarding the complicated problem of pharmaceutical pollution in water. They offer a long-lasting and effective way to solve this widespread global problem.

# 7.5. Other Organic Pollutants

Numerous organic contaminants, such as halogenated chemicals, oils, phenols, bacteria, pathogens, pesticides, and poisonous compounds, invade ecosystems and pose a serious concern worldwide. This has prompted a search for efficient methods to eliminate them, especially from polluted water supplies. The novel field of 3D graphene-based designs has emerged into the spotlight in recent years, as they display a wide range of characteristics adapted for the removal of numerous toxic organic contaminants [288]. Multiple factors contribute to the complex symphony that is the adsorption of organic contaminants onto these 3D GBMs. The electrostatic forces of interactions, hydrogen bonding, hydrophobic interactions, London forces, and Debye interactions are all present on the

J. Compos. Sci. 2025, 9, 18 37 of 53

surface of the macrostructure. There is strong evidence that these complex forces play a significant role in attracting and binding various organic contaminants [61].

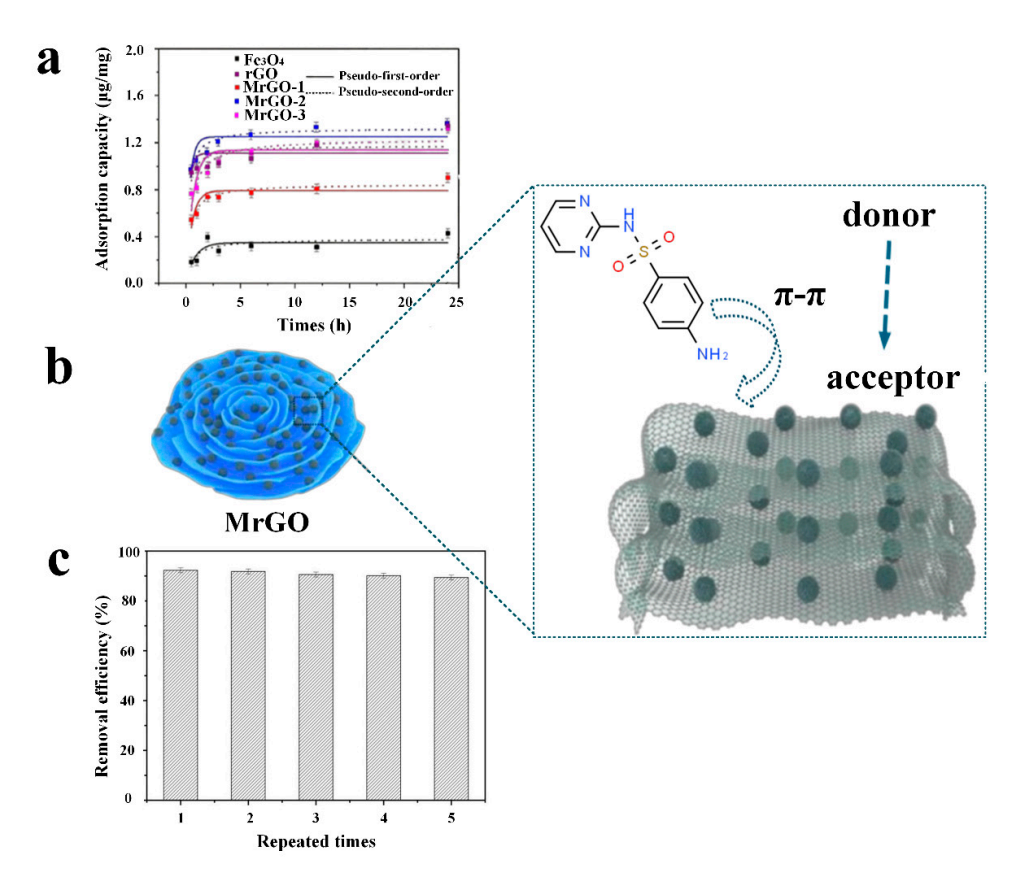


**Figure 12.** (a) Adsorption capacity of varying MrGOs showed better pseudo-second-order model fitting, suggesting chemical and physical adsorption, (b) MrGO's 3D petal-like interconnected structure improves SDZ adsorption. Effective SDZ removal relies on  $\pi$ - $\pi$  electron interaction with rGO during adsorption, (c) recyclability of MrGO-2 [277].

Novel adsorbents have been developed in the search for methods for the effective removal of harmful pesticides and herbicides [289]. The CM-CS-functionalized 3D Gr aerogel facilitates quick and easy glyphosate extraction from water via increased intermolecular contacts, and the CNF/GO hybrid aerogel's extraordinary reusability is due in large part to the reinforcement effects of its hydroxyl bonds [290]. Over a billion people are at risk of exposure to dangerous bacteria and deadly viruses in water, so effective removal solutions are urgently needed [291]. Three-dimensional graphene-based solutions, such as highly porous and lightweight GO foam, provide a formidable response to the aggregation of GO under saline circumstances. Additions to 3D porous GO membranes, such as peptides and glutathione-conjugated CNTs, have potent disinfecting powers against pathogenic microorganisms [292]. Even in low quantities, phenols and amines in environmental fluids are harmful to human health [293]. Table 7 presents a detailed summary of the underlying mechanisms and adsorption capacities of 3D GBCMs for organic pollutants, providing valuable insights for future research and development.

J. Compos. Sci. 2025, 9, 18 38 of 53

**Table 7.** Adsorption performances of diverse organic pollutants onto 3D GBCMs and mechanism analysis.

3D Graphene/Composite Materials	Organic Pollutants	pН	Adsorption Performances	Underlying Mechanism	References
3D GS	o-nitrophenol p-nitrophenol	7	1842 mg/g 879.6 mg/g	London and $\pi$ - $\pi$ , Debye interaction and hydrogen bond	[294]
3D SP-GOs	Bisphenol A (TBHQ) (PAP (PNP)	-	535.79 mg/g 22.17 mg/g 116.4 mg/g 44.78 mg/g	$\pi$ - $\pi$ and hydrogen bonding interactions,  Hydrogen bonding interaction, $\pi$ - $\pi$	[295]
3D GO-MA	(MNP (HQ) (ARS) (NR)	5	36.96 mg/g 16.10 mg/g 39.92 mg/g 24.23 mg/g	stacking interactions, electrostatic interactions, Lewis acid-base interactions	[224]
3D (r-GO-CD)	BPA	7	346.0 mg/g	π- $π$ interaction and hydrogen bonding	[296]
3D GO	Crude oil	-	95%	Physisorption	[297]
3D Ni-rGO	Hemoglobin	7	18,468.6 mg/g	Stronger $\pi$ - $\pi$ stacking interaction	[298]
3DG	Paraquat	6	119 mg/g	Electrostatic attraction, $\pi$ - $\pi$ interactions	[299]
FeNi <sub>3</sub> @3DGr	MG MB	6.4 7.1	100% 97.8%	Electrostatic interaction and $\pi$ - $\pi$ stacking	[287]

As a strategic reaction, hierarchical 3D GA-MS frameworks were developed with a uniform growth of mesoporous silica upon hydrothermally assembled Graphene aerogels that show improved adsorption capacity toward a spectrum of phenols [300]. Figure 13a shows the complex but effective sequence involved in the photocatalytic Fenton processes' synergistic degradation of CuBi<sub>2</sub>O<sub>4</sub>/rGH. Exposure to visible light enhances the catalytic degradation by initiating in situ photocatalytic Fenton reactions. The graphene-excitation of CuBi<sub>2</sub>O<sub>4</sub> causes the electron-hole pairs to rapidly separate, producing active  $\cdot$ O<sub>2</sub> and  $\cdot$ OH from the breakdown of  $H_2O_2$ . Copper-driven electron transfer enhances the photocatalysis and Fenton reaction in the Cu-Fenton system, leading to an increase in ·OH. The further production of ·O<sub>2</sub> results from Cu<sup>+</sup> interacting with molecular oxygen. After reaching adsorption equilibrium, the photocatalytic degradation efficiency was 40%, and the Fenton oxidation efficiency was 70%. In contrast, the combined photocatalysis-Fenton system achieved a 90% degradation rate in 20 min, demonstrating strong synergy (Figure 13b). The composite reached adsorption equilibrium after 40 min, and upon adding H<sub>2</sub>O<sub>2</sub> and light, the degradation efficiency peaked within 20 min, underscoring the importance of H<sub>2</sub>O<sub>2</sub> in the process (Figure 13c) [301]. Their hybridization of rGO and AgBr reveals 3D rGO-encapsulated AgBr hydrogels to be rapid and efficient solutions for the removal of BPA from aqueous solutions [171]. The protection of the environment requires immediate action, as oil spills and microemulsions in water pose a significant threat [302]. In line with this goal, the 3D Gr/GO-based sponges excel as oil absorbents because of graphene's oleophilic characteristic. The versatility and efficiency of 3D graphene materials in addressing a wide range of environmental concerns is highlighted by the fact that a 3D GO sponge was shown to exhibit a significant adsorption capability of 33.0 g/g toward crude oil [297]. Moreover, the revolutionary usage of 3D graphene sponges for the absorption of oils and the production of hydrogels for the fast removal of contaminants from aqueous solutions emphasize their variety of applications, placing 3D graphene as a vital actor in the fight for cleaner, safer water systems.

J. Compos. Sci. 2025, 9, 18 39 of 53

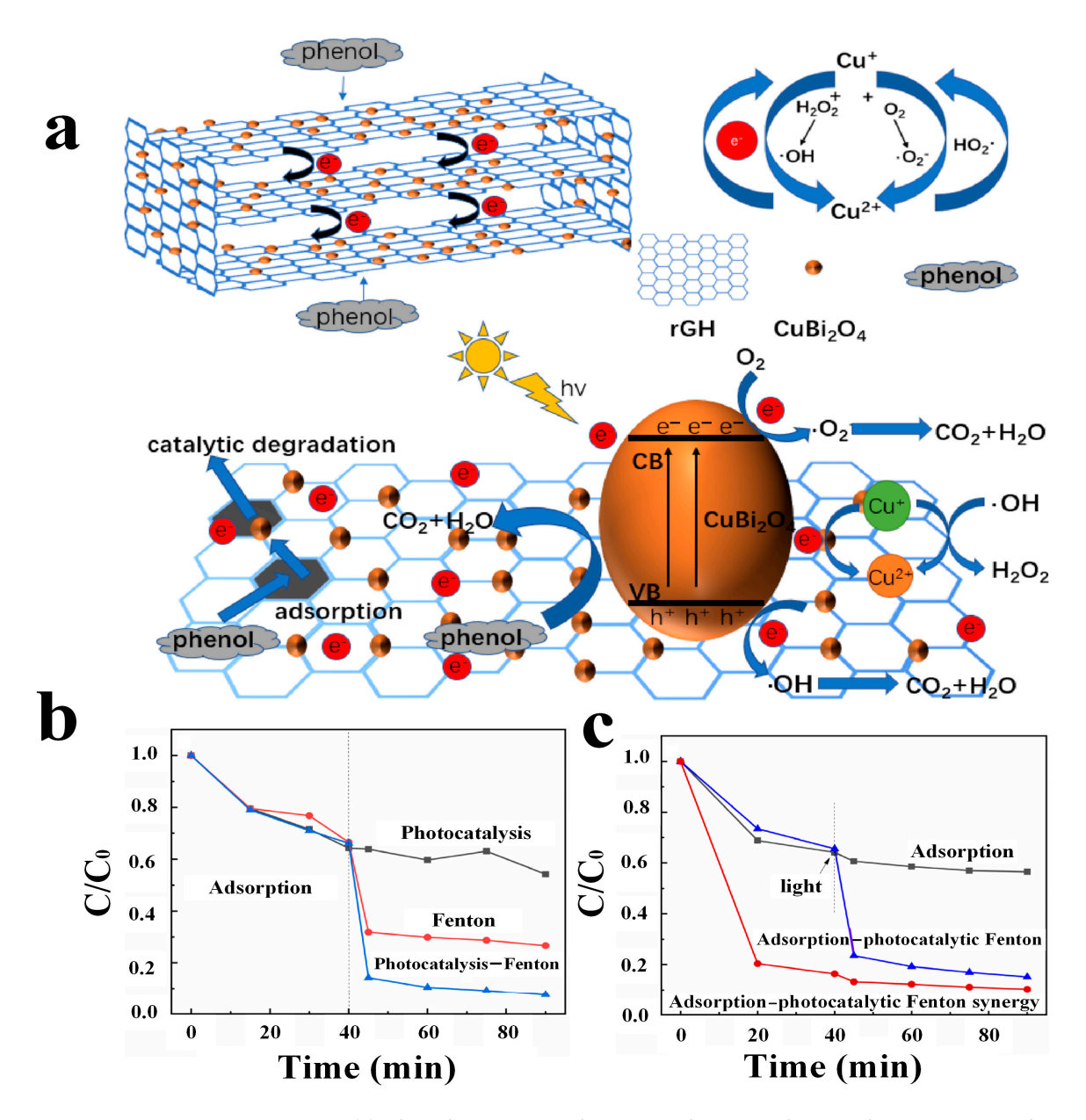


**Figure 13.** (a) The adsorption mechanism and in situ photocatalytic Fenton catalytic degradation of phenol by  $CuBi_2O_4/rGH$ , (b,c) adsorption and catalytic degradation performance of 20%  $CuBi_2O_4/rGH$  for phenol under various conditions [301].

## 8. Conclusive Remarks and Future Horizon

Three-dimensional GBCMs and nanomaterials offer promising solutions to the complex challenges of water pollution. Their versatility, efficiency, and sustainability make them valuable tools for creating clean and safe water sources. Three-dimensional GBCMs can revolutionize water treatment and contribute significantly to the preservation of our environment and the well-being of society. Most of these 3D GBCMs exhibit an absorption-dominated shielding mechanism, which is more acceptable, as reflection-induced secondary pollution is insignificant. There are obstacles and promising novel paths to explore as we look to the future of 3D graphene in wastewater treatment. First and foremost, there is an urgent need for a complete study to seamlessly incorporate the technologies provided by 3D-GBMs into existing water treatment systems due to the promising demonstrations of such technologies in water treatment applications. Second, these materials must be processed on an industrial scale, which is only possible using environmentally friendly

J. Compos. Sci. 2025, 9, 18 40 of 53

synthesis processes that allow for the cost-effective and sustainable manufacturing of 3D GBCMs. The mechanical-shearing exfoliation of graphite in aqueous solutions, a recent development in graphene synthesis, offers a promising route to cost-effective mass manufacturing. This opens the door for the further study of methods that use graphene as a precursor to make 3D GBCMs and other multifunctional macro-sized nanocomposite materials. Many open scientific questions and technical hurdles must be addressed because research on 3D GBCMs is still in its infancy. Research into the contribution of the preparation of catalysts for the adsorption and degradation of organic dyes in wastewater is required. While the research carried out on the composition of 3DGBMs for pollutant removal has been considerable, the morphology of catalysts placed onto graphene sheets has received less attention despite its potential importance. Oil/water separation, dye removal, and photocatalysis are just a few areas where researchers have focused their attention. However, the potential for disinfection and the elimination of persistent organic pollutants remains largely unexplored and demands serious attention. Improving the functionality of 3D GBCMs involves an organized approach that delves into the complex interactions between their structures and their properties. Understanding the basic processes and mechanisms that led to the creation of 3D graphene and 3D printing is crucial, since they are both unique methodologies and potential manufacturing techniques for structural composites for wastewater treatment. In recent years, there has been a rise in research into using 3D graphene as a nano-reinforcement in composites to enhance these materials' mechanical, electrical, and thermal characteristics. Concurrently, ground-breaking research publications have been released on the 3D printing of complex 3D graphene structures [303]. To optimize the structural performance of these materials in critical applications, 3D-printed graphene-reinforced composites hold great promise, but only if 3D graphene with the necessary characteristics is developed. However, significant flaws in this field need to be investigated and resolved before these materials can be effectively applied to environmental applications.

**Author Contributions:** T.S. (Tahreem Shahzad): Investigation, writing—original draft preparation; S.N.: writing—review and editing; H.J.: writing—review and editing; T.S. (Taiba Shahzad): writing—review and editing; F.A.: Supervision, writing—review and editing, funding acquisition; U.K.: Conceptualization, Visualization, Supervision, writing—review and editing, funding acquisition. All authors have read and agreed to the published version of the manuscript.

**Funding:** Urooj Kamran gratefully acknowledges the financial support provided by Luleå University of Technology, Luleå, Sweden, through the Excellent Postdoctoral Fellowship Program (grant number: 228121). Farid Akhtar acknowledges the funding support from Formas, The Swedish Research Council for Sustainable Development (grant number: 2022-01989).

Data Availability Statement: Not applicable.

**Acknowledgments:** The authors extend their gratitude to the University of Narowal, Narowal, Pakistan; University of Padua, Padua, Italy; Daegu Gyeongbuk Institute of Science & Technology, Daegu, Republic of Korea; Luleå University of Technology, Luleå, Sweden; Korea University, Seoul, Republic of Korea for their support, cooperation, and guidance in completion of this review paper.

Conflicts of Interest: The authors declare no conflicts of interest.

## References

- Waheed, A.; Baig, N.; Ullah, N.; Falath, W. Removal of Hazardous Dyes, Toxic Metal Ions and Organic Pollutants from Wastewater by Using Porous Hyper-Cross-Linked Polymeric Materials: A Review of Recent Advances. J. Environ. Manag. 2021, 287, 112360. [CrossRef] [PubMed]
- Ahmadian, M.; Jaymand, M. Interpenetrating Polymer Network Hydrogels for Removal of Synthetic Dyes: A Comprehensive Review. Coord. Chem. Rev. 2023, 486, 215152. [CrossRef]

J. Compos. Sci. 2025, 9, 18 41 of 53

3. Baig, N. Recent Progress on the Development of Superhydrophobic and Superoleophilic Meshes for Oil and Water Separation: A Review. In *Contaminants in Our Water: Identification and Remediation Methods*; ACS Symposium Series; American Chemical Society: Washington, DC, USA, 2020; Volume 1352, pp. 175–196, ISBN 978-0-8412-9894-1.

- 4. Hara, T.O.; Singh, B. Electrochemical Biosensors for Detection of Pesticides and Heavy Metal Toxicants in Water: Recent Trends and Progress. *ACS EST Water* **2021**, *1*, 462–478. [CrossRef]
- 5. Sharma, J.; Sharma, S.; Soni, V. Classification and Impact of Synthetic Textile Dyes on Aquatic Flora: A Review. *Reg. Stud. Mar. Sci.* **2021**, *45*, 101802. [CrossRef]
- 6. Pai, S.; Kini, M.S.; Selvaraj, R. A Review on Adsorptive Removal of Dyes from Wastewater by Hydroxyapatite Nanocomposites. *Environ. Sci. Pollut. Res.* **2021**, *28*, 11835–11849. [CrossRef] [PubMed]
- 7. Maddela, N.R.; Sheng, B.; Yuan, S.; Zhou, Z.; Villamar-Torres, R.; Meng, F. Roles of Quorum Sensing in Biological Wastewater Treatment: A Critical Review. *Chemosphere* **2019**, 221, 616–629. [CrossRef] [PubMed]
- 8. Yadav, D.; Karki, S.; Ingole, P.G. Current Advances and Opportunities in the Development of Nanofiltration (NF) Membranes in the Area of Wastewater Treatment, Water Desalination, Biotechnological and Pharmaceutical Applications. *J. Environ. Chem. Eng.* **2022**, *10*, 108109. [CrossRef]
- 9. Hand, S.; Cusick, R.D. Electrochemical Disinfection in Water and Wastewater Treatment: Identifying Impacts of Water Quality and Operating Conditions on Performance. *Environ. Sci. Technol.* **2021**, *55*, 3470–3482. [CrossRef] [PubMed]
- Chan, S.S.; Khoo, K.S.; Chew, K.W.; Ling, T.C.; Show, P.L. Recent Advances Biodegradation and Biosorption of Organic Compounds from Wastewater: Microalgae-Bacteria Consortium—A Review. *Bioresour. Technol.* 2022, 344, 126159. [CrossRef] [PubMed]
- 11. Lu, Q.; Xu, Q.; Meng, J.; How, Z.T.; Chelme-Ayala, P.; Wang, X.; Gamal El-Din, M.; Zhang, X. Surface Microlenses for Much More Efficient Photodegradation in Water Treatment. *ACS EST Water* **2022**, *2*, 644–657. [CrossRef]
- 12. Ma, X.; Zhao, S.; Tian, Z.; Duan, G.; Pan, H.; Yue, Y.; Li, S.; Jian, S.; Yang, W.; Liu, K.; et al. MOFs Meet Wood: Reusable Magnetic Hydrophilic Composites toward Efficient Water Treatment with Super-High Dye Adsorption Capacity at High Dye Concentration. *Chem. Eng. J.* 2022, 446, 136851. [CrossRef]
- Lan, D.; Zhu, H.; Zhang, J.; Li, S.; Chen, Q.; Wang, C.; Wu, T.; Xu, M. Adsorptive Removal of Organic Dyes via Porous Materials for Wastewater Treatment in Recent Decades: A Review on Species, Mechanisms and Perspectives. Chemosphere 2022, 293, 133464.
   [CrossRef]
- 14. Kamran, U.; Jamal, H.; Siddiqui, M.I.H.; Park, S.-J. Surfactant-Capped Silver-Doped Calcium Oxide Nanocomposite: Efficient Sorbents for Rapid Lithium Uptake and Recovery from Aqueous Media. *Water* 2023, 15, 3368. [CrossRef]
- Kamran, U.; Bhatti, H.N.; Noreen, S.; Tahir, M.A.; Park, S.-J. Chemically Modified Sugarcane Bagasse-Based Biocomposites for Efficient Removal of Acid Red 1 Dye: Kinetics, Isotherms, Thermodynamics, and Desorption Studies. *Chemosphere* 2022, 291, 132796. [CrossRef] [PubMed]
- 16. Kamran, U.; Park, S.-J. Hybrid Biochar Supported Transition Metal Doped MnO<sub>2</sub> Composites: Efficient Contenders for Lithium Adsorption and Recovery from Aqueous Solutions. *Desalination* **2022**, *522*, 115387. [CrossRef]
- 17. Li, W.; Wang, Z.; Li, Y.; Ghasemi, J.B.; Li, J.; Zhang, G. Visible-NIR Light-Responsive 0D/2D CQDs/Sb<sub>2</sub>WO<sub>6</sub> Nanosheets with Enhanced Photocatalytic Degradation Performance of RhB: Unveiling the Dual Roles of CQDs and Mechanism Study. *J. Hazard. Mater.* 2022, 424, 127595. [CrossRef]
- 18. Adel, M.; Ahmed, M.A.; Elabiad, M.A.; Mohamed, A.A. Removal of Heavy Metals and Dyes from Wastewater Using Graphene Oxide-Based Nanomaterials: A Critical Review. *Environ. Nanotechnol. Monit. Manag.* **2022**, *18*, 100719. [CrossRef]
- 19. Kamran, U.; Park, S.-J. Functionalized Titanate Nanotubes for Efficient Lithium Adsorption and Recovery from Aqueous Media. J. Solid State Chem. 2020, 283, 121157. [CrossRef]
- 20. Kumar, S.; Yadav, S.; Kataria, N.; Chauhan, A.K.; Joshi, S.; Gupta, R.; Kumar, P.; Chong, J.W.R.; Khoo, K.S.; Show, P.L. Recent Advancement in Nanotechnology for the Treatment of Pharmaceutical Wastewater: Sources, Toxicity, and Remediation Technology. *Curr. Pollut. Rep.* 2023, 9, 110–142. [CrossRef]
- 21. Abdullah, F.H.; Bakar, N.H.H.A.; Bakar, M.A. Current Advancements on the Fabrication, Modification, and Industrial Application of Zinc Oxide as Photocatalyst in the Removal of Organic and Inorganic Contaminants in Aquatic Systems. *J. Hazard. Mater.* 2022, 424, 127416. [CrossRef] [PubMed]
- 22. Kamran, U.; Heo, Y.-J.; Min, B.-G.; In, I.; Park, S.-J. Effect of Nickel Ion Doping in MnO<sub>2</sub>/Reduced Graphene Oxide Nanocomposites for Lithium Adsorption and Recovery from Aqueous Media. *RSC Adv.* **2020**, *10*, 9245–9257. [CrossRef] [PubMed]
- Zafar, L.; Khan, A.; Kamran, U.; Park, S.-J.; Bhatti, H.N. Eucalyptus (Camaldulensis) Bark-Based Composites for Efficient Basic Blue 41 Dye Biosorption from Aqueous Stream: Kinetics, Isothermal, and Thermodynamic Studies. Surf. Interfaces 2022, 31, 101897.
   [CrossRef]
- Ahmadijokani, F.; Molavi, H.; Bahi, A.; Wuttke, S.; Kamkar, M.; Rojas, O.J.; Ko, F.; Arjmand, M. Electrospun Nanofibers of Chitosan/Polyvinyl Alcohol/UiO-66/Nanodiamond: Versatile Adsorbents for Wastewater Remediation and Organic Dye Removal. Chem. Eng. J. 2023, 457, 141176. [CrossRef]

J. Compos. Sci. **2025**, 9, 18 42 of 53

25. Manikandan, S.; Subbaiya, R.; Saravanan, M.; Ponraj, M.; Selvam, M.; Pugazhendhi, A. A Critical Review of Advanced Nanotechnology and Hybrid Membrane Based Water Recycling, Reuse, and Wastewater Treatment Processes. *Chemosphere* 2022, 289, 132867. [CrossRef] [PubMed]

- 26. Kamran, U.; Bhatti, H.N.; Iqbal, M.; Jamil, S.; Zahid, M. Biogenic Synthesis, Characterization and Investigation of Photocatalytic and Antimicrobial Activity of Manganese Nanoparticles Synthesized from *Cinnamomum verum* Bark Extract. *J. Mol. Struct.* **2019**, 1179, 532–539. [CrossRef]
- 27. Khanna, N.; Singh, S.; Chatterji, T. Potential Application of Nanotechnology in Wastewater Management: A Paradigm Shift. *Mater. Lett.* **2022**, *315*, 131975. [CrossRef]
- 28. Yu, S.; Tang, H.; Zhang, D.; Wang, S.; Qiu, M.; Song, G.; Fu, D.; Hu, B.; Wang, X. MXenes as Emerging Nanomaterials in Water Purification and Environmental Remediation. *Sci. Total Environ.* **2022**, *811*, 152280. [CrossRef]
- 29. Corsi, I.; Venditti, I.; Trotta, F.; Punta, C. Environmental Safety of Nanotechnologies: The Eco-Design of Manufactured Nanomaterials for Environmental Remediation. *Sci. Total Environ.* **2023**, *864*, 161181. [CrossRef]
- 30. Saravanan, A.; Kumar, P.S.; Hemavathy, R.V.; Jeevanantham, S.; Jawahar, M.J.; Neshaanthini, J.P.; Saravanan, R. A Review on Synthesis Methods and Recent Applications of Nanomaterial in Wastewater Treatment: Challenges and Future Perspectives. *Chemosphere* 2022, 307, 135713. [CrossRef]
- 31. Kamath, S.V.; Mruthunjayappa, M.H.; Mondal, D.; Kotrappanavar, N.S. Nanocomposite-Based High-Performance Adsorptive Water Filters: Recent Advances, Limitations, Nanotoxicity and Environmental Implications. *Environ. Sci. Nano* 2022, *9*, 2320–2341. [CrossRef]
- 32. Saeed, K.; Kamran, U.; Khan, A.; Jamal, H.; Bhatti, H.N. Conversion of Phaseolus Vulgaris into Chemically Functionalized Biocomposites for Efficient Methylene Blue Removal: Kinetics, Isothermal, and Thermodynamics Analysis. *New J. Chem.* 2023, 47, 14157–14168. [CrossRef]
- 33. Baaloudj, O.; Badawi, A.K.; Kenfoud, H.; Benrighi, Y.; Hassan, R.; Nasrallah, N.; Assadi, A.A. Techno-Economic Studies for a Pilot-Scale Bi<sub>12</sub>TiO<sub>20</sub> Based Photocatalytic System for Pharmaceutical Wastewater Treatment: From Laboratory Studies to Commercial-Scale Applications. *J. Water Process Eng.* **2022**, *48*, 102847. [CrossRef]
- 34. Vatanpour, V.; Jouyandeh, M.; Akhi, H.; Mousavi Khadem, S.S.; Ganjali, M.R.; Moradi, H.; Mirsadeghi, S.; Badiei, A.; Esmaeili, A.; Rabiee, N.; et al. Hyperbranched Polyethylenimine Functionalized Silica/Polysulfone Nanocomposite Membranes for Water Purification. *Chemosphere* **2022**, 290, 133363. [CrossRef] [PubMed]
- 35. Gouda, M.H.; Elessawy, N.A.; Toghan, A. Development of Hybrid Green Nanocomposite Polymeric Beads Doped with Nano Sulfated Zirconia for Effective Removal of Cefotaxime Antibiotic from Aqueous Solution. *Sci. Rep.* **2022**, *12*, 12701. [CrossRef] [PubMed]
- 36. Fu, W.; Tang, T.; Chen, X.; Yang, Y.; Mi, B.; Yang, K.; Xu, X.; Zhang, X. Nano-Ceramic Membranes Combined with Ozonation for Water Treatment: Fundamentals and Engineering Applications. *J. Hazard. Mater. Adv.* **2023**, *10*, 100279. [CrossRef]
- 37. Li, W.; Feng, W.; Wu, S.; Wang, W.; Yu, D. Synergy of Photothermal Effect in Integrated 0D Ti<sub>2</sub>O<sub>3</sub> Nanoparticles/1D Carboxylated Carbon Nanotubes for Multifunctional Water Purification. *Sep. Purif. Technol.* **2022**, 292, 120989. [CrossRef]
- 38. Zhang, W.; Zhang, Z.; Ji, L.; Lu, Z.; Liu, R.; Nian, B.; Hu, Y. Laccase Immobilized on Nanocomposites for Wastewater Pollutants Degradation: Current Status and Future Prospects. *Bioprocess. Biosyst. Eng.* **2023**, *46*, 1513–1531. [CrossRef] [PubMed]
- 39. Ghosal, P.; Gupta, B.; Ambekar, R.S.; Rahman, M.M.; Ajayan, P.M.; Aich, N.; Gupta, A.K.; Tiwary, C.S. 3D Printed Materials in Water Treatment Applications. *Adv. Sustain. Syst.* **2022**, *6*, 2100282. [CrossRef]
- 40. Yousefi, N.; Lu, X.; Elimelech, M.; Tufenkji, N. Environmental Performance of Graphene-Based 3D Macrostructures. *Nat. Nanotechnol.* **2019**, *14*, 107–119. [CrossRef]
- 41. Wang, H.; Mi, X.; Li, Y.; Zhan, S. 3D Graphene-Based Macrostructures for Water Treatment. *Adv. Mater.* **2020**, 32, 1806843. [CrossRef] [PubMed]
- 42. Quan, Z.; Larimore, Z.; Wu, A.; Yu, J.; Qin, X.; Mirotznik, M.; Suhr, J.; Byun, J.-H.; Oh, Y.; Chou, T.-W. Microstructural Design and Additive Manufacturing and Characterization of 3D Orthogonal Short Carbon Fiber/Acrylonitrile-Butadiene-Styrene Preform and Composite. *Compos. Sci. Technol.* **2016**, 126, 139–148. [CrossRef]
- 43. Liu, Y.; Li, F.; Xia, Q.; Wu, J.; Liu, J.; Huang, M.; Xie, J. Conductive 3D Sponges for Affordable and Highly-Efficient Water Purification. *Nanoscale* **2018**, *10*, 4771–4778. [CrossRef] [PubMed]
- 44. Zhang, X.N.; Zheng, Q.; Wu, Z.L. Recent Advances in 3D Printing of Tough Hydrogels: A Review. *Compos. Part B Eng.* **2022**, 238, 109895. [CrossRef]
- 45. Ang, Z.R.; Kong, I.; Lee, R.S.Y.; Kong, C.; Kakarla, A.B.; Chai, A.B.; Kong, W. Preparation of 3D Graphene-Carbon Nanotube-Magnetic Hybrid Aerogels for Dye Adsorption. *New Carbon Mater.* **2022**, *37*, 424–432. [CrossRef]
- 46. Liang, W.; Wang, B.; Cheng, J.; Xiao, D.; Xie, Z.; Zhao, J. 3D, Eco-Friendly Metal-Organic Frameworks@carbon Nanotube Aerogels Composite Materials for Removal of Pesticides in Water. *J. Hazard. Mater.* 2021, 401, 123718. [CrossRef] [PubMed]
- 47. Liu, H.; Qiu, H. Recent Advances of 3D Graphene-Based Adsorbents for Sample Preparation of Water Pollutants: A Review. *Chem. Eng. J.* 2020, 393, 124691. [CrossRef]

J. Compos. Sci. 2025, 9, 18 43 of 53

48. Wang, J.; Duan, X.; Dong, Q.; Meng, F.; Tan, X.; Liu, S.; Wang, S. Facile Synthesis of N-Doped 3D Graphene Aerogel and Its Excellent Performance in Catalytic Degradation of Antibiotic Contaminants in Water. *Carbon* **2019**, *144*, 781–790. [CrossRef]

- 49. Tee, W.T.; Yong, J.E.; Chua, J.; Loh, N.Y.L.; Hiew, B.Y.Z.; Gan, S.; Lee, L.Y. A High-Performance 3D Phosphorus-Doped Graphene Oxide Adsorbent for Imipramine Wastewater Treatment. *Sep. Purif. Technol.* **2024**, *330*, 125266. [CrossRef]
- 50. Liu, T.; Liu, X.; Graham, N.; Yu, W.; Sun, K. Two-Dimensional MXene Incorporated Graphene Oxide Composite Membrane with Enhanced Water Purification Performance. *J. Membr. Sci.* **2020**, *593*, 117431. [CrossRef]
- 51. Brown, B.; Swain, B.; Hiltwine, J.; Brooks, D.B.; Zhou, Z. Carbon Nanosheet Buckypaper: A Graphene-Carbon Nanotube Hybrid Material for Enhanced Supercapacitor Performance. *J. Power Sources* **2014**, 272, 979–986. [CrossRef]
- 52. Pei, S.; Cheng, H.-M. The Reduction of Graphene Oxide. Carbon 2012, 50, 3210–3228. [CrossRef]
- 53. Wang, J.; Ellsworth, M. Graphene Aerogels. ECS Trans. 2009, 19, 241. [CrossRef]
- 54. Xu, Y.; Sheng, K.; Li, C.; Shi, G. Self-Assembled Graphene Hydrogel via a One-Step Hydrothermal Process. *ACS Nano* **2010**, *4*, 4324–4330. [CrossRef]
- 55. Worsley, M.A.; Olson, T.Y.; Lee, J.R.I.; Willey, T.M.; Nielsen, M.H.; Roberts, S.K.; Pauzauskie, P.J.; Biener, J.; Satcher, J.H., Jr.; Baumann, T.F. High Surface Area, sp<sup>2</sup>-Cross-Linked Three-Dimensional Graphene Monoliths. *J. Phys. Chem. Lett.* **2011**, *2*, 921–925. [CrossRef] [PubMed]
- 56. Chen, Z.; Ren, W.; Gao, L.; Liu, B.; Pei, S.; Cheng, H.-M. Three-Dimensional Flexible and Conductive Interconnected Graphene Networks Grown by Chemical Vapour Deposition. *Nat. Mater.* **2011**, *10*, 424–428. [CrossRef] [PubMed]
- 57. Wang, H.; Sun, K.; Tao, F.; Stacchiola, D.J.; Hu, Y.H. 3D Honeycomb-Like Structured Graphene and Its High Efficiency as a Counter-Electrode Catalyst for Dye-Sensitized Solar Cells. *Angew. Chem. Int. Ed.* **2013**, 52, 9210–9214. [CrossRef] [PubMed]
- 58. Liu, J.; Rinzler, A.G.; Dai, H.; Hafner, J.H.; Bradley, R.K.; Boul, P.J.; Lu, A.; Iverson, T.; Shelimov, K.; Huffman, C.B.; et al. Fullerene Pipes. *Science* 1998, 280, 1253–1256. [CrossRef]
- 59. Singh, M.; Dawsey, T.; Gupta, R.K. Recent Advancement in 3D Graphene for Metal-Sulfur Batteries. *J. Energy Storage* **2023**, 73, 109059. [CrossRef]
- 60. Cao, M.; Su, J.; Fan, S.; Qiu, H.; Su, D.; Li, L. Wearable Piezoresistive Pressure Sensors Based on 3D Graphene. *Chem. Eng. J.* **2021**, 406, 126777. [CrossRef]
- 61. Tee, W.T.; Loh, N.Y.L.; Lai, K.C.; Hiew, B.Y.Z.; Gan, S.; Lee, L.Y. Application of 3D Heteroatom-Doped Graphene in Adsorptive Removal of Water Pollutants: Review on Hydrothermal Synthesis and Its Influencing Factors. Sep. Purif. Technol. 2023, 320, 124072. [CrossRef]
- 62. Han, M.; Mu, Y.; Yuan, F.; Liang, J.; Jiang, T.; Bai, X.; Yu, J. Vertical Graphene Growth on Uniformly Dispersed Sub-Nanoscale SiO<sub>x</sub>/N-Doped Carbon Composite Microspheres with a 3D Conductive Network and an Ultra-Low Volume Deformation for Fast and Stable Lithium-Ion Storage. *J. Mater. Chem. A* **2020**, *8*, 3822–3833. [CrossRef]
- 63. Alencar, L.M.; Silva, A.W.B.N.; Trindade, M.A.G.; Salvatierra, R.V.; Martins, C.A.; Souza, V.H.R. One-Step Synthesis of Crumpled Graphene Fully Decorated by Copper-Based Nanoparticles: Application in H<sub>2</sub>O<sub>2</sub> Sensing. *Sens. Actuators B Chem.* **2022**, 360, 131649. [CrossRef]
- 64. Xiao, J.; Han, J.; Kong, D.; Shi, H.; Du, X.; Zhao, Z.; Chen, F.; Lan, P.; Wu, S.; Zhang, Y.; et al. "Nano-Spring" Confined in a Shrinkable Graphene Cage towards Self-Adaptable High-Capacity Anodes. *Energy Storage Mater.* 2022, 50, 554–562. [CrossRef]
- 65. Sun, Z.; Fang, S.; Hu, Y.H. 3D Graphene Materials: From Understanding to Design and Synthesis Control. *Chem. Rev.* **2020**, 120, 10336–10453. [CrossRef] [PubMed]
- 66. Wei, W.; Sun, K.; Hu, Y.H. Synthesis of 3D Cauliflower-Fungus-like Graphene from CO<sub>2</sub> as a Highly Efficient Counter Electrode Material for Dye-Sensitized Solar Cells. *J. Mater. Chem. A* **2014**, *2*, 16842–16846. [CrossRef]
- 67. Li, Z.; Gadipelli, S.; Yang, Y.; Guo, Z. Design of 3D Graphene-Oxide Spheres and Their Derived Hierarchical Porous Structures for High Performance Supercapacitors. *Small* **2017**, *13*, 1702474. [CrossRef] [PubMed]
- 68. Wen, X.; Xiang, K.; Zhu, Y.; Xiao, L.; Liao, H.; Chen, W.; Chen, X.; Chen, H. 3D Hierarchical Nitrogen-Doped Graphene/CNTs Microspheres as a Sulfur Host for High-Performance Lithium-Sulfur Batteries. *J. Alloys Compd.* **2020**, *815*, 152350. [CrossRef]
- 69. Zhang, E.; Liu, W.; Liu, X.; Zhao, Z.; Yang, Y. A Facile Route to Prepare Nitrogen-Doped Carbon Microspheres/Graphene Aerogel with High Compressibility and Superior Capacitive Property. *Mater. Today Commun.* **2020**, 24, 101125. [CrossRef]
- 70. Lungu, A.; Cernencu, A.I.; Vlasceanu, G.M.; Florea, N.M.; Ionita, M.; Iovu, H. 3D POSS Cages Decorated 2D Graphenic Sheets: A Versatile Platform for Silicon-Carbonaceous Nano-Additives Design. *Compos. Part B Eng.* **2021**, 207, 108578. [CrossRef]
- 71. Cao, X.; Pan, A.; Liu, S.; Zhou, J.; Li, S.; Cao, G.; Liu, J.; Liang, S. Chemical Synthesis of 3D Graphene-Like Cages for Sodium-Ion Batteries Applications. *Adv. Energy Mater.* **2017**, *7*, 1700797. [CrossRef]
- 72. Yuan, Y.; Tan, G.; Wen, J.; Lu, J.; Ma, L.; Liu, C.; Zuo, X.; Shahbazian-Yassar, R.; Wu, T.; Amine, K. Encapsulating Various Sulfur Allotropes within Graphene Nanocages for Long-Lasting Lithium Storage. *Adv. Funct. Mater.* **2018**, *28*, 1706443. [CrossRef]
- 73. Mathew, E.E.; Balachandran, M. Crumpled and Porous Graphene for Supercapacitor Applications: A Short Review. *Carbon Lett.* **2021**, *31*, 537–555. [CrossRef]

J. Compos. Sci. 2025, 9, 18 44 of 53

74. Fu, H.; Cai, H.; Gray, K.A. Metal Oxide Encapsulated by 3D Graphene Oxide Creates a Nanocomposite with Enhanced Organic Adsorption in Aqueous Solution. *J. Hazard. Mater.* **2023**, 444, 130340. [CrossRef] [PubMed]

- 75. Boruah, P.K.; Borthakur, P.; Neog, G.; Le Ouay, B.; Afzal, N.U.; Manna, P.; Das, M.R. Porous Nitrogen-Doped Crumpled Graphene Nanoparticles: A Metal-Free Nanozyme for Selective Detection of Dopamine in Aqueous Medium and Human Serum. *ACS Appl. Nano Mater.* 2023, 6, 1667–1677. [CrossRef]
- 76. Liu, Y.; Yang, L.; Xie, B.; Zhao, N.; Yang, L.; Zhan, F.; Pan, Q.; Han, J.; Wang, X.; Liu, J.; et al. Ultrathin Co<sub>3</sub>O<sub>4</sub> Nanosheet Clusters Anchored on Nitrogen Doped Carbon Nanotubes/3D Graphene as Binder-Free Cathodes for Al-Air Battery. *Chem. Eng. J.* **2020**, 381, 122681. [CrossRef]
- 77. Memisoglu, G.; Murugesan, R.C.; Zubia, J.; Rozhin, A.G. Graphene Nanocomposite Membranes: Fabrication and Water Treatment Applications. *Membranes* **2023**, *13*, 145. [CrossRef]
- 78. Aslam, M.M.-A.; Kuo, H.-W.; Den, W.; Usman, M.; Sultan, M.; Ashraf, H. Functionalized Carbon Nanotubes (CNTs) for Water and Wastewater Treatment: Preparation to Application. *Sustainability* **2021**, *13*, 5717. [CrossRef]
- 79. Gao, S.; Liu, W.; Wang, M.; Zhao, Z.; Liu, X. A Three-Dimensional in-Situ Self-Electrolysis System Based on Ni<sub>3</sub>(HITP)<sub>2</sub>/Graphene-Based Composite Aerogel Particle Electrodes for Efficient Deep Removal of Phenol from Coking Wastewater. *Appl. Catal. B Environ.* 2024, 340, 123276. [CrossRef]
- 80. Wang, X.; Zhang, J.; Wang, H.; Liang, M.; Wang, Q.; Chen, F. Revealing the Role of Defect in 3D Graphene-Based Photocatalytic Composite for Efficient Elimination of Antibiotic and Heavy Metal Combined Pollution. *Energy Environ. Mater.* **2023**, 7, e12616. [CrossRef]
- 81. Fung, K.; Li, Y.; Fan, S.; Fajrial, A.K.; Ding, Y.; Ding, X. Acoustically Excited Microstructure for On-Demand Fouling Mitigation in a Microfluidic Membrane Filtration Device. *J. Membr. Sci. Lett.* **2022**, *2*, 100012. [CrossRef]
- 82. Caudill, C.; Perry, J.L.; Iliadis, K.; Tessema, A.T.; Lee, B.J.; Mecham, B.S.; Tian, S.; DeSimone, J.M. Transdermal Vaccination via 3D-Printed Microneedles Induces Potent Humoral and Cellular Immunity. *Proc. Natl. Acad. Sci. USA* **2021**, *118*, e2102595118. [CrossRef] [PubMed]
- 83. Lin, Y.; Dylla, M.T.; Kuo, J.J.; Male, J.P.; Kinloch, I.A.; Freer, R.; Snyder, G.J. Graphene/Strontium Titanate: Approaching Single Crystal–Like Charge Transport in Polycrystalline Oxide Perovskite Nanocomposites through Grain Boundary Engineering. *Adv. Funct. Mater.* 2020, 30, 1910079. [CrossRef]
- 84. Nam, W.H.; Kim, B.B.; Seo, S.G.; Lim, Y.S.; Kim, J.-Y.; Seo, W.-S.; Choi, W.K.; Park, H.-H.; Lee, J.Y. Structurally Nanocrystalline-Electrically Single Crystalline ZnO-Reduced Graphene Oxide Composites. *Nano Lett.* **2014**, *14*, 5104–5109. [CrossRef]
- 85. Peng, G.; Xiang, M.; Wang, W.; Su, Z.; Liu, H.; Mao, Y.; Chen, Y.; Zhang, P. Engineering 3D Graphene-like Carbon-Assembled Layered Double Oxide for Efficient Microplastic Removal in a Wide pH Range. *J. Hazard. Mater.* **2022**, 433, 128672. [CrossRef] [PubMed]
- 86. Long, S.; Wang, H.; He, K.; Zhou, C.; Zeng, G.; Lu, Y.; Cheng, M.; Song, B.; Yang, Y.; Wang, Z.; et al. 3D Graphene Aerogel Based Photocatalysts: Synthesized, Properties, and Applications. *Colloids Surf. A Physicochem. Eng. Asp.* **2020**, 594, 124666. [CrossRef]
- 87. Idowu, A.; Boesl, B.; Agarwal, A. 3D Graphene Foam-Reinforced Polymer Composites—A Review. *Carbon* **2018**, *135*, 52–71. [CrossRef]
- 88. Li, J.; Zhao, X.; Wu, W.; Ji, X.; Lu, Y.; Zhang, L. Bubble-Templated rGO-Graphene Nanoplatelet Foams Encapsulated in Silicon Rubber for Electromagnetic Interference Shielding and High Thermal Conductivity. *Chem. Eng. J.* **2021**, *415*, 129054. [CrossRef]
- 89. Chhetri, S.; Kuila, T. Polymer Composites with 3D Graphene Architectures as High-Performance EMI Shielding Materials: A Review. RSC Appl. Polym. 2024, 2, 507–533. [CrossRef]
- 90. Zhang, X.; Zhang, T.; Wang, Z.; Ren, Z.; Yan, S.; Duan, Y.; Zhang, J. Ultralight, Superelastic, and Fatigue-Resistant Graphene Aerogel Templated by Graphene Oxide Liquid Crystal Stabilized Air Bubbles. *ACS Appl. Mater. Interfaces* **2019**, *11*, 1303–1310. [CrossRef] [PubMed]
- 91. Yang, H.; Li, Z.; Lu, B.; Gao, J.; Jin, X.; Sun, G.; Zhang, G.; Zhang, P.; Qu, L. Reconstruction of Inherent Graphene Oxide Liquid Crystals for Large-Scale Fabrication of Structure-Intact Graphene Aerogel Bulk toward Practical Applications. *ACS Nano* 2018, 12, 11407–11416. [CrossRef]
- 92. Huang, H.; Chen, P.; Zhang, X.; Lu, Y.; Zhan, W. Edge-to-Edge Assembled Graphene Oxide Aerogels with Outstanding Mechanical Performance and Superhigh Chemical Activity. *Small* **2013**, *9*, 1397–1404. [CrossRef]
- 93. Ye, S.; Liu, Y.; Feng, J. Low-Density, Mechanical Compressible, Water-Induced Self-Recoverable Graphene Aerogels for Water Treatment. *ACS Appl. Mater. Interfaces* **2017**, *9*, 22456–22464. [CrossRef] [PubMed]
- 94. Worsley, M.A.; Pauzauskie, P.J.; Olson, T.Y.; Biener, J.; Satcher, J.H., Jr.; Baumann, T.F. Synthesis of Graphene Aerogel with High Electrical Conductivity. *J. Am. Chem. Soc.* **2010**, *132*, 14067–14069. [CrossRef] [PubMed]
- 95. Weng, D.; Song, L.; Li, W.; Yan, J.; Chen, L.; Liu, Y. Review on Synthesis of Three-Dimensional Graphene Skeletons and Their Absorption Performance for Oily Wastewater. *Environ. Sci. Pollut. Res.* **2021**, *28*, 16–34. [CrossRef]
- 96. Chowdhury, S.; Balasubramanian, R. Three-Dimensional Graphene-Based Macrostructures for Sustainable Energy Applications and Climate Change Mitigation. *Prog. Mater. Sci.* **2017**, *90*, 224–275. [CrossRef]

J. Compos. Sci. 2025, 9, 18 45 of 53

97. Fang, Q.; Shen, Y.; Chen, B. Synthesis, Decoration and Properties of Three-Dimensional Graphene-Based Macrostructures: A Review. *Chem. Eng. J.* **2015**, 264, 753–771. [CrossRef]

- 98. Hirani, R.A.K.; Asif, A.H.; Rafique, N.; Shi, L.; Zhang, S.; Wu, H.; Sun, H. Wastewater Remediation Technologies Using Macroscopic Graphene-Based Materials: A Perspective. *Front. Nanotechnol.* **2021**, *3*, 688552. [CrossRef]
- 99. Shehzad, K.; Xu, Y.; Gao, C.; Duan, X. Three-Dimensional Macro-Structures of Two-Dimensional Nanomaterials. *Chem. Soc. Rev.* **2016**, *45*, 5541–5588. [CrossRef]
- 100. Singh, R.; Ullah, S.; Rao, N.; Singh, M.; Patra, I.; Darko, D.A.; Issac, C.P.J.; Esmaeilzadeh-Salestani, K.; Kanaoujiya, R.; Vijayan, V. Synthesis of Three-Dimensional Reduced-Graphene Oxide from Graphene Oxide. *J. Nanomater.* **2022**, 2022, e8731429. [CrossRef]
- 101. Aboutalebi, S.H.; Gudarzi, M.M.; Zheng, Q.B.; Kim, J.-K. Spontaneous Formation of Liquid Crystals in Ultralarge Graphene Oxide Dispersions. *Adv. Funct. Mater.* **2011**, 21, 2978–2988. [CrossRef]
- 102. Kavadiya, S.; Raliya, R.; Schrock, M.; Biswas, P. Crumpling of Graphene Oxide through Evaporative Confinement in Nanodroplets Produced by Electrohydrodynamic Aerosolization. *J. Nanoparticle Res.* **2017**, *19*, 43. [CrossRef]
- 103. Hensleigh, R.M.; Cui, H.; Oakdale, J.S.; Ye, J.C.; Campbell, P.G.; Duoss, E.B.; Spadaccini, C.M.; Zheng, X.; Worsley, M.A. Additive Manufacturing of Complex Micro-Architected Graphene Aerogels. *Mater. Horiz.* **2018**, *5*, 1035–1041. [CrossRef]
- 104. Yu, Z.; Wei, L.; Lu, L.; Shen, Y.; Zhang, Y.; Wang, J.; Tan, X. Structural Manipulation of 3D Graphene-Based Macrostructures for Water Purification. *Gels* **2022**, *8*, 622. [CrossRef] [PubMed]
- 105. Huang, Y.; Tang, Y.; Mai, Y.; Wang, X.; Wang, C.; Han, S.; Zhang, F.; Wu, D.; Feng, X. Three-Dimensional Carbon Nitride/Graphene Framework as a High-Performance Cathode for Lithium-Ion Batteries. *Chem. Asian J.* **2016**, *11*, 1194–1198. [CrossRef]
- 106. Xu, Y.; Shi, G.; Duan, X. Self-Assembled Three-Dimensional Graphene Macrostructures: Synthesis and Applications in Supercapacitors. *Acc. Chem. Res.* **2015**, *48*, 1666–1675. [CrossRef] [PubMed]
- 107. Li, J.; Ji, B.; Jiang, R.; Zhang, P.; Chen, N.; Zhang, G.; Qu, L. Hierarchical Hole-Enhanced 3D Graphene Assembly for Highly Efficient Capacitive Deionization. *Carbon* **2018**, *129*, 95–103. [CrossRef]
- 108. Hiew, B.Y.Z.; Lee, L.Y.; Lee, X.J.; Thangalazhy-Gopakumar, S.; Gan, S.; Lim, S.S.; Pan, G.-T.; Yang, T.C.-K.; Chiu, W.S.; Khiew, P.S. Review on Synthesis of 3D Graphene-Based Configurations and Their Adsorption Performance for Hazardous Water Pollutants. *Process Saf. Environ. Prot.* 2018, 116, 262–286. [CrossRef]
- 109. Li, Y.; Chen, N.; Li, Z.; Shao, H.; Sun, X.; Liu, F.; Liu, X.; Guo, Q.; Qu, L. Reborn Three-Dimensional Graphene with Ultrahigh Volumetric Desalination Capacity. *Adv. Mater.* **2021**, *33*, 2105853. [CrossRef] [PubMed]
- 110. Li, H.; Jia, D.; Ding, M.; Zhou, L.; Wang, K.; Liu, J.; Liu, C.-Y.; Li, C. Robust 3D Graphene/Cellulose Nanocrystals Hybrid Lamella Network for Stable and Highly Efficient Solar Desalination. *Sol. RRL* **2021**, *5*, 2100317. [CrossRef]
- 111. He, K.; Chen, G.; Zeng, G.; Chen, A.; Huang, Z.; Shi, J.; Huang, T.; Peng, M.; Hu, L. Three-Dimensional Graphene Supported Catalysts for Organic Dyes Degradation. *Appl. Catal. B Environ.* **2018**, 228, 19–28. [CrossRef]
- 112. Qiu, B.; Xing, M.; Zhang, J. Recent Advances in Three-Dimensional Graphene Based Materials for Catalysis Applications. *Chem. Soc. Rev.* **2018**, 47, 2165–2216. [CrossRef]
- 113. Liu, Y.; Miao, W.; Feng, Y.; Fang, X.; Li, Q.; Du, N.; Wang, D.; Mao, S. Enhanced Peroxydisulfate Oxidation via Cu(III) Species with a Cu-MOF-Derived Cu Nanoparticle and 3D Graphene Network. *J. Hazard. Mater.* **2021**, *403*, 123691. [CrossRef] [PubMed]
- 114. Kong, Q.; Shi, X.; Ma, W.; Zhang, F.; Yu, T.; Zhao, F.; Zhao, D.; Wei, C. Strategies to Improve the Adsorption Properties of Graphene-Based Adsorbent towards Heavy Metal Ions and Their Compound Pollutants: A Review. *J. Hazard. Mater.* 2021, 415, 125690. [CrossRef] [PubMed]
- 115. Saxena, R.; Saxena, M.; Lochab, A. Recent Progress in Nanomaterials for Adsorptive Removal of Organic Contaminants from Wastewater. *ChemistrySelect* **2020**, *5*, 335–353. [CrossRef]
- 116. Shen, Y.; Fang, Q.; Chen, B. Environmental Applications of Three-Dimensional Graphene-Based Macrostructures: Adsorption, Transformation, and Detection. *Environ. Sci. Technol.* **2015**, *49*, 67–84. [CrossRef] [PubMed]
- 117. Jiang, W.; Cui, W.-R.; Liang, R.-P.; Qiu, J.-D. Zwitterionic Surface Charge Regulation in Ionic Covalent Organic Nanosheets: Synergistic Adsorption of Fluoroquinolone Antibiotics. *Chem. Eng. J.* **2021**, *417*, 128034. [CrossRef]
- 118. Suresh Kumar, P.; Korving, L.; Keesman, K.J.; van Loosdrecht, M.C.M.; Witkamp, G.-J. Effect of Pore Size Distribution and Particle Size of Porous Metal Oxides on Phosphate Adsorption Capacity and Kinetics. *Chem. Eng. J.* **2019**, *358*, 160–169. [CrossRef]
- 119. Li, X.; Zhang, L.; Yang, Z.; Wang, P.; Yan, Y.; Ran, J. Adsorption Materials for Volatile Organic Compounds (VOCs) and the Key Factors for VOCs Adsorption Process: A Review. *Sep. Purif. Technol.* **2020**, *235*, 116213. [CrossRef]
- 120. Kumar, P.S.; Prot, T.; Korving, L.; Keesman, K.J.; Dugulan, I.; van Loosdrecht, M.C.M.; Witkamp, G.-J. Effect of Pore Size Distribution on Iron Oxide Coated Granular Activated Carbons for Phosphate Adsorption—Importance of Mesopores. *Chem. Eng. J.* 2017, 326, 231–239. [CrossRef]
- 121. Lin, Y.; Tian, Y.; Sun, H.; Hagio, T. Progress in Modifications of 3D Graphene-Based Adsorbents for Environmental Applications. *Chemosphere* **2021**, 270, 129420. [CrossRef] [PubMed]
- 122. Bai, J.; Zhou, A.; Huang, Z.; Wu, J.; Bai, H.; Li, L. Ultra-Light and Elastic Graphene Foams with a Hierarchical Structure and a High Oil Absorption Capacity. *J. Mater. Chem. A* 2015, 3, 22687–22694. [CrossRef]

J. Compos. Sci. **2025**, 9, 18 46 of 53

123. Kang, J.; Min, J.; Kim, S.-I.; Kim, S.-W.; Jang, J.-H. Three-Level Micro–Meso–Macroporous Three-Dimensional Graphene for Highly Fast Capacitive Deionization. *Mater. Today Energy* **2020**, *18*, 100502. [CrossRef]

- 124. Yang, X.-Y.; Chen, L.-H.; Li, Y.; Rooke, J.C.; Sanchez, C.; Su, B.-L. Hierarchically Porous Materials: Synthesis Strategies and Structure Design. *Chem. Soc. Rev.* **2017**, *46*, 481–558. [CrossRef] [PubMed]
- 125. Pérez-Page, M.; Yu, E.; Li, J.; Rahman, M.; Dryden, D.M.; Vidu, R.; Stroeve, P. Template-Based Syntheses for Shape Controlled Nanostructures. *Adv. Colloid Interface Sci.* **2016**, 234, 51–79. [CrossRef] [PubMed]
- 126. Hwang, J.; Ejsmont, A.; Freund, R.; Goscianska, J.; Schmidt, B.V.K.J.; Wuttke, S. Controlling the Morphology of Metal–Organic Frameworks and Porous Carbon Materials: Metal Oxides as Primary Architecture-Directing Agents. *Chem. Soc. Rev.* 2020, 49, 3348–3422. [CrossRef]
- 127. Cai, G.; Yan, P.; Zhang, L.; Zhou, H.-C.; Jiang, H.-L. Metal–Organic Framework-Based Hierarchically Porous Materials: Synthesis and Applications. *Chem. Rev.* **2021**, 121, 12278–12326. [CrossRef] [PubMed]
- 128. Tang, S.; Zhang, H.; Lee, H.K. Advances in Sample Extraction. Anal. Chem. 2016, 88, 228–249. [CrossRef] [PubMed]
- 129. Pavlenko, V.; Khosravi, H.S.; Żółtowska, S.; Haruna, A.B.; Zahid, M.; Mansurov, Z.; Supiyeva, Z.; Galal, A.; Ozoemena, K.I.; Abbas, Q.; et al. A Comprehensive Review of Template-Assisted Porous Carbons: Modern Preparation Methods and Advanced Applications. *Mater. Sci. Eng. R Rep.* 2022, 149, 100682. [CrossRef]
- 130. Shao, G.; Hanaor, D.A.H.; Shen, X.; Gurlo, A. Freeze Casting: From Low-Dimensional Building Blocks to Aligned Porous Structures—A Review of Novel Materials, Methods, and Applications. *Adv. Mater.* **2020**, *32*, 1907176. [CrossRef]
- 131. Li, C.; Yang, J.; Pachfule, P.; Li, S.; Ye, M.-Y.; Schmidt, J.; Thomas, A. Ultralight Covalent Organic Framework/Graphene Aerogels with Hierarchical Porosity. *Nat. Commun.* **2020**, *11*, 4712. [CrossRef]
- 132. Qin, W.; Zhu, W.; Ma, J.; Yang, Y.; Tang, B. Carbon Fibers Assisted 3D N-Doped Graphene Aerogel on Excellent Adsorption Capacity and Mechanical Property. *Colloids Surf. A Physicochem. Eng. Asp.* **2021**, *608*, 125602. [CrossRef]
- 133. Li, Y.; Yang, J.; Zheng, S.; Zeng, W.; Zhao, N.; Shen, M. One-Pot Synthesis of 3D TiO<sub>2</sub>-Reduced Graphene Oxide Aerogels with Superior Adsorption Capacity and Enhanced Visible-Light Photocatalytic Performance. *Ceram. Int.* **2016**, 42, 19091–19096. [CrossRef]
- 134. Teng, J.; Zeng, X.; Xu, X.; Yu, J.-G. Assembly of a Novel Porous 3D Graphene Oxide-Starch Architecture by a Facile Hydrothermal Method and Its Adsorption Properties toward Metal Ions. *Mater. Lett.* **2018**, 214, 31–33. [CrossRef]
- 135. Peng, W.; Wang, W.; Han, G.; Huang, Y.; Zhang, Y. Fabrication of 3D Flower-like MoS<sub>2</sub>/Graphene Composite as High-Performance Electrode for Capacitive Deionization. *Desalination* **2020**, *473*, 114191. [CrossRef]
- 136. Amini, A.; Khajeh, M.; Oveisi, A.R.; Daliran, S.; Ghaffari-Moghaddam, M.; Delarami, H.S. A Porous Multifunctional and Magnetic Layered Graphene Oxide/3D Mesoporous MOF Nanocomposite for Rapid Adsorption of Uranium(VI) from Aqueous Solutions. *J. Ind. Eng. Chem.* **2021**, *93*, 322–332. [CrossRef]
- 137. Lee, S.P.; Ali, G.A.M.; Algarni, H.; Chong, K.F. Flake Size-Dependent Adsorption of Graphene Oxide Aerogel. *J. Mol. Liq.* **2019**, 277, 175–180. [CrossRef]
- 138. Shen, Y.; Zhu, X.; Chen, B. Size Effects of Graphene Oxide Nanosheets on the Construction of Three-Dimensional Graphene-Based Macrostructures as Adsorbents. *J. Mater. Chem. A* **2016**, *4*, 12106–12118. [CrossRef]
- 139. Shen, S.; Pan, X.; Wang, J.; Bao, T.; Liu, X.; Tang, Z.; Xiu, H.; Li, J. Size Effect of Graphene Oxide on Graphene-Aerogel-Supported Au Catalysts for Electrochemical CO<sub>2</sub> Reduction. *Materials* **2023**, *16*, 7042. [CrossRef] [PubMed]
- 140. Fuxiang, S.; Jingxiang, Z.; Tao, D.; Na, W.; Zhuoyue, W.; Zhen, Z.; Bin, L.; Qiangqiang, Z. Three-Dimensional-Printed Hierarchical Reduced Graphene Oxide/Ethylenediamine Filter with Super-High Uranyl Ions with Recycling Capacity and Unique Selectivity. *Carbon* **2021**, *182*, 1–10. [CrossRef]
- 141. Haghighi Poudeh, L.; Cakiroglu, D.; Cebeci, F.Ç.; Yildiz, M.; Menceloglu, Y.Z.; Saner Okan, B. Design of Pt-Supported 1D and 3D Multilayer Graphene-Based Structural Composite Electrodes with Controlled Morphology by Core–Shell Electrospinning/Electrospraying. *ACS Omega* 2018, *3*, 6400–6410. [CrossRef] [PubMed]
- 142. Tao, E.; Ma, D.; Yang, S.; Hao, X. Graphene Oxide-Montmorillonite/Sodium Alginate Aerogel Beads for Selective Adsorption of Methylene Blue in Wastewater. *J. Alloys Compd.* **2020**, *832*, 154833. [CrossRef]
- 143. Wu, Z.; Huang, W.; Shan, X.; Li, Z. Preparation of a Porous Graphene Oxide/Alkali Lignin Aerogel Composite and Its Adsorption Properties for Methylene Blue. *Int. J. Biol. Macromol.* **2020**, *143*, 325–333. [CrossRef] [PubMed]
- 144. Ilyas, M.; Ahmad, W.; Khan, H.; Yousaf, S.; Yasir, M.; Khan, A. Environmental and Health Impacts of Industrial Wastewater Effluents in Pakistan: A Review. *Rev. Environ. Health* **2019**, *34*, 171–186. [CrossRef]
- 145. Akhtar, N.; Syakir Ishak, M.I.; Bhawani, S.A.; Umar, K. Various Natural and Anthropogenic Factors Responsible for Water Quality Degradation: A Review. *Water* 2021, 13, 2660. [CrossRef]
- 146. Vardhan, K.H.; Kumar, P.S.; Panda, R.C. A Review on Heavy Metal Pollution, Toxicity and Remedial Measures: Current Trends and Future Perspectives. *J. Mol. Liq.* **2019**, 290, 111197. [CrossRef]

J. Compos. Sci. **2025**, 9, 18 47 of 53

147. Khan, F.S.A.; Mubarak, N.M.; Tan, Y.H.; Khalid, M.; Karri, R.R.; Walvekar, R.; Abdullah, E.C.; Nizamuddin, S.; Mazari, S.A. A Comprehensive Review on Magnetic Carbon Nanotubes and Carbon Nanotube-Based Buckypaper for Removal of Heavy Metals and Dyes. J. Hazard. Mater. 2021, 413, 125375. [CrossRef] [PubMed]

- 148. Saravanan, A.; Senthil Kumar, P.; Jeevanantham, S.; Karishma, S.; Tajsabreen, B.; Yaashikaa, P.R.; Reshma, B. Effective Water/Wastewater Treatment Methodologies for Toxic Pollutants Removal: Processes and Applications towards Sustainable Development. *Chemosphere* 2021, 280, 130595. [CrossRef] [PubMed]
- 149. Hussain, K.; Haris, M.; Qamar, H.; Hussain, T.; Ahmad, G.; Ansari, M.S.; Khan, A.A. Bioremediation of Waste Gases and Polluted Soils. In *Microbial Rejuvenation of Polluted Environment*; Panpatte, D.G., Jhala, Y.K., Eds.; Microorganisms for Sustainability; Springer: Singapore, 2021; Volume 2, pp. 111–137, ISBN 9789811574559.
- 150. Wei, X.; Peng, Y.; Fang, W.; Hu, Z.; Li, W.; Zhang, S.; Jin, J. A Polyaniline Nanofiber Array Supported Ultrathin Polyamide Membrane for Solar-Driven Volatile Organic Compound Removal. *J. Mater. Chem. A* **2022**, *10*, 20424–20430. [CrossRef]
- 151. Ogidi, O.I.; Akpan, U.M. Aquatic Biodiversity Loss: Impacts of Pollution and Anthropogenic Activities and Strategies for Conservation. In *Biodiversity in Africa: Potentials, Threats and Conservation*; Chibueze Izah, S., Ed.; Sustainable Development and Biodiversity; Springer Nature: Singapore, 2022; pp. 421–448, ISBN 978-981-19332-6-4.
- 152. Geist, J.; Hoess, R.; Rytterstam, J.; Söderberg, H. Substratum Raking Can Restore Interstitial Habitat Quality in Swedish Freshwater Pearl Mussel Streams. *Diversity* **2023**, *15*, 869. [CrossRef]
- 153. Rashid, R.; Shafiq, I.; Akhter, P.; Iqbal, M.; Hussain, M. A State-of-the-Art Review on Wastewater Treatment Techniques: The Effectiveness of Adsorption Method. *Environ. Sci. Pollut. Res.* **2021**, *28*, 9050–9066. [CrossRef] [PubMed]
- 154. Momina; Ahmad, K. Feasibility of the Adsorption as a Process for Its Large Scale Adoption across Industries for the Treatment of Wastewater: Research Gaps and Economic Assessment. *J. Clean. Prod.* 2023, 388, 136014. [CrossRef]
- 155. Suliman, M.A.; Sajid, M.; Nazal, M.K.; Islam, M.A. Carbon-Based Materials as Promising Sorbents for Analytical Sample Preparation: Recent Advances and Trends in Extraction of Toxic Metal Pollutants from Various Media. *TrAC Trends Anal. Chem.* **2023**, *167*, 117265. [CrossRef]
- 156. Majeed, F.; Razzaq, A.; Rehmat, S.; Azhar, I.; Mohyuddin, A.; Rizvi, N.B. Enhanced Dye Sequestration with Natural Polysaccharides-Based Hydrogels: A Review. *Carbohydr. Polym.* **2024**, *330*, 121820. [CrossRef]
- 157. Zhang, Y.; Zhang, G.; Zhao, S.; Gao, A.; Cui, J.; Yan, Y. Three-Dimensional MXene-Based Functional Materials for Water Treatment: Preparation, Functional Tailoring, and Applications. *Ind. Eng. Chem. Res.* **2023**, *62*, 7297–7335. [CrossRef]
- 158. Arsalani, N.; Nasiri, R.; Zarei, M. Synthesis of Magnetic 3D Graphene Decorated with CaCO<sub>3</sub> for Anionic Azo Dye Removal from Aqueous Solution: Kinetic and RSM Modeling Approach. *Chem. Eng. Res. Des.* **2018**, *136*, 795–805. [CrossRef]
- 159. Khan, S.; Achazhiyath Edathil, A.; Banat, F. Sustainable Synthesis of Graphene-Based Adsorbent Using Date Syrup. *Sci. Rep.* **2019**, 9, 18106. [CrossRef] [PubMed]
- 160. Oh, M.J.; Yoo, P.J. Graphene-Based 3D Lightweight Cellular Structures: Synthesis and Applications. *Korean J. Chem. Eng.* **2020**, 37, 189–208. [CrossRef]
- 161. Maiti, U.N.; Lee, W.J.; Lee, J.M.; Oh, Y.; Kim, J.Y.; Kim, J.E.; Shim, J.; Han, T.H.; Kim, S.O. 25th Anniversary Article: Chemically Modified/Doped Carbon Nanotubes & Graphene for Optimized Nanostructures & Nanodevices. *Adv. Mater.* 2014, 26, 40–67. [CrossRef] [PubMed]
- 162. Kheirabadi, M.; Samadi, M.; Asadian, E.; Zhou, Y.; Dong, C.; Zhang, J.; Moshfegh, A.Z. Well-Designed Ag/ZnO/3D Graphene Structure for Dye Removal: Adsorption, Photocatalysis and Physical Separation Capabilities. *J. Colloid Interface Sci.* **2019**, 537, 66–78. [CrossRef]
- 163. Mei, J.-Y.; Qi, P.; Wei, X.-N.; Zheng, X.-C.; Wang, Q.; Guan, X.-X. Assembly and Enhanced Elimination Performance of 3D Graphene Aerogel-Zinc Oxide Hybrids for Methylene Blue Dye in Water. *Mater. Res. Bull.* **2019**, *109*, 141–148. [CrossRef]
- 164. Liu, X.; Wang, J.; Dong, Y.; Li, H.; Xia, Y.; Wang, H. One-Step Synthesis of Bi<sub>2</sub>MoO<sub>6</sub>/Reduced Graphene Oxide Aerogel Composite with Enhanced Adsorption and Photocatalytic Degradation Performance for Methylene Blue. *Mater. Sci. Semicond. Process.* **2018**, 88, 214–223. [CrossRef]
- 165. Ahmadi, Y.; Kim, K.-H. Modification Strategies for Visible-Light Photocatalysts and Their Performance-Enhancing Effects on Photocatalytic Degradation of Volatile Organic Compounds. *Renew. Sustain. Energy Rev.* **2024**, *189*, 113948. [CrossRef]
- 166. Zhang, B.; Shan, X.; Yu, J.; Zhang, H.; Alali, K.T.; Liu, Q.; Zhu, J.; Yu, J.; Liu, J.; Li, R.; et al. Facile Synthesis of TiO<sub>2</sub>-PAN Photocatalytic Membrane with Excellent Photocatalytic Performance for Uranium Extraction from Seawater. *Sep. Purif. Technol.* **2024**, *328*, 125026. [CrossRef]
- 167. Ferrand, A.; Siaj, M.; Claverie, J.P. Graphene, the Swiss Army Knife of Nanomaterials Science. *ACS Appl. Nano Mater.* **2020**, *3*, 7305–7313. [CrossRef]
- 168. Zhao, G.; Zhu, H. Cation–π Interactions in Graphene-Containing Systems for Water Treatment and Beyond. *Adv. Mater.* **2020**, *32*, 1905756. [CrossRef] [PubMed]

J. Compos. Sci. 2025, 9, 18 48 of 53

169. Fadeel, B.; Bussy, C.; Merino, S.; Vázquez, E.; Flahaut, E.; Mouchet, F.; Evariste, L.; Gauthier, L.; Koivisto, A.J.; Vogel, U.; et al. Safety Assessment of Graphene-Based Materials: Focus on Human Health and the Environment. *ACS Nano* 2018, 12, 10582–10620. [CrossRef] [PubMed]

- 170. Nassar, G.; Daou, E.; Najjar, R.; Bassil, M.; Habchi, R. A Review on the Current Research on Graphene-Based Aerogels and Their Applications. *Carbon Trends* **2021**, *4*, 100065. [CrossRef]
- 171. Chen, F.; An, W.; Liu, L.; Liang, Y.; Cui, W. Highly Efficient Removal of Bisphenol A by a Three-Dimensional Graphene Hydrogel-AgBr@rGO Exhibiting Adsorption/Photocatalysis Synergy. *Appl. Catal. B Environ.* **2017**, 217, 65–80. [CrossRef]
- 172. Yan, S.; Chen, X.; Yang, Y.; Zhou, T. Peroxymonosulfate Activation by N-Doped 3D Graphene from Spent Lithium-Ion Batteries for Organic Pollutants Degradation: An Insight into the Degradation Mechanism. *Chem. Eng. J.* **2024**, *484*, 149379. [CrossRef]
- 173. Zhang, Z.; Zhai, S.; Wang, M.; Ji, H.; He, L.; Ye, C.; Wang, C.; Fang, S.; Zhang, H. Photocatalytic Degradation of Rhodamine B by Using a Nanocomposite of Cuprous Oxide, Three-Dimensional Reduced Graphene Oxide, and Nanochitosan Prepared via One-Pot Synthesis. *J. Alloys Compd.* 2015, 659, 101–111. [CrossRef]
- 174. Liu, P.; Yan, T.; Zhang, J.; Shi, L.; Zhang, D. Separation and Recovery of Heavy Metal Ions and Salt Ions from Wastewater by 3D Graphene-Based Asymmetric Electrodes via Capacitive Deionization. *J. Mater. Chem. A* **2017**, *5*, 14748–14757. [CrossRef]
- 175. Han, B.; Cheng, G.; Wang, Y.; Wang, X. Structure and Functionality Design of Novel Carbon and Faradaic Electrode Materials for High-Performance Capacitive Deionization. *Chem. Eng. J.* **2019**, *360*, 364–384. [CrossRef]
- 176. Wu, Q.; Liang, D.; Lu, S.; Zhang, J.; Wang, H.; Xiang, Y.; Aurbach, D. Novel Inorganic Integrated Membrane Electrodes for Membrane Capacitive Deionization. *ACS Appl. Mater. Interfaces* **2021**, *13*, 46537–46548. [CrossRef] [PubMed]
- 177. Vafakhah, S.; Sim, G.J.; Saeedikhani, M.; Li, X.; y Alvarado, P.V.; Yang, H.Y. 3D Printed Electrodes for Efficient Membrane Capacitive Deionization. *Nanoscale Adv.* 2019, 1, 4804–4811. [CrossRef] [PubMed]
- 178. Wang, M.; Duan, X.; Xu, Y.; Duan, X. Functional Three-Dimensional Graphene/Polymer Composites. *ACS Nano* **2016**, *10*, 7231–7247. [CrossRef]
- 179. Zhang, X.; Li, Y.; Yang, Z.; Yang, P.; Wang, J.; Shi, M.; Yu, F.; Ma, J. Industrially-Prepared Carbon Aerogel for Excellent Fluoride Removal by Membrane Capacitive Deionization from Brackish Groundwaters. Sep. Purif. Technol. 2022, 297, 121510. [CrossRef]
- 180. Dasgupta, A.; Rajukumar, L.P.; Rotella, C.; Lei, Y.; Terrones, M. Covalent Three-Dimensional Networks of Graphene and Carbon Nanotubes: Synthesis and Environmental Applications. *Nano Today* **2017**, *12*, 116–135. [CrossRef]
- 181. Shu, R.; Zhang, G.; Zhang, C.; Wu, Y.; Zhang, J. Nitrogen-Doping-Regulated Electromagnetic Wave Absorption Properties of Ultralight Three-Dimensional Porous Reduced Graphene Oxide Aerogels. *Adv. Electron. Mater.* **2021**, *7*, 2001001. [CrossRef]
- 182. Wang, H.; Zhang, D.; Yan, T.; Wen, X.; Zhang, J.; Shi, L.; Zhong, Q. Three-Dimensional Macroporous Graphene Architectures as High Performance Electrodes for Capacitive Deionization. *J. Mater. Chem. A* **2013**, *1*, 11778–11789. [CrossRef]
- 183. Shi, W.; Li, H.; Cao, X.; Leong, Z.Y.; Zhang, J.; Chen, T.; Zhang, H.; Yang, H.Y. Ultrahigh Performance of Novel Capacitive Deionization Electrodes Based on A Three-Dimensional Graphene Architecture with Nanopores. *Sci. Rep.* **2016**, *6*, 18966. [CrossRef]
- 184. Hosseinzadeh, M.; Mozaffari, S.A.; Ebrahimi, F. Porous 3D-Graphene Functionalized with MnO<sub>2</sub> Nanospheres and NiO Nanoparticles as Highly Efficient Electrodes for Asymmetric Capacitive Deionization: Evaluation by Impedance-Derived Capacitance Spectroscopy. *Electrochim. Acta* 2022, 427, 140844. [CrossRef]
- 185. Rangaraj, V.M.; Yoo, J.-I.; Song, J.-K.; Mittal, V. MOF-Derived 3D MnO<sub>2</sub>@graphene/CNT and Ag@graphene/CNT Hybrid Electrode Materials for Dual-Ion Selective Pseudocapacitive Deionization. *Desalination* **2023**, *550*, 116369. [CrossRef]
- 186. Chen, T.-H.; Yeh, K.-H.; Lin, C.-F.; Lee, M.; Hou, C.-H. Technological and Economic Perspectives of Membrane Capacitive Deionization (MCDI) Systems in High-Tech Industries: From Tap Water Purification to Wastewater Reclamation for Water Sustainability. *Resour. Conserv. Recycl.* 2022, 177, 106012. [CrossRef]
- 187. Wu, J.; Zhang, T.; Qu, J.; Jiao, F.-Z.; Hu, C.; Zhao, H.-Y.; Li, X.; Yu, Z.-Z. Hydrothermally Modified 3D Porous Loofah Sponges with MoS<sub>2</sub> Sheets and Carbon Particles for Efficient Solar Steam Generation and Seawater Desalination. *ACS Appl. Mater. Interfaces* **2023**, *15*, 29457–29467. [CrossRef]
- 188. Shao, B.; Wang, Y.; Wu, X.; Lu, Y.; Yang, X.; Chen, G.Y.; Owens, G.; Xu, H. Stackable Nickel–Cobalt@polydopamine Nanosheet Based Photothermal Sponges for Highly Efficient Solar Steam Generation. *J. Mater. Chem. A* **2020**, *8*, 11665–11673. [CrossRef]
- 189. Loo, S.-L.; Vásquez, L.; Zahid, M.; Costantino, F.; Athanassiou, A.; Fragouli, D. 3D Photothermal Cryogels for Solar-Driven Desalination. *ACS Appl. Mater. Interfaces* **2021**, *13*, 30542–30555. [CrossRef] [PubMed]
- 190. Zhao, D.; Ding, M.; Lin, T.; Duan, Z.; Wei, R.; Feng, P.; Yu, J.; Liu, C.-Y.; Li, C. Gradient Graphene Spiral Sponges for Efficient Solar Evaporation and Zero Liquid Discharge Desalination with Directional Salt Crystallization. *Adv. Sci.* **2024**, *11*, 2400310. [CrossRef]
- 191. Ding, M.; Lu, H.; Sun, Y.; He, Y.; Yu, J.; Kong, H.; Shao, C.; Liu, C.-Y.; Li, C. Superelastic 3D Assembled Clay/Graphene Aerogels for Continuous Solar Desalination and Oil/Organic Solvent Absorption. *Adv. Sci.* **2022**, *9*, 2205202. [CrossRef]
- 192. Bezza, F.A.; Iwarere, S.A.; Brink, H.G.; Chirwa, E.M.N. Design and Fabrication of Porous Three-dimensional Ag-Doped Reduced Graphene Oxide (3D Ag@rGO) Composite for Interfacial Solar Desalination. *Sci. Rep.* **2024**, *14*, 13793. [CrossRef] [PubMed]

J. Compos. Sci. **2025**, 9, 18 49 of 53

193. Wang, Q.; Wang, L.; Song, S.; Li, Y.; Jia, F.; Feng, T.; Hu, N. Flexible 2D@3D Janus Evaporators for High-Performance and Continuous Solar Desalination. *Desalination* **2022**, 525, 115483. [CrossRef]

- 194. Yang, Y.; Liu, C.; Wang, J.; Xu, G.; Ren, T. Janus 3D Graphene Based Evaporator with Controllable Wettability for Highly Efficient Solar Desalination. *Desalination* **2023**, *558*, 116639. [CrossRef]
- 195. Jiao, F.-Z.; Wu, J.; Zhang, T.; Pan, R.-J.; Wang, Z.-H.; Yu, Z.-Z.; Qu, J. Simultaneous Solar-Thermal Desalination and Catalytic Degradation of Wastewater Containing Both Salt Ions and Organic Contaminants. *ACS Appl. Mater. Interfaces* **2023**, *15*, 41007–41018. [CrossRef]
- 196. Mohanavelu, A.; Shrivastava, S.; Naganna, S.R. Streambed Pollution: A Comprehensive Review of Its Sources, Eco-Hydro-Geo-Chemical Impacts, Assessment, and Mitigation Strategies. *Chemosphere* **2022**, *300*, 134589. [CrossRef]
- 197. Sharma, S.; Bhattacharya, A. Drinking Water Contamination and Treatment Techniques. *Appl. Water Sci.* **2017**, 7, 1043–1067. [CrossRef]
- 198. Hiew, B.Y.Z.; Lee, L.Y.; Lai, K.C.; Gan, S.; Thangalazhy-Gopakumar, S.; Pan, G.-T.; Yang, T.C.-K. Adsorptive Decontamination of Diclofenac by Three-Dimensional Graphene-Based Adsorbent: Response Surface Methodology, Adsorption Equilibrium, Kinetic and Thermodynamic Studies. *Environ. Res.* 2019, 168, 241–253. [CrossRef]
- 199. Mora, A.; Torres-Martínez, J.A.; Capparelli, M.V.; Zabala, A.; Mahlknecht, J. Effects of Wastewater Irrigation on Groundwater Quality: An Overview. *Curr. Opin. Environ. Sci. Health* 2022, 25, 100322. [CrossRef]
- 200. Hussain, R.; Khattak, S.; Ali, L.; Sattar, S.; Zeb, M.; Luqman, M. Impacts of the Linear Flowing Industrial Wastewater on the Groundwater Quality and Human Health in Swabi, Pakistan. *Environ. Sci. Pollut. Res.* **2021**, *28*, 56741–56757. [CrossRef] [PubMed]
- 201. Farhan, A.; Rashid, E.U.; Waqas, M.; Ahmad, H.; Nawaz, S.; Munawar, J.; Rahdar, A.; Varjani, S.; Bilal, M. Graphene-Based Nanocomposites and Nanohybrids for the Abatement of Agro-Industrial Pollutants in Aqueous Environments. *Environ. Pollut.* 2022, 308, 119557. [CrossRef] [PubMed]
- 202. Aguilar-Pérez, K.M.; Avilés-Castrillo, J.I.; Ruiz-Pulido, G. Nano-Sorbent Materials for Pharmaceutical-Based Wastewater Effluents—An Overview. *Case Stud. Chem. Environ. Eng.* **2020**, 2, 100028. [CrossRef]
- Zamora-Ledezma, C.; Negrete-Bolagay, D.; Figueroa, F.; Zamora-Ledezma, E.; Ni, M.; Alexis, F.; Guerrero, V.H. Heavy Metal Water Pollution: A Fresh Look about Hazards, Novel and Conventional Remediation Methods. *Environ. Technol. Innov.* 2021, 22, 101504. [CrossRef]
- 204. Petlovanyi, M.; Kuzmenko, O.; Lozynskyi, V.; Popovych, V.; Sai, K.; Saik, P. Review of Man-Made Mineral Formations Accumulation and Prospects of Their Developing in Mining Industrial Regions in Ukraine. *Min. Miner. Depos.* 2019, 13, 24–38. [CrossRef]
- 205. Shi, L.; Li, Y.; Rong, X.; Wang, Y.; Ding, S. Facile Fabrication of a Novel 3D Graphene Framework/Bi Nanoparticle Film for Ultrasensitive Electrochemical Assays of Heavy Metal Ions. *Anal. Chim. Acta* 2017, 968, 21–29. [CrossRef] [PubMed]
- 206. Hundessa, N.K.; Hu, C.-C.; Kang, D.-Y.; Ajebe, E.G.; Habet, B.A.; Hung, W.-S.; Lee, K.-R.; Lai, J.-Y. A Novel Trimesoyl Chloride/Hyper Branched Polyethyleneimine/MOF (MIL-303)/P84 Co-Polyimide Nanocomposite Mixed Matrix Membranes with an Ultra-Thin Surface Cross Linking Layer for Removing Toxic Heavy Metal Ions from Wastewater. *J. Hazard. Mater.* 2024, 480, 136221. [CrossRef] [PubMed]
- 207. Chen, G.; Liu, Y.; Liu, F.; Zhang, X. Fabrication of Three-Dimensional Graphene Foam with High Electrical Conductivity and Large Adsorption Capability. *Appl. Surf. Sci.* **2014**, *311*, 808–815. [CrossRef]
- 208. Xie, Z.; Diao, S.; Xu, R.; Wei, G.; Wen, J.; Hu, G.; Tang, T.; Jiang, L.; Li, X.; Li, M.; et al. Construction of Carboxylated-GO and MOFs Composites for Efficient Removal of Heavy Metal Ions. *Appl. Surf. Sci.* 2023, 636, 157827. [CrossRef]
- 209. Zeng, T.; Yu, Y.; Li, Z.; Zuo, J.; Kuai, Z.; Jin, Y.; Wang, Y.; Wu, A.; Peng, C. 3D MnO<sub>2</sub> Nanotubes@reduced Graphene Oxide Hydrogel as Reusable Adsorbent for the Removal of Heavy Metal Ions. *Mater. Chem. Phys.* **2019**, 231, 105–108. [CrossRef]
- 210. Liu, J.; Ge, X.; Ye, X.; Wang, G.; Zhang, H.; Zhou, H.; Zhang, Y.; Zhao, H. 3D Graphene /δ-MnO<sub>2</sub> Aerogels for Highly Efficient and Reversible Removal of Heavy Metal Ions. *J. Mater. Chem. A* **2016**, *4*, 1970–1979. [CrossRef]
- 211. Zhao, X.; Jiang, X.; Peng, D.; Teng, J.; Yu, J. Behavior and Mechanism of Graphene Oxide-Tris(4-Aminophenyl)Amine Composites in Adsorption of Rare Earth Elements. *J. Rare Earths* **2021**, *39*, 90–97. [CrossRef]
- 212. Yu, S.; Wei, D.; Shi, L.; Ai, Y.; Zhang, P.; Wang, X. Three-Dimensional Graphene/Titanium Dioxide Composite for Enhanced U(VI) Capture: Insights from Batch Experiments, XPS Spectroscopy and DFT Calculation. *Environ. Pollut.* 2019, 251, 975–983. [CrossRef] [PubMed]
- 213. Lai, K.C.; Lee, L.Y.; Hiew, B.Y.Z.; Thangalazhy-Gopakumar, S.; Gan, S. Facile Synthesis of Xanthan Biopolymer Integrated 3D Hierarchical Graphene Oxide/Titanium Dioxide Composite for Adsorptive Lead Removal in Wastewater. *Bioresour. Technol.* 2020, 309, 123296. [CrossRef]
- 214. Ding, Z.; Liang, J.; Zhang, W.; Wang, W.; Geng, R.; Wang, Y.; Li, P.; Fan, Q. Efficiency and Active Sites of the Synergetic Sorption and Photocatalysis in Cr(VI) Decontamination on a 3D Oxidized Graphene Ribbon Framework. *J. Mater. Chem. A* 2020, 8, 11362–11369. [CrossRef]

J. Compos. Sci. 2025, 9, 18 50 of 53

215. Huo, J.; Yu, G.; Wang, J. Selective Adsorption of Cesium (I) from Water by Prussian Blue Analogues Anchored on 3D Reduced Graphene Oxide Aerogel. *Sci. Total Environ.* **2021**, *761*, 143286. [CrossRef] [PubMed]

- 216. Lei, Y.; Chen, F.; Luo, Y.; Zhang, L. Three-Dimensional Magnetic Graphene Oxide Foam/Fe<sub>3</sub>O<sub>4</sub> Nanocomposite as an Efficient Absorbent for Cr(VI) Removal. *J. Mater. Sci.* **2014**, *49*, 4236–4245. [CrossRef]
- 217. Zhou, Y.; Liang, C.; Yu, J.; Jiang, X. Adsorption Properties of a Novel 3D Graphene/MgO Composite for Heavy Metal Ions. *J. Cent. South Univ.* **2019**, 26, 813–823. [CrossRef]
- 218. You, S.-M.; Tasi, C.-K.; Millet, P.; Doong, R.-A. Electrochemically Capacitive Deionization of Copper (II) Using 3D Hierarchically Reduced Graphene Oxide Architectures. *Sep. Purif. Technol.* **2020**, *251*, 117368. [CrossRef]
- 219. Zhao, X.-R.; Xu, X.; Teng, J.; Zhou, N.; Zhou, Z.; Jiang, X.-Y.; Jiao, F.-P.; Yu, J.-G. Three-Dimensional Porous Graphene Oxide-Maize Amylopectin Composites with Controllable Pore-Sizes and Good Adsorption-Desorption Properties: Facile Fabrication and Reutilization, and the Adsorption Mechanism. *Ecotoxicol. Environ. Saf.* 2019, 176, 11–19. [CrossRef] [PubMed]
- 220. Xu, X.; Zou, J.; Zhao, X.-R.; Jiang, X.-Y.; Jiao, F.-P.; Yu, J.-G.; Liu, Q.; Teng, J. Facile Assembly of Three-Dimensional Cylindrical Egg White Embedded Graphene Oxide Composite with Good Reusability for Aqueous Adsorption of Rare Earth Elements. *Colloids Surf. A Physicochem. Eng. Asp.* 2019, 570, 127–140. [CrossRef]
- 221. Kasap, S.; Aslan, E.N.; Öztürk, İ. Investigation of MnO<sub>2</sub> Nanoparticles-Anchored 3D-Graphene Foam Composites (3DGF-MnO<sub>2</sub>) as an Adsorbent for Strontium Using the Central Composite Design (CCD) Method. *New J. Chem.* **2019**, *43*, 2981–2989. [CrossRef]
- 222. Nasiri, R.; Arsalani, N.; Panahian, Y. One-Pot Synthesis of Novel Magnetic Three-Dimensional Graphene/Chitosan/Nickel Ferrite Nanocomposite for Lead Ions Removal from Aqueous Solution: RSM Modelling Design. *J. Clean. Prod.* 2018, 201, 507–515. [CrossRef]
- 223. Wang, Z.; Lin, F.; Huang, L.; Chang, Z.; Yang, B.; Liu, S.; Zheng, M.; Lu, Y.; Chen, J. Cyclodextrin Functionalized 3D-Graphene for the Removal of Cr(VI) with the Easy and Rapid Separation Strategy. *Environ. Pollut.* 2019, 254, 112854. [CrossRef] [PubMed]
- 224. Huang, Z.-W.; Li, Z.-J.; Zheng, L.-R.; Wu, W.-S.; Chai, Z.-F.; Shi, W.-Q. Adsorption of Eu(III) and Th(IV) on Three-Dimensional Graphene-Based Macrostructure Studied by Spectroscopic Investigation. *Environ. Pollut.* 2019, 248, 82–89. [CrossRef] [PubMed]
- 225. Zhou, F.; Feng, X.; Yu, J.; Jiang, X. High Performance of 3D Porous Graphene/Lignin/Sodium Alginate Composite for Adsorption of Cd(II) and Pb(II). *Environ. Sci. Pollut. Res.* **2018**, 25, 15651–15661. [CrossRef]
- 226. Tan, B.; Zhao, H.; Zhang, Y.; Quan, X.; He, Z.; Zheng, W.; Shi, B. Amphiphilic PA-Induced Three-Dimensional Graphene Macrostructure with Enhanced Removal of Heavy Metal Ions. *J. Colloid Interface Sci.* **2018**, *512*, 853–861. [CrossRef] [PubMed]
- 227. Peng, X.; Gao, F.; Zhao, J.; Li, J.; Qu, J.; Fan, H. Self-Assembly of a Graphene Oxide/MnFe<sub>2</sub>O<sub>4</sub> Motor by Coupling Shear Force with Capillarity for Removal of Toxic Heavy Metals. *J. Mater. Chem. A* **2018**, *6*, 20861–20868. [CrossRef]
- 228. Leão, M.B.; Bordin, J.R.; de Matos, C.F. Specific Surface Area Versus Adsorptive Capacity: An Application View of 3D Graphene-Based Materials for the Removal of Emerging Water Pollutants. *Water Air Soil Pollut.* **2023**, 234, 136. [CrossRef]
- 229. Chen, Y.-Y.; Lan, X.-W.; Ren, H.; Li, W.-J.; Chen, J.; Jiang, X.-Y.; Yu, J.-G. Three-Dimensional Hybrid Nitrogen/Oxygen-Containing Components Modified Graphene Oxide as a Recyclable Adsorbent for Rapid Adsorption of REEs. *J. Environ. Chem. Eng.* **2021**, 9, 106500. [CrossRef]
- 230. He, J.; Ni, F.; Cui, A.; Chen, X.; Deng, S.; Shen, F.; Huang, C.; Yang, G.; Song, C.; Zhang, J.; et al. New Insight into Adsorption and Co-Adsorption of Arsenic and Tetracycline Using a Y-Immobilized Graphene Oxide-Alginate Hydrogel: Adsorption Behaviours and Mechanisms. *Sci. Total Environ.* **2020**, 701, 134363. [CrossRef] [PubMed]
- 231. Islam, T.; Repon, M.R.; Islam, T.; Sarwar, Z.; Rahman, M. Impact of Textile Dyes on Health and Ecosystem: A Review of Structure, Causes, and Potential Solutions. *Environ. Sci. Pollut. Res.* 2022, 30, 9207–9242. [CrossRef] [PubMed]
- 232. Capodaglio, A. Biorefinery of Sewage Sludge: Overview of Possible Value-Added Products and Applicable Process Technologies. *Water* 2023, 15, 1195. [CrossRef]
- 233. Li, C.; Sun, W.; Lu, Z.; Ao, X.; Li, S. Ceramic Nanocomposite Membranes and Membrane Fouling: A Review. *Water Res.* **2020**, *175*, 115674. [CrossRef] [PubMed]
- 234. Babuponnusami, A.; Sinha, S.; Ashokan, H.; Veliyath, M.; Hariharan, S.; Jayaseelan, A.; Kannappan Panchamoorthy, G.; Le, Q.; Pugazhendhi, A. Advanced Oxidation Process (AOP) Combined Biological Process for Wastewater Treatment: A Review on Advancements, Feasibility and Practicability of Combined Techniques. *Environ. Res.* 2023, 237, 116944. [CrossRef]
- 235. Xin, X.; Li, S.-H.; Zhang, N.; Tang, Z.-R.; Xu, Y.-J. 3D Graphene/AgBr/Ag Cascade Aerogel for Efficient Photocatalytic Disinfection. *Appl. Catal. B Environ.* **2019**, 245, 343–350. [CrossRef]
- 236. Dong, S.; Cui, L.; Liu, C.; Zhang, F.; Li, K.; Xia, L.; Su, X.; Feng, J.; Zhu, Y.; Sun, J. Fabrication of 3D Ultra-Light Graphene Aerogel/Bi<sub>2</sub>WO<sub>6</sub> Composite with Excellent Photocatalytic Performance: A Promising Photocatalysts for Water Purification. *J. Taiwan Inst. Chem. Eng.* **2019**, *97*, 288–296. [CrossRef]
- 237. Tee, W.T.; Loh, N.Y.L.; Hiew, B.Y.Z.; Chiu, W.S.; Khiew, P.S.; Thangalazhy-Gopakumar, S.; Gan, S.; Lee, L.Y. Design and Development of a High-Performance 3D Graphene System for Adsorptive Removal of Organic Toxins from Wastewater: Mechanisms and Process Optimization. *Chem. Eng. Res. Des.* 2023, 195, 132–150. [CrossRef]

J. Compos. Sci. **2025**, 9, 18 51 of 53

238. Lai, K.C.; Lee, L.Y.; Hiew, B.Y.Z.; Yang, T.C.-K.; Pan, G.-T.; Thangalazhy-Gopakumar, S.; Gan, S. Utilisation of Eco-Friendly and Low Cost 3D Graphene-Based Composite for Treatment of Aqueous Reactive Black 5 Dye: Characterisation, Adsorption Mechanism and Recyclability Studies. *J. Taiwan Inst. Chem. Eng.* 2020, 114, 57–66. [CrossRef]

- 239. Liu, Y.; Huang, S.; Zhao, X.; Zhang, Y. Fabrication of Three-Dimensional Porous β-Cyclodextrin/Chitosan Functionalized Graphene Oxide Hydrogel for Methylene Blue Removal from Aqueous Solution. *Colloids Surf. A Physicochem. Eng. Asp.* **2018**, 539, 1–10. [CrossRef]
- 240. Zhang, J.-J.; Fang, S.-S.; Mei, J.-Y.; Zheng, G.-P.; Zheng, X.-C.; Guan, X.-X. High-Efficiency Removal of Rhodamine B Dye in Water Using g-C<sub>3</sub>N<sub>4</sub> and TiO<sub>2</sub> Co-Hybridized 3D Graphene Aerogel Composites. *Sep. Purif. Technol.* **2018**, 194, 96–103. [CrossRef]
- 241. Yang, Q.; Lu, R.; Ren, S.; Chen, C.; Chen, Z.; Yang, X. Three Dimensional Reduced Graphene Oxide/ZIF-67 Aerogel: Effective Removal Cationic and Anionic Dyes from Water. *Chem. Eng. J.* **2018**, *348*, 202–211. [CrossRef]
- 242. Nasiri, R.; Arsalani, N. Synthesis and Application of 3D Graphene Nanocomposite for the Removal of Cationic Dyes from Aqueous Solutions: Response Surface Methodology Design. *J. Clean. Prod.* **2018**, *190*, 63–71. [CrossRef]
- 243. Zhao, Q.; Zhu, X.; Chen, B. Stable Graphene Oxide/Poly(Ethyleneimine) 3D Aerogel with Tunable Surface Charge for High Performance Selective Removal of Ionic Dyes from Water. *Chem. Eng. J.* 2018, 334, 1119–1127. [CrossRef]
- 244. Labiadh, L.; Kamali, A.R. 3D Graphene Nanoedges as Efficient Dye Adsorbents with Ultra-High Thermal Regeneration Performance. *Appl. Surf. Sci.* **2019**, 490, 383–394. [CrossRef]
- 245. Liu, C.; Liu, H.; Xu, A.; Tang, K.; Huang, Y.; Lu, C. In Situ Reduced and Assembled Three-Dimensional Graphene Aerogel for Efficient Dye Removal. *J. Alloys Compd.* **2017**, 714, 522–529. [CrossRef]
- 246. Yunus, R.M.; Rosman, N.N.; Shah, N.R.A.M. 3D Graphene as a Photocatalyst for Water Splitting. In 3D Graphene; Springer: Berlin/Heidelberg, Germany, 2023; pp. 359–374, ISBN 978-3-031-36248-4.
- 247. Fan, K.; Lu, M.L.; Li, D.Y.; Li, L.F.; Li, J.H.; Xu, F.L. The Synthesis of 3D Graphene/Fe<sub>3</sub>O<sub>4</sub> Aerogel via γ-Ray and Its Application for the Absorption of Organic Liquids. *High Energy Chem.* **2023**, *57*, 77–82. [CrossRef]
- 248. Zhao, C.; Sun, H.; Li, C.; Wang, M.; Wu, J.; Chen, M.; Jiang, S.; Niu, T.; Liu, D. Facile Synthesis of 3D Interconnected Porous G-C<sub>3</sub>N<sub>4</sub>/rGO Composite for Hydrogen Production and Dye Elimination. *Catalysts* **2023**, *13*, 1079. [CrossRef]
- 249. Liu, H.; Tian, Z.; Huang, C.; Wang, P.; Huang, S.; Yang, X.; Cheng, H.; Zheng, X.; Tian, H.; Liu, Z. A Novel 3D Co/Mo Co-Catalyzed Graphene Sponge-Mediated Peroxymonosulfate Activation for the Highly Efficient Pollutants Degradation. *Sep. Purif. Technol.* 2022, 301, 122035. [CrossRef]
- 250. Li, X.; Liu, Z.; Zhu, Y.; Song, L.; Dong, Z.; Niu, S.; Lyu, C. Facile Synthesis and Synergistic Mechanism of CoFe<sub>2</sub>O<sub>4</sub>@three-Dimensional Graphene Aerogels towards Peroxymonosulfate Activation for Highly Efficient Degradation of Recalcitrant Organic Pollutants. *Sci. Total Environ.* **2020**, 749, 141466. [CrossRef] [PubMed]
- 251. Ayoub, G.; Korban, L.; Al-Hindi, M.; Zayyat, R. Brackish Water Desalination: An Effective Pretreatment Process for Reverse Osmosis Systems. *Water Air Soil Pollut.* **2019**, 230, 238. [CrossRef]
- 252. Qing, W.; Liu, F.; Yao, H.; Sun, S.; Chen, C.; Zhang, W. Functional Catalytic Membrane Development: A Review of Catalyst Coating Techniques. *Adv. Colloid Interface Sci.* 2020, 282, 102207. [CrossRef] [PubMed]
- 253. Gu, X.; Deng, Y.; Wang, C. Fabrication of Anion-Exchange Polymer Layered Graphene–Melamine Electrodes for Membrane Capacitive Deionization. *ACS Sustain. Chem. Eng.* **2017**, *5*, 325–333. [CrossRef]
- 254. Pathan, S.; Islam, S.; Gupta, R.; Maity, B.; Reddy, R.; Mondal, S.; Katha, A.; Bose, S. Fundamental Understanding of Ultrathin, Highly Stable Self-Assembled Liquid Crystalline Graphene Oxide Membranes Leading to Precise Molecular Sieving through Non-Equilibrium Molecular Dynamics. *ACS Nano* 2023, 17, 7272–7284. [CrossRef] [PubMed]
- 255. Mohd Firdaus, R.; Berrada, N.; Desforges, A.; Mohamed, A.R.; Vigolo, B. From 2D Graphene Nanosheets to 3D Graphene-Based Macrostructures. *Chem. Asian J.* **2020**, *15*, 2902–2924. [CrossRef] [PubMed]
- 256. Liu, Q.; Tan, G.; Lei, Y.; Xiao, D. 3D Interconnected Porous Graphene Architecture as a High-Performance Capacitive Deionization Electrode. *Sep. Purif. Technol.* **2024**, *336*, 126300. [CrossRef]
- 257. Talebi, M.; Ahadian, M.M.; Shahrokhian, S. Binder-Free 3D Graphene Nanostructures on Ni Foam Substrate for Application in Capacitive Deionization. *Diam. Relat. Mater.* **2021**, *120*, 108612. [CrossRef]
- 258. Dianbudiyanto, W.; Liu, S.-H. Outstanding Performance of Capacitive Deionization by a Hierarchically Porous 3D Architectural Graphene. *Desalination* **2019**, 468, 114069. [CrossRef]
- 259. Khan, Z.U.; Yan, T.; Shi, L.; Zhang, D. Improved Capacitive Deionization by Using 3D Intercalated Graphene Sheet–Sphere Nanocomposite Architectures. *Environ. Sci. Nano* 2018, *5*, 980–991. [CrossRef]
- 260. Xu, X.; Liu, Y.; Wang, M.; Zhu, C.; Lu, T.; Zhao, R.; Pan, L. Hierarchical Hybrids with Microporous Carbon Spheres Decorated Three-Dimensional Graphene Frameworks for Capacitive Applications in Supercapacitor and Deionization. *Electrochim. Acta* 2016, 193, 88–95. [CrossRef]
- 261. Chang, L.; Hang Hu, Y. 3D Channel-Structured Graphene as Efficient Electrodes for Capacitive Deionization. *J. Colloid Interface Sci.* 2019, 538, 420–425. [CrossRef]

J. Compos. Sci. **2025**, 9, 18 52 of 53

262. El-Deen, A.G.; Boom, R.M.; Kim, H.Y.; Duan, H.; Chan-Park, M.B.; Choi, J.-H. Flexible 3D Nanoporous Graphene for Desalination and Bio-Decontamination of Brackish Water via Asymmetric Capacitive Deionization. *ACS Appl. Mater. Interfaces* **2016**, *8*, 25313–25325. [CrossRef]

- 263. Wang, H.; Yan, T.; Liu, P.; Chen, G.; Shi, L.; Zhang, J.; Zhong, Q.; Zhang, D. In Situ Creating Interconnected Pores across 3D Graphene Architectures and Their Application as High Performance Electrodes for Flow-through Deionization Capacitors. *J. Mater. Chem. A* 2016, 4, 4908–4919. [CrossRef]
- 264. Liu, P.; Wang, H.; Yan, T.; Zhang, J.; Shi, L.; Zhang, D. Grafting Sulfonic and Amine Functional Groups on 3D Graphene for Improved Capacitive Deionization. *J. Mater. Chem. A* 2016, 4, 5303–5313. [CrossRef]
- 265. Gu, X.; Yang, Y.; Hu, Y.; Hu, M.; Huang, J.; Wang, C. Nitrogen-Doped Graphene Composites as Efficient Electrodes with Enhanced Capacitive Deionization Performance. *RSC Adv.* **2014**, *4*, 63189–63199. [CrossRef]
- 266. Xing, W.; Liang, J.; Tang, W.; He, D.; Yan, M.; Wang, X.; Luo, Y.; Tang, N.; Huang, M. Versatile Applications of Capacitive Deionization (CDI)-Based Technologies. *Desalination* **2020**, *482*, 114390. [CrossRef]
- 267. Qian, M.; Duan, M.; Gong, Z. Nitrogen-Doped Self-Shrinking Porous 3D Graphene Capacitor Deionization Electrode. *Int. J. Energy Res.* 2019, 43, 7583–7593. [CrossRef]
- 268. Leong, Z.Y.; Lu, G.; Yang, H.Y. Three-Dimensional Graphene Oxide and Polyvinyl Alcohol Composites as Structured Activated Carbons for Capacitive Desalination. *Desalination* **2019**, *451*, 172–181. [CrossRef]
- 269. Han, D.-C.; Zhang, C.-M.; Guan, J.; Gai, L.-H.; Yue, R.-Y.; Liu, L.-N.; Afzal, M.Z.; Song, C.; Wang, S.-G.; Sun, X.-F. High-Performance Capacitive Deionization Using Nitrogen and Phosphorus-Doped Three-Dimensional Graphene with Tunable Pore Size. *Electrochim. Acta* 2020, 336, 135639. [CrossRef]
- 270. Zhang, G.; Li, W.; Chen, Z.; Long, J.; Xu, C. Freestanding N-Doped Graphene Membrane Electrode with Interconnected Porous Architecture for Efficient Capacitive Deionization. *Carbon* **2022**, *187*, 86–96. [CrossRef]
- 271. Khan, A.; Wang, J.; Li, J.; Wang, X.; Chen, Z.; Alsaedi, A.; Hayat, T.; Chen, Y.; Wang, X. The Role of Graphene Oxide and Graphene Oxide-Based Nanomaterials in the Removal of Pharmaceuticals from Aqueous Media: A Review. *Environ. Sci. Pollut. Res.* 2017, 24, 7938–7958. [CrossRef]
- 272. Wang, J.; Wang, S. Removal of Pharmaceuticals and Personal Care Products (PPCPs) from Wastewater: A Review. *J. Environ. Manag.* 2016, 182, 620–640. [CrossRef] [PubMed]
- 273. Chaturvedi, P.; Shukla, P.; Giri, B.S.; Chowdhary, P.; Chandra, R.; Gupta, P.; Pandey, A. Prevalence and Hazardous Impact of Pharmaceutical and Personal Care Products and Antibiotics in Environment: A Review on Emerging Contaminants. *Environ. Res.* **2021**, *194*, 110664. [CrossRef]
- 274. Sharma, K.; Thakur, I.S.; Kaushik, G. Occurrence and Distribution of Pharmaceutical Compounds and Their Environmental Impacts: A Review. *Bioresour. Technol. Rep.* **2021**, *16*, 100841. [CrossRef]
- 275. Al-Khateeb, L.A.; Hakami, W.; Salam, M.A. Removal of Non-Steroidal Anti-Inflammatory Drugs from Water Using High Surface Area Nanographene: Kinetic and Thermodynamic Studies. *J. Mol. Liq.* **2017**, *241*, 733–741. [CrossRef]
- 276. Liu, Q.; Shen, J.; Yang, X.; Zhang, T.; Tang, H. 3D Reduced Graphene Oxide Aerogel-Mediated Z-Scheme Photocatalytic System for Highly Efficient Solar-Driven Water Oxidation and Removal of Antibiotics. *Appl. Catal. B Environ.* **2018**, 232, 562–573. [CrossRef]
- 277. Zhong, J.; Feng, Y.; Li, J.-L.; Yang, B.; Ying, G.-G. Removal of Sulfadiazine Using 3D Interconnected Petal-Like Magnetic Reduced Graphene Oxide (MrGO) Nanocomposites. *Water* 2020, 12, 1933. [CrossRef]
- 278. Zhuang, Y.; Yu, F.; Ma, J.; Chen, J. Graphene as a Template and Structural Scaffold for the Synthesis of a 3D Porous Bio-Adsorbent to Remove Antibiotics from Water. *RSC Adv.* **2015**, *5*, 27964–27969. [CrossRef]
- 279. Niu, P.; Nie, X.; Li, Y.; Liang, X.; Wang, L.; Guo, Y. Magnetic N-Doped 3D Graphene-like Framework Carbon for Extraction of Cephalexin Monohydrate and Ceftiofur Hydrochloride. *Talanta* 2020, 215, 120932. [CrossRef] [PubMed]
- 280. Shen, Y.; Zhu, X.; Zhu, L.; Chen, B. Synergistic Effects of 2D Graphene Oxide Nanosheets and 1D Carbon Nanotubes in the Constructed 3D Carbon Aerogel for High Performance Pollutant Removal. *Chem. Eng. J.* 2017, 314, 336–346. [CrossRef]
- 281. Umbreen, N.; Sohni, S.; Ahmad, I.; Khattak, N.U.; Gul, K. Self-Assembled Three-Dimensional Reduced Graphene Oxide-Based Hydrogel for Highly Efficient and Facile Removal of Pharmaceutical Compounds from Aqueous Solution. *J. Colloid Interface Sci.* 2018, 527, 356–367. [CrossRef]
- 282. Shan, D.; Deng, S.; Jiang, C.; Chen, Y.; Wang, B.; Wang, Y.; Huang, J.; Yu, G.; Wiesner, M.R. Hydrophilic and Strengthened 3D Reduced Graphene Oxide/Nano-Fe<sub>3</sub>O<sub>4</sub> Hybrid Hydrogel for Enhanced Adsorption and Catalytic Oxidation of Typical Pharmaceuticals. *Environ. Sci. Nano* 2018, 5, 1650–1660. [CrossRef]
- 283. Ehtesabi, H.; Bagheri, Z.; Yaghoubi-Avini, M. Application of Three-Dimensional Graphene Hydrogels for Removal of Ofloxacin from Aqueous Solutions. *Environ. Nanotechnol. Monit. Manag.* **2019**, *12*, 100274. [CrossRef]
- 284. Wang, S.; Ma, X.; Zheng, P. Sulfo-Functional 3D Porous Cellulose/Graphene Oxide Composites for Highly Efficient Removal of Methylene Blue and Tetracycline from Water. *Int. J. Biol. Macromol.* **2019**, *140*, 119–128. [CrossRef] [PubMed]
- 285. Feng, X.; Qiu, B.; Sun, D. Enhanced Naproxen Adsorption by a Novel β-Cyclodextrin Immobilized the Three-Dimensional Macrostructure of Reduced Graphene Oxide and Multiwall Carbon Nanotubes. *Sep. Purif. Technol.* **2022**, 290, 120837. [CrossRef]

J. Compos. Sci. 2025, 9, 18 53 of 53

286. Fard, N.T.; Tadayon, F.; Panahi, H.A.; Moniri, E. Synthesize, Characterization and Application of a Novel Three-Dimensional Magnetic Graphene Oxide Decorated with Polyester Dendrimers for Detection of Donepezil Hydrochloride in Pharmaceutical Formulation and Biological Fluid. *Synth. Met.* **2022**, *290*, 117141. [CrossRef]

- 287. Ghaly, H.A.; Souaya, E.R.; Allam, N.K.; El-Deen, A.G. Constructing of FeNi<sub>3</sub> Nano-Necklaces Intercalated 3D Graphene as an Efficient and Robust Heterogeneous Catalyst for Photo-Fenton Degradation of Hazardous Organic Pollutants. *Colloids Surf. A Physicochem. Eng. Asp.* 2023, 681, 132704. [CrossRef]
- 288. Hu, J.; Zhang, P.; Cui, J.; An, W.; Liu, L.; Liang, Y.; Yang, Q.; Yang, H.; Cui, W. High-Efficiency Removal of Phenol and Coking Wastewater via Photocatalysis-Fenton Synergy over a Fe-g-C<sub>3</sub>N<sub>4</sub> Graphene Hydrogel 3D Structure. *J. Ind. Eng. Chem.* **2020**, *84*, 305–314. [CrossRef]
- 289. Sajid, M.; Asif, M.; Baig, N.; Kabeer, M.; Ihsanullah, I.; Mohammad, A.W. Carbon Nanotubes-Based Adsorbents: Properties, Functionalization, Interaction Mechanisms, and Applications in Water Purification. *J. Water Process Eng.* **2022**, *47*, 102815. [CrossRef]
- 290. Ding, C.; Wang, X.; Liu, H.; Li, Y.; Sun, Y.; Lin, Y.; Sun, W.; Zhu, X.; Dai, Y.; Luo, C. Glyphosate Removal from Water by Functional Three-Dimensional Graphene Aerogels. *Environ. Chem.* **2018**, *15*, 325–335. [CrossRef]
- 291. Zhou, P.; Yang, X.-L.; Wang, X.-G.; Hu, B.; Zhang, L.; Zhang, W.; Si, H.-R.; Zhu, Y.; Li, B.; Huang, C.-L.; et al. A Pneumonia Outbreak Associated with a New Coronavirus of Probable Bat Origin. *Nature* 2020, 579, 270–273. [CrossRef] [PubMed]
- 292. Viraka Nellore, B.P.; Kanchanapally, R.; Pedraza, F.; Sinha, S.S.; Pramanik, A.; Hamme, A.T.; Arslan, Z.; Sardar, D.; Ray, P.C. Bio-Conjugated CNT-Bridged 3D Porous Graphene Oxide Membrane for Highly Efficient Disinfection of Pathogenic Bacteria and Removal of Toxic Metals from Water. ACS Appl. Mater. Interfaces 2015, 7, 19210–19218. [CrossRef]
- 293. De Farias, M.B.; Prediger, P.; Vieira, M.G.A. Conventional and Green-Synthesized Nanomaterials Applied for the Adsorption and/or Degradation of Phenol: A Recent Overview. *J. Clean. Prod.* **2022**, *367*, 132980. [CrossRef]
- 294. Severo, L.S.; Thue, P.S.; Lima, D.R.; Didó, C.A.; Vasconcellos, M.A.Z.; Armas, L.E.G.; Lima, E.C.; Benvenutti, E.V.; de Menezes, E.W. 3D Graphene Sponge Biomass-Derived with High Surface Area Applied as Adsorbent for Nitrophenols. *J. Environ. Chem. Eng.* 2023, 11, 109924. [CrossRef]
- 295. Zhang, T.; Li, H.; Wei, J.; Ma, J.-G.; Cheng, P. Tailored Sky-Parking Architectures of 3D Graphene Oxide Towards Highly-Efficient Water Purification. *ChemSusChem* **2023**, *16*, e202201974. [CrossRef] [PubMed]
- 296. Sun, Z.; Zhao, L.; Liu, C.; Zhen, Y.; Zhang, W.; Ma, J. A Novel 3D Adsorbent of Reduced Graphene Oxide-β-Cyclodextrin Aerogel Coupled Hardness with Softness for Efficient Removal of Bisphenol A. *Chem. Eng. J.* **2019**, 372, 896–904. [CrossRef]
- 297. Bagoole, O.; Rahman, M.M.; Shah, S.; Hong, H.; Chen, H.; Al Ghaferi, A.; Younes, H. Functionalized Three-Dimensional Graphene Sponges for Highly Efficient Crude and Diesel Oil Adsorption. *Environ. Sci. Pollut. Res.* 2018, 25, 23091–23105. [CrossRef] [PubMed]
- 298. Chen, L.; Xu, Z.-R. A Three-Dimensional Nickel-Doped Reduced Graphene Oxide Composite for Selective Separation of Hemoglobin with a High Adsorption Capacity. *RSC Adv.* **2016**, *6*, 56278–56286. [CrossRef]
- 299. Huang, Y.; Li, C.; Lin, Z. EDTA-Induced Self-Assembly of 3D Graphene and Its Superior Adsorption Ability for Paraquat Using a Teabag. ACS Appl. Mater. Interfaces 2014, 6, 19766–19773. [CrossRef] [PubMed]
- 300. Wang, X.; Lu, M.; Wang, H.; Pei, Y.; Rao, H.; Du, X. Three-Dimensional Graphene Aerogels–Mesoporous Silica Frameworks for Superior Adsorption Capability of Phenols. *Sep. Purif. Technol.* **2015**, *153*, 7–13. [CrossRef]
- 301. An, W.; Yang, T.; Liu, C.; Hu, J.; Cui, W.; Liang, Y. CuBi<sub>2</sub>O<sub>4</sub> Surface-Modified Three-Dimensional Graphene Hydrogel Adsorption and in Situ Photocatalytic Fenton Synergistic Degradation of Organic Pollutants. *Appl. Surf. Sci.* **2023**, *615*, 156396. [CrossRef]
- 302. Guo, X.; Qu, L.; Zhu, S.; Tian, M.; Zhang, X.; Sun, K.; Tang, X. Preparation of Three-Dimensional Chitosan–Graphene Oxide Aerogel for Residue Oil Removal. *Water Environ. Res.* **2016**, *88*, 768–778. [CrossRef]
- 303. Kondapalli, V.K.R.; He, X.; Khosravifar, M.; Khodabakhsh, S.; Collins, B.; Yarmolenko, S.; y Puente, A.P.; Shanov, V. CVD Synthesis of 3D-Shaped 3D Graphene Using a 3D-Printed Nickel–PLGA Catalyst Precursor. *ACS Omega* **2021**, *6*, 29009–29021. [CrossRef]

**Disclaimer/Publisher's Note:** The statements, opinions and data contained in all publications are solely those of the individual author(s) and contributor(s) and not of MDPI and/or the editor(s). MDPI and/or the editor(s) disclaim responsibility for any injury to people or property resulting from any ideas, methods, instructions or products referred to in the content.